

Aus der II. Medizinischen Klinik
(Gastroenterologie, Hepatologie, Infektiologie)

der Medizinischen Fakultät Mannheim
(Direktor: Prof. Dr. med. Matthias Ebert)

Crosstalk of Myotubularin-related protein 7 with RAS/WNT Driver Pathways in Colorectal Cancer

Inauguraldissertation
zur Erlangung des medizinischen Doktorgrades
der
Medizinischen Fakultät Mannheim
der Ruprecht-Karls-Universität
zu
Heidelberg

vorgelegt von
Yanxiong Yu
aus
Hunan, China
2024

Dekan: Herr Prof. Dr. med. Sergij Goerd
Referent(in): Frau Priv.-Doz. Dr. rer. nat. Elke Burgermeister

CONTENTS

	Page
ABBREVIATIONS.....	1
1 Introduction	2
1.1 Colorectal Cancer	2
1.1.1 Epidemiology in colorectal cancer	2
1.1.2 Etiology	3
1.1.3 Molecular pathways in colorectal cancer.....	4
1.1.4 Current treatments and limitations	7
1.1.5 Prevention.....	8
1.2 Myotubularin family of Lipid-Phosphatases.....	9
1.2.1 Cellular functions.....	9
1.2.2 Association with human diseases.....	10
1.2.3 Myotubularin-related protein 7	10
1.3 Aim of thesis.....	16
2 Material and Methods	17
2.1 Material.....	17
2.1.1 Cell lines	17
2.1.2 Mouse model and treatments	17
2.1.3 Plasmids and oligonucleotide primers.....	17
2.1.4 Drugs and antibodies.....	18
2.1.5 Peptides	20
2.1.6 Reagents	20
2.1.7 Materials and equipment	22
2.2 Methods.....	24
2.2.1 Cell culture.....	24
2.2.2 Immunocytochemistry (IHC).....	24
2.2.3 Plasmid DNA purification.....	25
2.2.4 Co-immunoprecipitation (Co-IP)	25
2.2.5 Immunoprecipitation (IP).....	26
2.2.6 Cell transfection and drug treatments.....	26
2.2.7 Luciferase Reporter gene assay	27
2.2.8 Reverse transcription (RT) PCR and real-time quantitative PCR (qPCR)	27
2.2.9 Immunofluorescence (IF).....	27
2.2.10 Proximity Ligation Assays (PLA).....	28
2.2.11 Cellular peptide uptake	30
2.2.12 Western blotting.....	30
2.3 Ethics statement.....	32
2.4 Statistics and software.....	32
3 Results	33
3.1 Overexpression of MTMR7 in HEK293T cells.....	33
3.2 In vitro analysis of WNT signaling after MTMR7 overexpression.....	34
3.2.1 MTMR7 reduces TCF/LEF-dependent transcription.....	34
3.2.2 MTMR7 and KYA1797K inhibit the transcriptional response of TCF/LEF.....	36
3.2.3 MTMR7 inhibits WNT signaling in presence of GSK3i.....	37
3.3 In vivo analysis of WNT signaling after MTMR7 peptide treatment.....	38
3.3.1 Therapy of APC ^{min/+} and SV40-Tag mice.....	38
3.3.2 MTMR7 peptide inhibits WNT signaling <i>in vivo</i>	39
3.3.3 MTMR7 peptide reduces WNT-target gene expression.....	41

3.4	<i>MTMR7 regulates β-catenin translocation in vitro.</i>	42
3.5	<i>MTMR7 inhibits WNT signaling by interfering with RAS-β-catenin interaction.</i>	44
3.5.1	<i>RAS and β-catenin form a protein interaction complex.</i>	44
3.5.2	<i>MTMR7 does not directly interact with full-length (FL) RAS by Co-IP.</i>	45
3.5.3	<i>Inhibition of WNT signaling by MTMR7 through destabilization of RAS and β-catenin.</i>	47
3.6	<i>Cellular uptake of Biotin-MTMR7 peptide.</i>	49
4	Discussion	51
4.1	<i>Expression and function of MTMR7.</i>	51
4.2	<i>MTMR7 and the WNT pathway in colorectal cancer cells.</i>	52
4.3	<i>Pathways involved in MTMR7 regulation.</i>	55
4.4	<i>MTMR7 as novel therapeutic target for colorectal cancer.</i>	57
5	CONCLUSION	59
6	REFERENCES	60
7	CURRICULUM VITAE	69
8	ACKNOWLEDGEMENTS	70

ABBREVIATIONS

Ab	Antibody
APC	Adenomatous Polyposis Coli
AP	Ammonium persulfate
BSA	Bovine Serum Albumin
B2M	B-2-microglobulin
CRC	Colorectal Cancer
Co-IP	Co-immunoprecipitation
CC	Coiled Coil Domain
DMEM	Dulbecco's modified eagle medium
DMSO	Dimethyl sulfoxide
DNA	Deoxyribonucleic acid
ECL	Enhanced chemiluminescence
EV	Empty Vector
FBS	Fetal bovine serum
FFPE	Formalin-fixed and paraffin-embedded
FL	Full Length
GSK3b	Glycogen synthase kinase 3 β
p-GSK3b	Phospho-Glycogen synthase kinase 3 β
HSP90	Hot Shock Protein 90
IB	Immuno Blot
IF	Immunofluorescence
IHC	Immunohistochemistry
IP	Input
LEF	Lymphoid enhancer factor family
MT	MTMR7-CC peptide
MTM	Myotubularin
MTMR	Myotubularin-related protein
MSS	Microsatellite stable
MSI	Microsatellite instability
OD	Optical Density
PAGE	Polyacrylamide gel electrophoresis
PBS	Phosphate buffered saline
PCR	Polymerase chain reaction
PLA	Proximity Ligation Assay
RAS	Rat sarcoma viral oncogene homolog
RNA	Ribonucleic acid
Rpm	Revolutions per minute
RT-qPCR	Reverse transcription polymerase chain reaction
RT	Room temperature
SC	Scrambled peptide
SDS	Sodium dodecyl sulfate
TCF	T cell factor
TCL	Total Cell Lysate
TEMED	N, N, N', N'-Tetramethyl ethylenediamine
VC	Vehicle control
WT	Wild-Type

1 Introduction

1.1 Colorectal Cancer

1.1.1 Epidemiology in colorectal cancer

Colorectal cancer (CRC) stands as the third most prevalent cancer and the fourth major contributor to cancer-related fatalities, resulting in an estimated 700,000 fatalities annually. Although the exact causes of CRC remain elusive, its incidence and mortality rates vary depending on multiple factors like gender, geography, and age [1].

Gender remarkably influences CRC incidence. As reported earlier, the *2014 World Cancer Report* reveals that CRC incidence ranks second to breast cancer among females, accounting for 9.2%, and third to lung and gastric cancers among males at 10% [2].

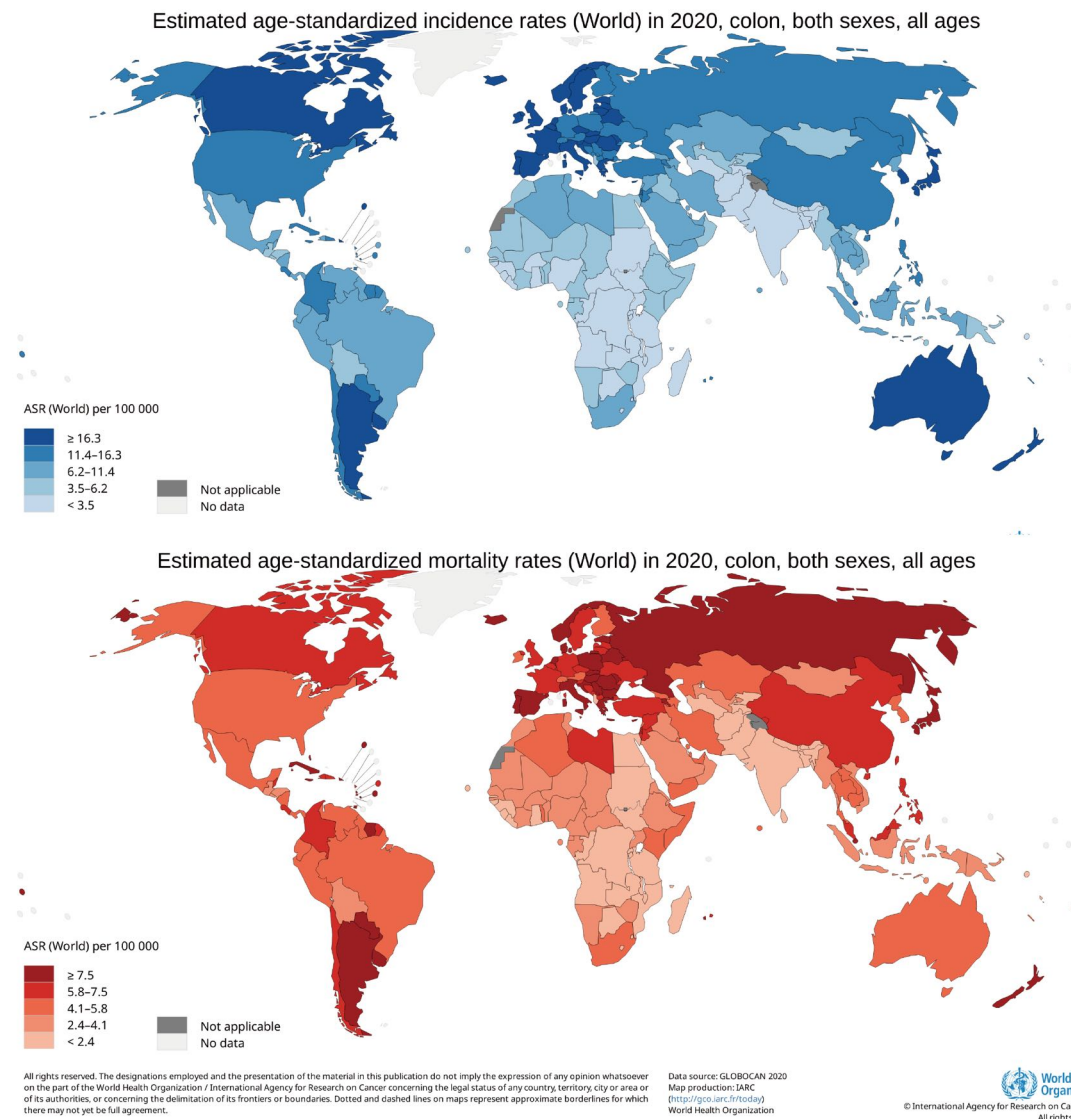


Figure 1. Incidence and mortality rates of CRC in males worldwide (age-adjusted to the world standard population, per 100,000) in 2020. Figure was adapted from GLOBOCAN 2020 [3].

Geographical disparities serve as another pivotal determinant. CRC incidences are higher in Australia, New Zealand, Europe, and North America, whereas they are comparatively lower in Africa, Central, and South Asia. Developed nations exhibit CRC incidence rates approximately four times higher than those in developing regions [4,5]. Figure 1 illustrates the global incidence and mortality rates of CRC in both sexes in 2020, which are shown in different colors, are age-adjusted based on the global standard population per 100,000, as reported by *GLOBOCAN 2020* [3]. Studies have identified dietary and environmental differences as potential contributors to the geographical disparities in CRC. Diets low in fiber and high in red meat, particularly prevalent in Europe, are linked with an elevated CRC risk [6].

In addition to gender and geography mentioned above, age emerges as another crucial factor contributing significantly to the increased onset and mortality of CRC.

There is a noticeable increase in the incidence and mortality of CRC among older individuals [4,7]. Paradoxically, this disease remains more prevalent and lethal in younger individuals, despite advancements in early detection and treatment. Considering the escalating global aging issue, it becomes imperative to enhance our comprehension of the initiation and progression mechanisms underlying CRC.

1.1.2 Etiology

The exact cause of CRC remains uncertain, but several risk factors contribute to identified as contributors to an increased risk of developing CRC. These factors can be broadly classified as genetic or environmental. The genetic risk factors are further categorized into hereditary nonpolyposis (HNPCC) and polyposis syndromes, while the environmental risk factors encompass obesity, smoking, and excessive alcohol consumption.

Hereditary CRC syndromes fall into general subcategories of Lynch (also known as HNPCC) and polyposis[1]. The latter can be further subclassified as MUTYH-associated polyposis (MAP), familial adenomatous polyposis (FAP), serrated polyposis syndrome (SPS), and other hamartomatous polyposis conditions. Notably, polyposis is more easily recognizable by physicians because of the presence of numerous polyps under endoscopy. On the other hand, Lynch syndrome is often overlooked because patients experience few adenomas, which are similar to those found in sporadic cases [8,9].

Among various environmental factors, obesity exerts a crucial role and is correlated to higher mortality and a compromised response to chemotherapy, especially targeted therapy. Meta-analyses and systematic reviews have demonstrated a notable increase in CRC incidence among men with obesity, with a relative risk (RR) varying from 1.37 (95% confidence interval (CI) = 1.21-1.56) [10] and in women with RR = 1.5 and 95%CI = 1.06-1.24 [10–12]. While the precise reason for the link between obesity and increased CRC mortality remains unclear, it might be associated with being in a state of metabolic dysregulation, specifically metabolic syndrome (MS) [13], which concurrently elevates the levels of visceral adipose tissue [14] and adipocytokine levels [15]. Furthermore, this association could be attributed to hyperinsulinemia [16], which serves as a crucial element influencing the proliferation of colonic mucosal cells and simultaneously stimulates the proliferation of colonic tumor cells at the same time [17].

However, the limited available research pointed out that weight loss might be linked to a decreased CRC incidence.

Besides, smoking is strongly linked to elevated morbidity and mortality in CRC. According to a meta-analysis, current smokers face an increased possibility of developing adenomatous polyps and CRC compared to non-smokers, with RR of 2.1 (95%CI = 1.9-2.5) and 1.8 (95%CI = 1.7-2.0) for current and never smokers, respectively [18]. This risk may further elevate the risk of CRC development in patients suffering from HNPCC.

In addition to the factors listed above, alcohol consumption stands out as a significant risk factor for elevated incidence of CRC, potentially ranking among the most substantial avoidable contributors. As indicated by a meta-analysis, both moderate (2-3 drinks/day), and high (≥ 4 drinks/day) alcohol consumption contribute to a significantly elevated risk of CRC, showing RR of 1.21 (95%CI = 1.13-1.28) and 1.52 (95%CI = 1.27-1.81) respectively, compared to a lifetime of low alcohol consumption [19].

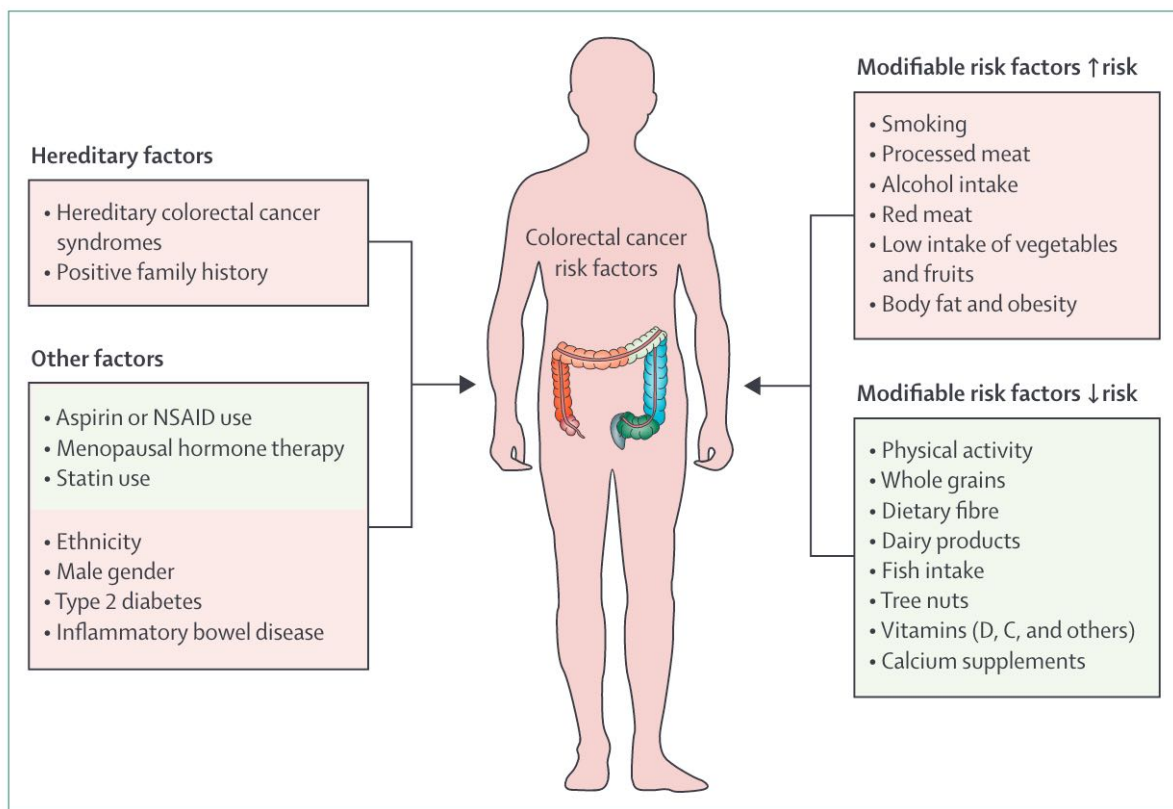


Figure 2. Etiology and factors increasing or decreasing CRC risk , adapted from Dekker et al [7].

1.1.3 Molecular pathways in colorectal cancer

The progression of CRC involves complex molecular pathways that are regulated by genetic and epigenetic alterations. Studies have indicated the emergence of at least three pathways: chromosomal instability (CIN), microsatellite instability (MSI), and the CpG island methylator phenotype (CIMP).

CIN

CIN constitutes the most prevalent of the three pathways, accounting for 80-85%, in CRC [20]. Sporadic CRC is primarily associated with CIN, characterized by an abundance of deficiency of chromosome fragments, structural abnormalities in chromosomes, and frequent loss of heterozygosity (LOH) at sites of tumor suppressor genes. The mechanisms driving CIN might involve responses to DNA damage, telomere dysfunction, and alterations in chromosome segregation, which arise from the activation of oncogenes or the deactivation of tumor suppressor genes, such as *TP53*, *APC*, and *KRAS*. *APC* mutations trigger the translocation of β -catenin from the cytoplasm to the nucleus, initiating the transcription of WNT target genes implicated in tumorigenesis [21]. *KRAS* and *phosphoinositide 3-kinase (PI3K)* induce continuous activation of mitogen-activated protein kinases (MAPKs), fostering sustained cell proliferation. *TP53*, which works as the main “gate keeper” in tumorigenesis, is inactive in the cell cycle to control DNA-damage and apoptosis when mutated. In summary, these processes collectively drive the initiation of CRC [22].

MSI

MSI, characterized by a hypermutable phenotype, results from dysfunction in deoxyribonucleic acid (DNA) mismatch repair during processes like DNA recombination, replication, and damage [22,23]. Microsatellites, which refer to repetitive DNA sequences consisting of a few nucleotides (1-6 base pairs) dispersed throughout the genome, are prone to replication errors. These errors can affect non-coding regions and microsatellites, leading to tumor growth when alterations occur in the Open Reading Frame (ORF) of tumor suppressor genes coded in microsatellites. Specifically, the DNA mismatch repair (MMR) protein *Mlh1* corrects such errors. Nevertheless, in the case of *Mlh1* defects (dMMR), these errors accumulate, leading to MSI and an elevated risk of HNPCC [23]. Consequently, hypermutated tumors produce misfolded proteins (neoantigens) and can be highly immunogenic.

CIMP

CIMP represents the third prevailing molecular pathway in CRC, originating from the activity of DNA methyltransferases (DNMTs). CIMP is distinguished by the hypermethylation of CpG-rich regions within promoter regions, causing reduced transcription and subsequent inactivation of tumor suppressor genes, thus facilitating the progression of CRC [24,25].

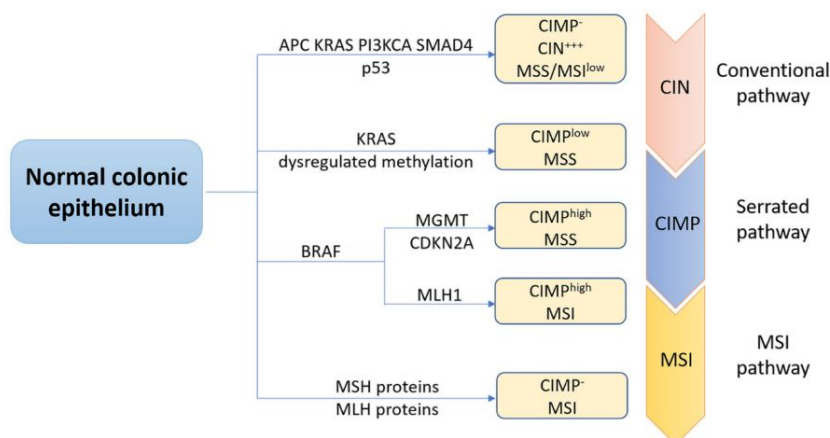


Figure 3. The three major molecular pathways of CRC, adapted from Huang et al [26].

Recent research has brought to light additional mechanisms contributing to the onset of CRC, extending beyond the conventional three pathways. These additional mechanisms include DNA methylation and non-coding DNA. It is now well-established that the development of CRC is intricately shaped by the interplay of multiple pathways, like epidermal growth factor receptor (EGFR)/ MAPK, neurogenic locus notch homolog protein (Notch), PI3K, transforming growth factor- β (TGF- β), and wingless-related integration site (WNT)/ β -catenin. They govern crucial cellular processes, encompassing cell proliferation, differentiation, angiogenesis, invasion, and metastasis [17,27]. Noteworthy is the interconnectedness of these pathways, capable of mutually amplifying their effects through cascading interactions [26,28]. Figure 4 here shows multiple signaling pathways involved in activation of CRC development and progression from normal epithelium to carcinoma.

Consensus molecular subtypes (CMS)

Although the traditional TNM staging system classifies CRC based on tumor size (T), lymph node involvement (N), and the presence of distant metastases (M), it inadequately captures the complete biological behavior of the disease due to its limited integration of the molecular and genetic characteristics of tumors and the variability among patients. Consequently, a personalized staging model grounded in the molecular and genetic profiles of tumors is imperative for guiding therapeutic strategies more precisely and enhancing prognostic accuracy [29].

In 2015, an international consortium of cancer researchers introduced the Consensus Molecular Subtypes (CMS) classification, which was derived from comprehensive gene expression analyses across six CRC subtyping algorithms [21]. This classification categorizes CRC into four distinct subtypes as depicted in Figure 4: CMS1 (MSI immune subtype, 14%), CMS2 (canonical subtype, 37%, characterized by high WNT and MYC signaling activation), CMS3 (metabolic subtype, 13%), and CMS4 (mesenchymal subtype, 23%) [21,30]. Each subtype encapsulates unique biological traits of the tumors, offering divergent prognostic values. Notably, samples exhibiting mixed features (13%) may suggest either a transitional phenotype or intratumoral heterogeneity [21]. For example, CMS1 is typically associated with high levels of immune infiltration, correlating with a favorable prognosis [31,32]. Conversely, CMS4, marked by extensive stromal components, tends to elicit poorer treatment responses, consistently leading to poorer relapse-free and overall survival rates [33–35].

Moreover, the CMS framework enhances clinical stratification and supports tailored intervention strategies in CRC treatment, marking a shift from generalized to precision medicine. This biologically informed classification not only deepens our comprehension of CRC heterogeneity but also underpins more scientifically rigorous and precise clinical decision-making processes. The CMS classification is poised to be a pivotal direction in future CRC research and therapy [21,29,34].

CMS1 MSI immune	CMS2 Canonical	CMS3 Metabolic	CMS4 Mesenchymal
14%	37%	13%	23%
MSI, CIMP high, hypermethylation	SCNA high	Mixed MSI status, SCNA low, CIMP low	SCNA high
<i>BRAF</i> mutations		<i>KRAS</i> mutations	
Immune infiltration and activation	WNT and MYC activation	Metabolic deregulation	Stromal infiltration, TGF- β activation, angiogenesis
Worse survival after relapse			Worse relapse-free and overall survival

Figure 4. Novel classification of CRC based on distinct molecular subtypes derived from gene expression differences, adapted from Guinney et al [21].

1.1.4 Current treatments and limitations

CRC, characterized by multiple mutations and stages, presents a formidable challenge for developing a comprehensive therapeutic approach. The current treatment modalities encompass endoscopic treatment, surgical interventions, chemotherapy, radiotherapy, biologic treatments, targeted therapies, and immunotherapy. Figure 5 illustrates the classes of drugs used in patients with CRC [7].

Endoscopic treatment is primarily applicable in the early stages of CRC due to the small size and non-invasive stage of the tumor. Upon diagnosis under cancer screening, some malignant polyps might be resected directly by endoscopy [7,36].

Surgical treatment and chemotherapy stand as the predominant and foundational modalities in CRC treatment [37]. Radiotherapy is usually employed to mitigate the absolute risk before surgery [38]. Chemotherapy agents such as fluoropyrimidines, oxaliplatin, and irinotecan serve as key components in two- or three-drug regimens. However, a substantial proportion (60-70%) of metastatic colorectal cancer (mCRC) cases are diagnosed in advanced stages, leading to an unfavorable prognosis, and rendering the tumor challenging to treat.

Nowadays, significant advancements in CRC treatment have been realized through the progress of biologics, targeted therapies, or immunotherapy. Bevacizumab, classified as an anti-vascular endothelial growth factor (VEGF) agent, stands out as the first biologic treatment approved for mCRC, demonstrating notable efficacy across all stages [39]. Regorafenib (tyrosine-kinase inhibitor) [40,41] and TAS-102 (trifluridine plus tipiracil) [42] are two innovative drugs employed for patients who do not respond to systemic therapies. Moreover, immune checkpoint inhibitors (ICIs) present a promising avenue for durable and curative outcomes. PD-1 blockade through drugs like nivolumab and pembrolizumab is now utilized for CRC with dMMR or high MSI [43–45]. However, this approach proves ineffective for MMR-proficient CRC, which occupies the majority of CRC cases [43]. In patients with left-sided CRC with *RAS* wild-

type (WT) status, treatment with anti-EGFR therapies like cetuximab or panitumumab yields favorable outcomes [46,47]. Conversely, in right-sided CRC, these therapies are less effective. This disparity may stem from differences in cells of origins between the two cancer types [7]. In addition, *BRAF-V600E* mutant CRC represents an aggressive tumor which does not respond to most systemic therapies. As a results, patients with such CRC can be intervened using combinatorial strategies (BRAF or BRAF plus MEK inhibitors) [46,47].

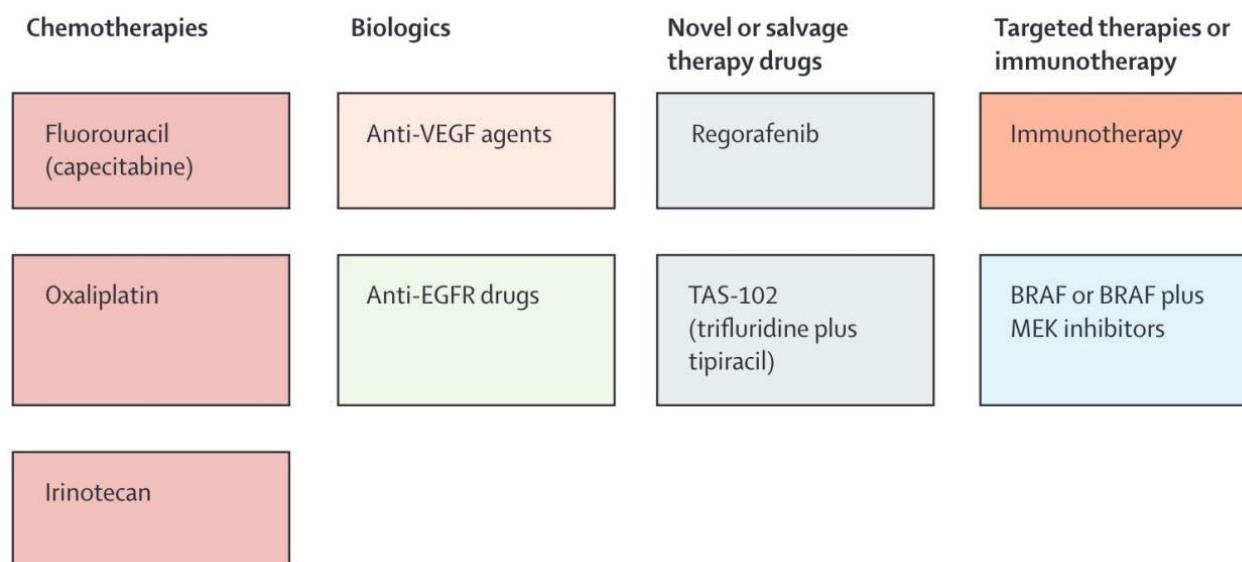


Figure 5. Classifications of drugs used for patients with CRC, adapted from Dekker et al [7].

1.1.5 Prevention

Considerable research suggests that CRC has a substantial lifestyle-related component, which opens avenues for effective prevention. In general, behavioral modification, encompassing screenings, diets, and medications, plays a pivotal role in this endeavor.

In various countries, especially the developed world, CRC screenings have witnessed a significant reduction in mortality in recent years. To be more specific, research suggests that individuals undergoing colonoscopy, tomographic colonography (CTG) every 10 years, or flexible sigmoidoscopies every 5 years, achieve a balanced benefit of screenings and manageable burden [48].

Dietary interventions further contribute to reducing the risk and mortality of CRC. As mentioned above, a low fiber intake and high consumption of red meat exhibit correlations to an elevated risk of CRC. In contrast, higher fiber intake and lower red meat consumption have been demonstrated to reduce the risk. Additionally, the intake of calcium and vitamin D intake have been proven to contribute to the reduction of CRC risk by binding to bile acids and fatty acids in the intestine, facilitating the diminishment of irritation and proliferation of intestinal tissues [49–51].

Importantly, certain medications have exhibited the potential to decrease the CRC risk, including NSAIDs, statins, and bisphosphonates. For example, aspirin, has been

shown to reduce long-term incidences especially for proximal colon cancer when it is administrated at a dose of 75 mg and more per day continuously for several years [52,53].

1.2 Myotubularin family of Lipid-Phosphatases

1.2.1 Cellular functions

The myotubularin family (MTM) comprises a large group of conserved proteins, denoted by MTM1 and MTMR1 to MTMR13 [54]. While the primary functions of MTMs are well-established in endocytosis and membrane trafficking. Recently, findings suggest potential additional roles encompassing cell proliferation, autophagy, and cell junction dynamics [54,55,55,56].

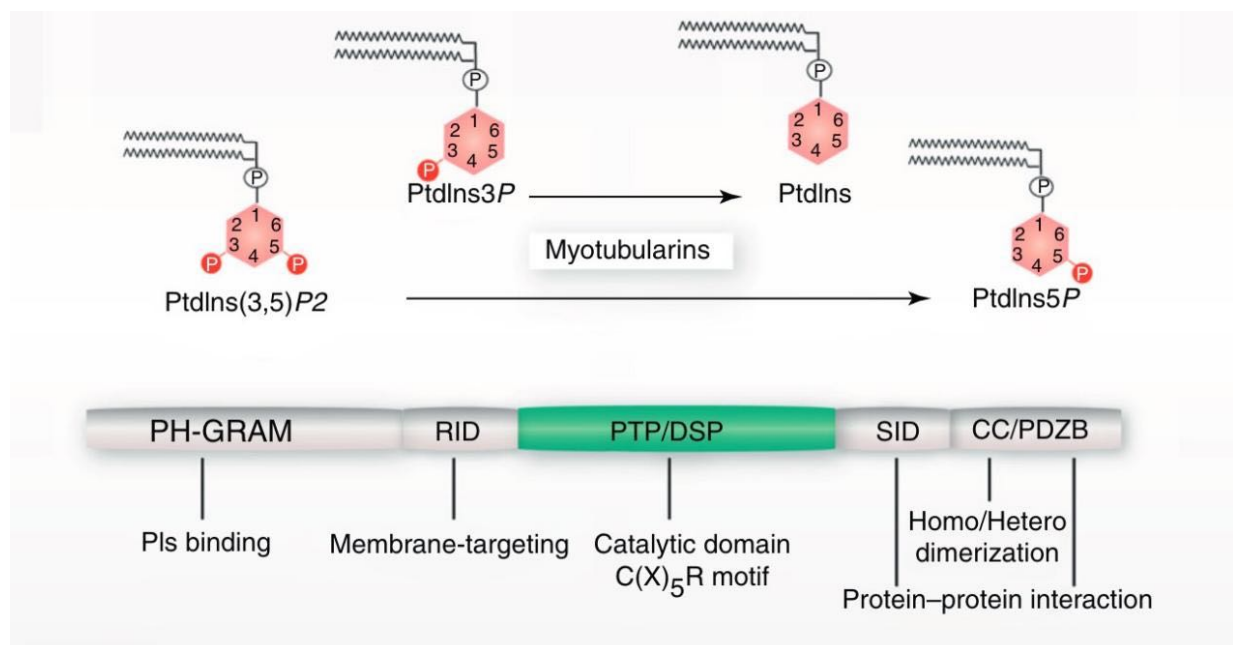


Figure 6. Schematic structure of MTM protein family and the process of catalytic activity, adapted from Hnia et al [57].

As depicted in Figure 6, the MTM protein family consists of Pleckstrin Homology Glucosyltransferase Rab-like GTPase Activator (PH-GRAM), RAC-induced recruitment domain (RID), protein tyrosine phosphatase domain)/dual specificity phosphatase (PTP/DSP), SET-interacting domain (SID) and coiled coil/PDZ-binding motif (CC/PDZB) [57]. Phosphoinositides (PIs) serve as membrane-derived second messengers. The PH-GRAM domain could mediate the activities of proteins in binding PIs [58–61]. The RID works as a membrane-targeting domain, while the PTP/DSP domain, containing the catalytic domain C(X)₅R motif, can dephosphorylate phosphatidylinositol 3-monophosphate (PtdIns3P) and PtdIns(3,5)P₂ to PtdIns and PtdIns5P, respectively. The CC/PDZB domain exerts a crucial effect in homodimerization and/or heterodimerization of MTMs. In addition to all the features described above, the SID domain plays an essential role in mediating protein-protein interaction.

1.2.2 Association with human diseases

Several diseases are linked with MTMs, including myotubular myopathy (XLMTM) and Charcot-Marie-Tooth (CMT) [62].

XLMTM, a severe congenital myopathy, typically manifests as hypotonia at birth [63]. *MTM1* mutations play a vital role in XLMTM, which has been reported in over 300 cases with more than 60 distinct mutation types [64]. Research has indicated that the muscle histology of *MTM1* knockout mice appears normal at birth. However, they subsequently develop histological symptoms associated with XLMTM and experience progressive myopathy within several weeks after birth. This implies that the disarrayed structure of muscle fibers results from defects in structural maintenance, contrary to the previously hypothesized impairment of myogenesis [65]. Additionally, the mouse model displayed no indications of active regeneration.

Another condition, CMT, is the most prevalent group of genetic disorders affecting the peripheral nervous system and is categorized as demyelinating and axonal neuropathies. There exists an interaction between the disease and mutations of *MTMR2* and *MTMR13/Sbf2*. CMT typically manifests with symmetrical distal and proximal muscle weakness, initiating in the lower extremities, accompanied by sensory loss and a notable decrease in nerve conduction velocity, often starting in childhood [62].

Interestingly, *MTMR5*, has been linked to spermatogenesis and azoospermia, as evidenced in mouse models. This highlights the human gene on chromosome 22qter as a promising candidate for male infertility [66]. In addition, *MTMR3* is correlated with an upregulated risk of CRC [67].

1.2.3 Myotubularin-related protein 7

1.2.3.1 Structure and Expression

Myotubularin-related protein 7 (MTMR7), under the MTMs family, is predominantly found in brain and neuronal cells, as illustrated in Figures 7B and 8A. *MTMR7* mRNA in normal human tissues is documented in various databases such as GTEX, Illumina, BioGPS, and SAGE. In humans, the *MTMR7* cDNA comprises 1,983 base pairs (bp). According to NCBI, the *MTMR7* gene is situated in the genomic region of the cytogenetic band 8p22 as depicted in Figure 7A, a finding corroborated by Ensembl and GeneLoc. Reports indicate its localization in the cytosol and granules near the nucleus [68].

MTMR7 consists of 660 amino acids (aa) with a molecular mass of approximately 75,833 Da [68]. Meanwhile, it has its three-dimensional structures predicted by AlphaFold as given in Figure 7C. The interactions between *MTMR7* and other proteins, analyzed using the STRING interaction Network, are depicted in Figure 7D, which highlights the top 5 interactants. The results unveil that *MTMR7* can bind with proteins such as *MTMR3*, *MTMR4*, *MTMR6*, *MTMR8*, and *MTMR9*. Notably, it is reported that only the CC domain is necessary for *MTMR9* to bind to *MTMR7*, enhancing the

phosphatase activity of MTMR7. Consequently, MTMR7 and MTMR9 collaborate in the dephosphorylation of their substrates [68].

MTMR7 expression levels vary across different cancers and show distinctions between tumor tissues and adjacent normal tissues. In general, most tumor data indicate higher MTMR7 expression in tumor tissues, as demonstrated in Figure 8B. However, the functional role of MTMR7 in tumors remains largely unexplored. Figure 8C provides a visual representation of MTMR7 expression across various CRC cell lines.

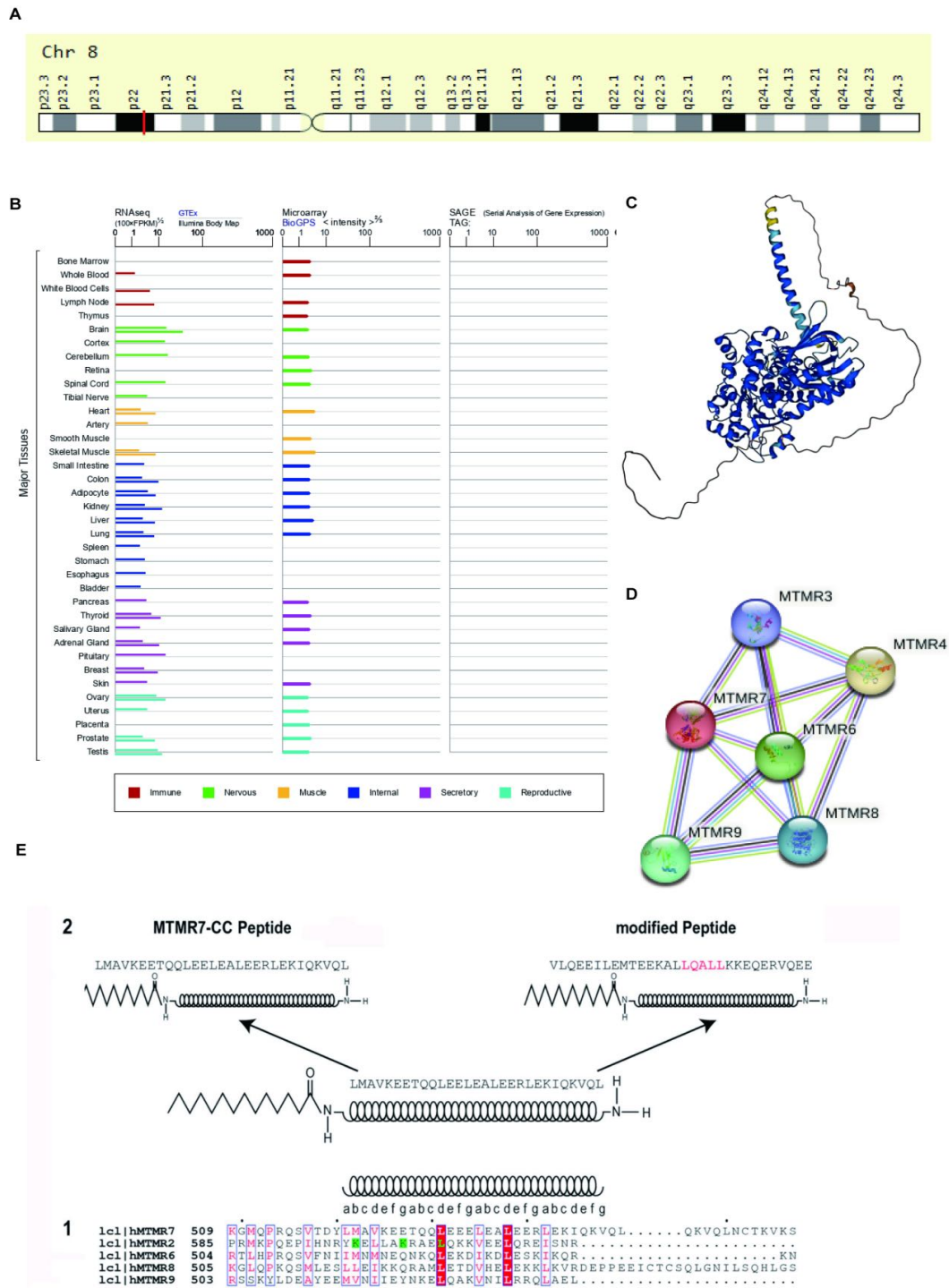


Figure 7. The structure and expression of MTMR7. **A.** Genomic location of *MTMR7* Gene: Cytogenetic band 8p22 (NCBI) (<https://www.ncbi.nlm.nih.gov/gene/9108>), with banding (Ensembl) (https://www.ensembl.org/Homo_sapiens/Gene/Summary?g=ENSG0000003987;r=8:17296794-17413528) and location details (GeneLoc) (<https://www.genecards.org/cgi-bin/carddisp.pl?gene=MTMR7>). **B.** *MTMR7* mRNA expression in normal human tissues, sourced from GTEx (<https://www.gtexportal.org/home/gene/MTMR7>), Illumina (https://rapid.ensembl.org/Homo_sapiens_GCA_009914755.4/Gene/Summary?db=core;g=ENSG05220042114;r=8:17564397-17680799), and BioGPS (<http://biogps.org/#goto=genereport&id=9108>). **C.** Predicted three-dimensional structures of *MTMR7* from AlphaFold (<https://alphafold.ebi.ac.uk/entry/Q9Y216>). **D.** Top 5 interacting proteins with *MTMR7* from the STRING Interaction Network Preview (<https://string-db.org/cgi/network?taskId=bsqJCz7t4Mi0&sessionId=bgkT3aQTn93D>). **E.** Design of *MTMR7*-CC mimicry peptides, previously published by Weidner et al [69].

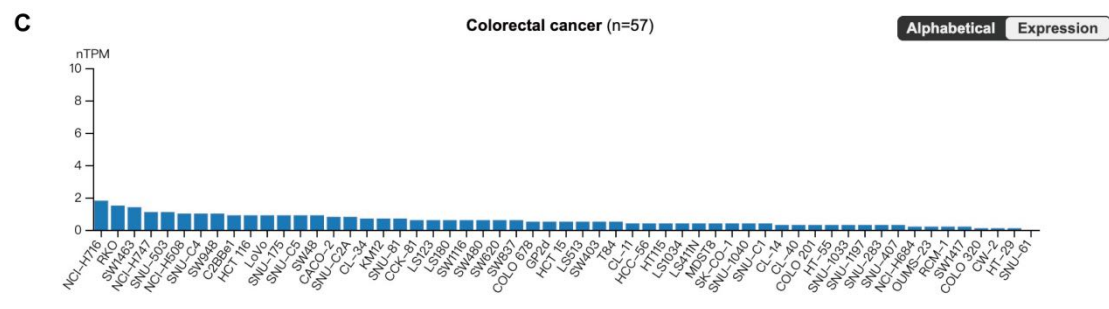
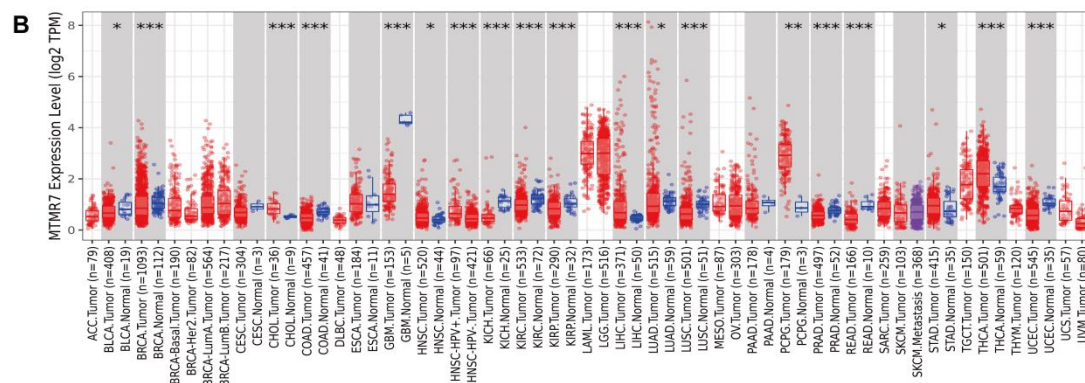
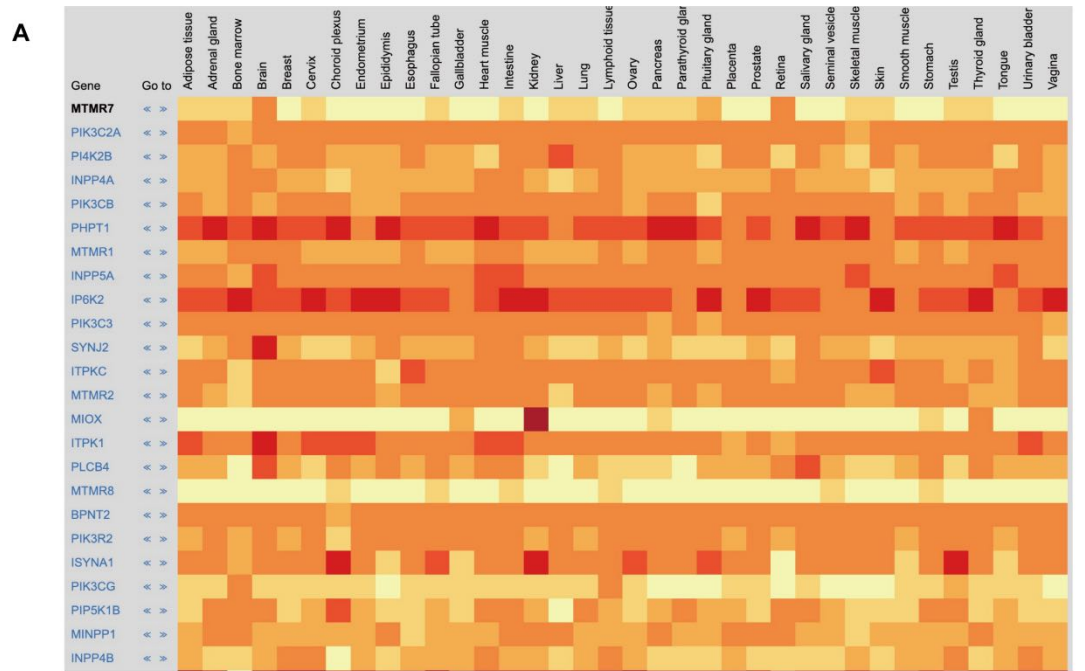


Figure 8. The expression of MTMR7 from public database.
A. MetabolicAtlas (<https://metabolicatlas.org/>) **B.** MTMR7 gene expression in tumors and adjacent normal tissues across all TCGA tumors which are determined by the database (<http://timer.cistrome.org/>). Gene expression levels are depicted using box plots. Statistical significance, determined by Wilcoxon test, is denoted by stars. (*: p-value < 0.05; **: p-value < 0.01; ***: p-value < 0.001). **C.** Human Protein Atlas (<https://www.proteinatlas.org/ENSG0000003987-MTMR7>). MTMR7 expression as normalized transcript per million (nTPM) values in cancer cells.

1.2.3.2 Previous Research

1.2.3.2.1 MTMR7 inhibits RAS/ ERK 1/2 signaling.

Since 2016, our research group has embarked on an exploration into the link between MTMR7 and CRC. The results revealed that MTMR7 effectively impedes the insulin-driven activation of both the AKT and ERK 1/2 signaling pathways [70].

Figure 9 demonstrates that MTMR7 functions as an inhibitor of two downstream pathways in receptor tyrosine kinase (RTK) signaling: AKT and ERK1/2 [70], thus greatly weakening the proliferation of CRC cells. These findings underscore the pivotal role of MTMR7 as a central mediator in the intricate interplay between growth factors and CRC. Additionally, we observed a notable downregulation of MTMR7 protein in human CRC cells and patient-derived clinical samples. These findings signify no remarkable link between MTMR7 expression in tumor tissues and patient prognosis. However, increased MTMR7 expression in adjacent stromal tissues is notably associated with an unfavorable prognosis. In summary, these intriguing findings imply that MTMR7 holds promise as a potential target or marker for CRC, while also playing a crucial role in modulating the intricate interplay between lipid phosphatase and growth factor pathways [70].

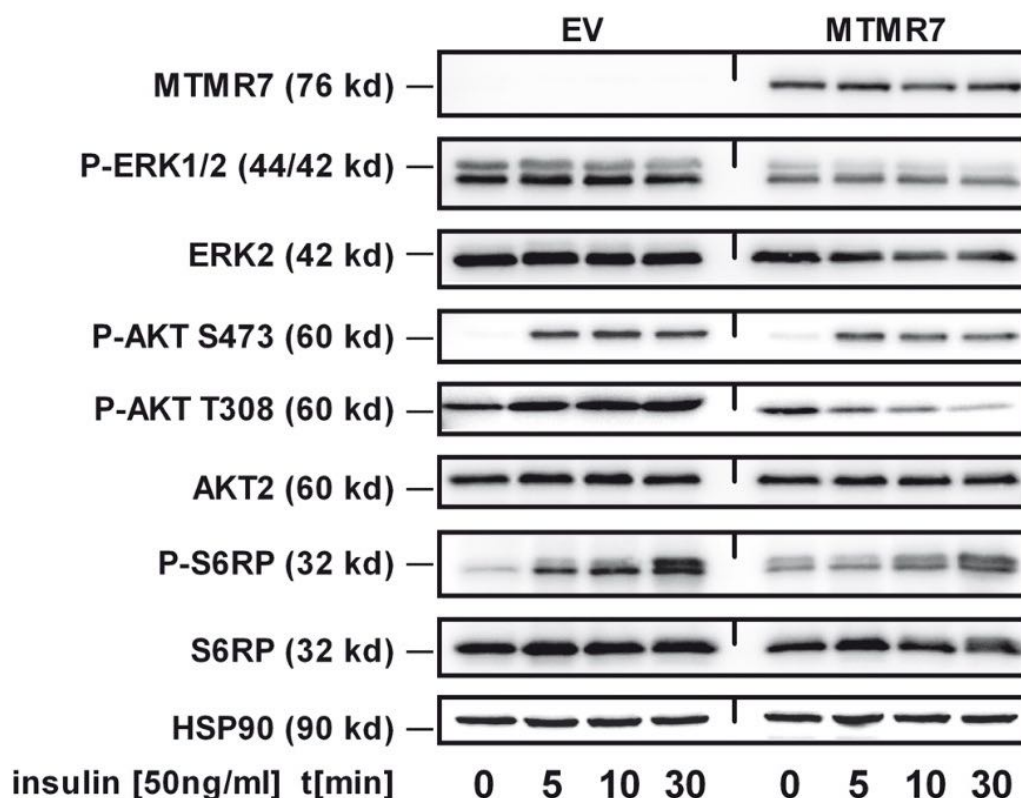


Figure 9. Inhibition of cellular RTK-signaling by MTMR7 adapted from Weidner et al [70].

HEK293T cells were transfected with either an empty vector (EV) or a full-length MTMR7 (MTMR7) plasmid for 48 hours, followed by serum deprivation for 24 hours. The cells were then stimulated with 50 ng/ml insulin at various time points (0, 5, 10, and 30 minutes). Cell lysates were collected for Western blot analysis to detect phosphorylated and total proteins including p-ERK1/2, ERK2, P-AKT (S473 and T308), p-S6RP and S6RP. HSP90 served as a loading control, and the expression of MTMR7 was used to confirm the efficacy of the transfection.

1.2.3.2.2 MTMR7 activates the tumor suppressor PPAR γ

The indistinct impact of peroxisome proliferator-activated receptor γ (PPAR γ) in CRC intervention may stem from its intricate regulation by the RAS-ERK1/2 signaling cascade [71]. Within this cascade, RAS downstream effectors inhibit PPAR γ through mechanisms like ERK1/2-dependent phosphorylation, while MEK1 in the nucleus exports and confines it to the cytoplasm [72].

In 2020, building upon our previous work, our team further delved into the association between MTMR7 and CRC. Through a MALDI-MS screen, we initially identified PPAR γ as a cytoplasmic binding chaperone for MTMR7 [69]. Subsequently, by comprehensively analyzing the aa sequences of MTMR7, MTMR2, MTMR6, MTMR8, and MTMR9, a 30-aa segment was pinpointed at the C-terminal end of MTMR7. Utilizing this information, a peptide was assigned for MTMR7-CC (MT) for comparative analysis. Additionally, a scramble modified peptide (SC) was crafted, which comprised of the same aa residues but arranged in a shuffled order and retained the characteristic LXXLL coactivator motifs of nuclear receptors (including PPAR γ). Figure 7E depicts the MTMR7-CC mimicry peptides previously published by our team [69]. Conclusively, our research demonstrated that MTMR7, by forming a complex with PPAR γ , enhances its transcriptional activity both *in vitro* and *in vivo*. Moreover, this interaction also diminishes the ERK1/2-dependent phosphorylation of PPAR γ . Consequently, the MTMR7-PPAR γ complex might serve as promising pharmacological target in treating *KRAS*-mutated CRC [69].

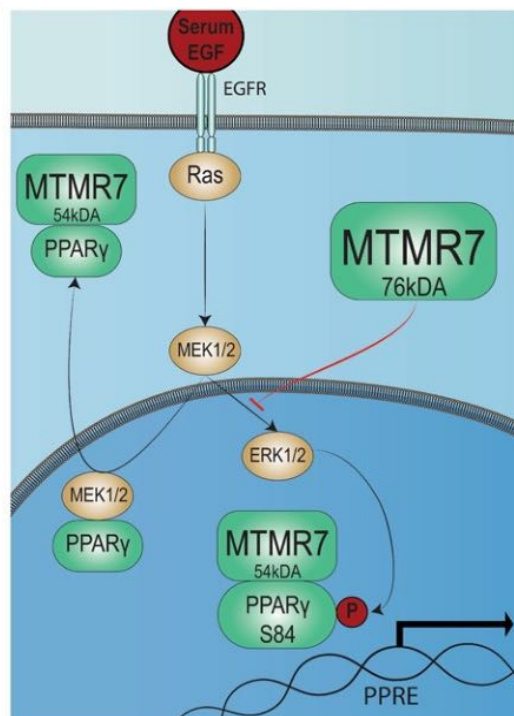


Figure 10. Model of MTMR7-PPAR γ signaling, adapted from Weidner et al [69].

Activation by external stimuli: In the presence of EGF or serum, the RAS-MEK1/2-ERK1/2 signaling pathway is activated. This pathway inactivates PPAR γ via two mechanisms: ERK1/2 phosphorylates PPAR γ on Ser84, and MEK1/2 mediates the translocation of PPAR γ from the nucleus to the cytoplasm, suppressing its transcriptional activity. However, MTMR7 inhibits MEK1/2-dependent ERK1/2 activation and thereby antagonizes the kinase-induced inhibition of PPAR γ and, by forming a coiled-coil (CC) complex with PPAR γ , enhances its transcriptional activity both *in vitro* and *in vivo*.

1.3 Aim of thesis

Colorectal Cancer, serving as a disease involving multiple mutations and different stages, poses a challenge in terms of non-responsiveness to current therapies, necessitating the identification of new druggable targets.

The WNT/ β -catenin and RAS pathways are extensively accepted as two essential contributors to CRC tumorigenesis. *APC* and *KRAS* mutations occur in CRC commonly and jointly [27]. However, the intricate crosstalk between *APC* and *KRAS* remains poorly understood. Recent studies have highlighted the collaborative role of these pathways in advancing tumorigenesis, metastasis [73,74], and resistance to therapy in CRC [27].

This thesis primarily focused on investigating the interaction between myotubularin-related protein 7 (MTMR7) and the RAS/WNT driver pathways in CRC. Our previous work has shown the inhibitory effect of MTMR7 on RAS/ERK 1/2 signaling [70] and its ability to activate the tumor suppressor PPAR γ [69]. Building upon this, now we have discovered that the MTMR7 enzyme and a peptide derived from its CC-domain also act as an inhibitor in the WNT signaling pathway, as evidenced by both *in vitro* and *in vivo* studies. Additionally, we found that the stability of β -catenin is contingent upon its interaction with RAS. Disruption of the interaction leads to separate degradation processes for both β -catenin and RAS. Using the MTMR7-full length (FL) plasmid for transfection into three distinct cell lines (HEK293T, SW480, HCT116), Co-immunoprecipitation (Co-IP) was employed to demonstrate that MTMR7 interferes with the interaction of β -catenin and RAS. In summary, MTMR7 functions as a potent WNT signaling inhibitor, showcasing its potential as a therapeutic agent for treatment-resistant CRC.

2 Material and Methods

2.1 Material

2.1.1 Cell lines

Human embryonic kidney (HEK) 293T cells as well as the CRC cell lines SW480, HT29, and HCT116 were all acquired from the American Type Culture Collection (ATCC, USA). The table below (Table 1) lists the cell lines utilized herein, along with their corresponding mutation sites.

Table 1: Mutation status of cell lines

	<i>TP53</i>	<i>KRAS</i>	<i>BRAF</i>	<i>APC</i>	MSI	CIN	CIMP
HEK293T	WT	WT	WT	WT	WT	WT	WT
SW480	p.R273H; p. P309S	p. G12V	WT	Mu	MSS	Mu	CIMP-
HCT116	WT	p. G13D	WT	WT	MSI	WT	CIMP+

Note: MSS, microsatellite stable. MSI, microsatellite instability. CIN, chromosomal instability. WT, wide type. CIMP, CpG island methylator phenotype. Mu, mutation. (Mutation status source was from [75])

2.1.2 Mouse model and treatments

All procedures involving mice adhered to approved guidelines (Aktenzeichen G188-18, RP Karlsruhe, Germany). Two distinct genetically modified mouse strains, SV40-Tag gastric cancer mice and *APC*^{min/+} intestinal cancer mice [69,76,77], were utilized throughout the experiments. Peptides were synthesized by J Bode et al. (ETH Zürich, Switzerland) and were dissolved in sterile DMSO in PBS and applied intraperitoneally (i.p.) as a daily dosage of 30 mg/kg administered as a single dose, 4 times per week for a duration of 2 weeks [69].

2.1.3 Plasmids and oligonucleotide primers

The pRK5-HA-Ubiquitin-WT plasmid was procured from Addgene (Addgene plasmid # 17608; <https://www.addgene.org/17608/>; RRID: Addgene_17608). The complete human cDNA sequence of MTMR7 (initiation codon MEHIRT, amino acids 1-660, 76 kDa, NM_004686.4) was amplified from total RNA derived from HEK293T cells. Subsequently, it was inserted, both with and without an N-terminal FLAG-tag, into the pTarget (pT) vector (Promega GmbH, Mannheim, DE) [69,70]. The empty vector (EV) pT was utilized as a negative control. For ubiquitin experiments in Chapter 3.5.3, HA-MTMR9 was set as a control. Furthermore, the oligonucleotide primers were synthesized by Eurofins Genomics (Ebersberg, DE), and detailed primer information is provided in Table 2 below.

Table 2: Oligonucleotides for RT-qPCR

Gene	Primer (mouse)	Sequence (5' > 3')	Amplicon (bp)
<i>mB2m</i>	<i>5-mB2m</i>	TTCTGGTGCTTGTCTCACTGA	104
	<i>3-mB2m</i>	CAGTATGTTCCGGCTTCCCATTCC	
<i>Axin2</i>	<i>5-Axin2</i>	TGACTCTCCTTCCAGATCCCA	105
	<i>3-Axin2</i>	TGCCACACTAGGCTGACA	
<i>Ephb</i>	<i>5-Ephb</i>	TTGAGAATGGCACCGTCT	150
	<i>3-Ephb</i>	TTGAGAATGGCACCGTCT	
<i>Lgr5</i>	<i>5-Lgr5</i>	CCTACTCGAAGACTTACCCAGT	165
	<i>3-Lgr5</i>	GCATTGGGGTGAATGATAGCA	
<i>Asclc</i>	<i>5-Asclc</i>	GCAACCGGGTCAAGTTGGT	218
	<i>3-Asclc</i>	GTCGTTGGAGTAGTTGGGGG	

2.1.4 Drugs and antibodies

All the drugs and antibodies adopted were as followed (Table 3).

Table 3: Antibodies

Application	Clone (Add-Ons)	Cat. No.	Company
Western blotting (WB)			
Axin1	Rabbit IgG	2087S	Cell Signaling Technology (CST)
Axin2	Rabbit IgG	2151S	CST
MTMR7	Rabbit IgG	MBS9406043	Mybiosource
MTMR7	Rabbit IgG	PA5-113535	Invitrogen
MTMR7	Rabbit IgG	25990-1-AP	Proteintech
ERK1/2	Rabbit IgG	9102S	CST
β-catenin	Rabbit IgG	8480S	CST
Phospho β-catenin	Rabbit IgG	9565S	CST
Non-phospho β-catenin	Rabbit IgG	19807S	CST
GSK3b	Rabbit IgG	12456S	CST
Phospho GSK3b	Rabbit IgG	9332S	CST
Pan-RAS	Mouse IgG	Sc-166691	Santa Cruz
K-RAS	Rabbit IgG	415700	CST
HSP90	Mouse IgG	sc-13119	Santa Cruz

β actin	Mouse IgG	sc-47778	Santa Cruz
Anti-HA	Rabbit IgG	3724S	CST
Cortactin	Rabbit IgG	3503S	CST
GAPDH	Mouse IgG	sc-47724	Santa Cruz
Lamin A/C	Rabbit IgG	sc-7292	Santa Cruz
Anti-rabbit IgG	Goat IgG	7074	CST
Anti-mouse IgG	Horse IgG	7076	CST

Immunohistochemistry (IHC)

β-catenin	Rabbit IgG	8480S	CST
Non-phospho β-catenin	Rabbit IgG	19807S	CST
MTMR7	Rabbit IgG	25990-1AP	Proteintech
Antigen Unmasking Solution		H-3300-250	Vector Laboratories
ABC kit		PK-4001	Vector Laboratories
DAB kit		SK-4100	Vector Laboratories
Goat serum	Goat IgG	Ab7481	Abcam

Immunofluorescence (IF)

Pan-RAS	Mouse IgG	Sc-166691	Santa Cruz
β-catenin	Rabbit IgG	8480S	CST
Non-phospho β-catenin	Rabbit IgG	19807S	CST
Phalloidin	Alexa Fluor 488	A12381	Invitrogen
Streptavidin	Alexa Fluor 594	S11227	Invitrogen
DAPI		D1306	Invitrogen
Alexa Fluor 594	Donkey anti-rabbit	A21207	CST
Alexa Fluor 488	Donkey anti-mouse	A21206	CST
Mounting buffer		GM304	DAKO

Proximity Ligation Assay (PLA)

Pan-RAS	Mouse IgG	Sc-166691	Santa Cruz
β-catenin	Rabbit IgG	8480S	CST
Non-phospho β-catenin	Rabbit IgG	19807S	CST
Phalloidin	Alexa 488	A12381	Invitrogen
DAPI		D1306	Invitrogen

Duolink® in Situ
PLA
Note: CST: Cell signaling Technology

DUO92101

Olink Bioscience

Table 4: Drugs

Name	Cat. No	Company
Dimethyl sulfoxide	J66650.AK	Thermo Scientific
MG132	S2619	Selleckchem
SAR405	S7682	Selleckchem
Chir99021	S2934	Selleckchem
XAV939	S7682	Selleckchem
KYA1797K	S8327	Selleckchem
Importazole	S8446	Selleckchem
Leptomycin B	S7580	Selleckchem

2.1.5 Peptides

The MTMR7 peptide imitates the natural leucine-rich aa sequence of MTMR7, precisely spanning amino acids 521-550 (30 aa). This sequence corresponds to the original leucine-rich aa sequence of MTMR7 (aa 521-550; Swissprot ID: Q9Y216.3: LMAVKEETQQLLEEELEEALEERLEKIQKVQL).

Furthermore, we synthesized two variants of MTMR7 based on its C-terminal aa sequence. The first variant, prepared using automated solid-phase peptide synthesis on Rink amide resin, featured N-terminal attachment of myristic acid and was employed for the animal treatment, as previously mentioned (MT). In parallel, a scramble modified peptide (SC) was crafted, which comprised of the same aa residues but arranged in a shuffled order and retained the characteristic LXXLL coactivator motifs of nuclear receptors (including PPAR γ). The other variant was made of Biotin and myristic acid at the N-terminus, specifically designed for cellular uptake experiments and Co-IP (Biotin-MTMR7). Prof. J Bode from the ETH Zürich in Switzerland synthesized all peptides, and their purity and sequences were verified using HPLC and MALDI-MS. Finally, the resulted peptide was supplied as a lyophilized powder and was dissolved in DMSO prior to experimental use.

2.1.6 Reagents

Table 5: Reagents

Name	Cat.	Company
Gibco® Dulbecco's Modified Eagle's Medium (DMEM)	12491015	Thermo Fisher Scientific
Gibco® Advanced RPMI 1640 Medium	12633012	Thermo Fisher Scientific
Gibco® Penicillin-Streptomycin (PS)	15140122	Thermo Fisher Scientific
Gibco® L-glutamine	A2916801	Thermo Fisher Scientific

Gibco® Trypsin-EDTA	25200072	Thermo Fisher Scientific
Tween® 20	9127.1	Roth GmbH
PBS (pH 7.4)	10010015	Thermo Fisher Scientific
DPBS	14190144	Thermo Fisher Scientific
Fetal Bovine Serum (FBS)	26140079	Thermo Fisher Scientific
Trypsin-EDTA (0.25%), phenol red	25200072	Thermo Fisher Scientific
Bovine Serum Albumin (BSA)	8076.5	Roth GmbH
HEPES buffer (pH 7.2–7.5)	J67485.AK	Thermo Fisher Scientific
UltraPure™ DNase/RNase-Free Distilled Water	10977049	Thermo Fisher Scientific
RevertAid First Strand cDNA Synthesis Kit	K621	Thermo Fisher Scientific
Thermo Scientific™ TurboFect transfection reagent	R0532	Thermo Fisher Scientific
SuperSignal™ West Atto Ultimate Sensitivity Substrate	A38556	Thermo Fisher Scientific
GlutaMAX™ supplement	35050061	Thermo Fisher Scientific
Matrigel® matrix	354230	Corning
Non-Fat Dry Milk (NFDM)	T145.2	Sigma-Aldrich
Thermo Scientific™ Pierce™ BCA ProteinAssay Kits	23225	Thermo Fisher Scientific
Goat serum	Ab7481	Abcam
cOmplete™ Protease Inhibitor Cocktail	04693124062	Roche
Luciferase assay reagent	E1910	Promega
Cell Culture Lysis 5X buffer	E194A	Promega
2-Propanol Dithiothreitol (DTT)	1.114.740.004	Roth GmbH
Ethanol, 96%	46139	Roth GmbH
Ethanol, absolute, ≥ 98 % (GC)	24194-5L R	Sigma Aldrich
Methanol	P717.1	Roth GmbH
Xylol (mixture of isomers)	4436.2	Roth GmbH
Tris PUFFERAN≥ 99,9 % Ultra	AE15.5	Roth GmbH
SDS ultra-pure	2326.5	Roth GmbH
ROTIPHORESE® NF-Acrylamide/Bis solution 30 (29:1), 1 l, glass	A124.2	Roth GmbH
Ammonium peroxodisulfate (APS), pure	9592.5	Roth GmbH
TEMED	2367.4	Roth GmbH

PageRuler™ Plus Prestained Protein Ladder	26619	Thermo Fisher Scientific
LB-Agar	X965.1	Roth GmbH
LB-Medium	X964.1	Roth GmbH
Magnesium chloride	5833 1000	Merk
Ampicillin > 99%	K029.1	Roth GmbH
Eukitt	03989	Sigma-Aldrich
Formaldehyde 37% ROTIPURAN	4979.2	Roth GmbH
Hydrochloric acid (1N)	1.090.571.000	Merck
Magnesium chloride	5833 1000	Merck
Power SYBR Green PCR Master Mix	4368577	Applied Biosystems
Protein G Plus/Protein A-Agarose	IP05	Merck
Sodium Chloride	31434-500G-R	Sigma-Aldrich
Sodium Orthovanadate	S6508	Sigma-Aldrich
Top 10 one shot competent cells	C404010	Invitrogen
Triton X-100	1.122.980.101	Sigma-Aldrich
Lithium chloride	3739.1	Roth GmbH
DAB kit	SK-4100	Vector Laboratories
ABC kit	PK-4001	Vector Laboratories
Duolink in Situ PLA	DUO92101	Olink Bioscience
HighSpeed Plasmid Midi Kit	12643	QIAGEN GmbH
QIAquick Gel Extraction Kit	28704	QIAGEN GmbH
Pure Yield Plasmid Mini prep kit	A1222	Promega
Thermo Scientific™ RIPA lysis and extraction buffer	89900	Thermo Fisher Scientific

2.1.7 Materials and equipment

Table 6: Materials and equipment

Name	Company	Cat.No
Materials		
Blue-Cap-Greiner 15 ml	Greiner bio-one	188261
Blue-Cap-Greiner 50 ml	Greiner bio-one	227261
Cellstar cell culture flask 75 mm ³	Greiner bio-one	658175
Cellstar cell culture flask 25 mm ³	Greiner bio-one	690175
Cellstar cell culture dishes 10 cm	Greiner bio-one	664160

Cellstar cell culture dishes 14,5 cm	Greiner bio-one	639160
Cellstar cell culture dishes 6 cm	Greiner bio-one	628160
Cellstar 6-well cell culture plate	Greiner bio-one	657160
Cellstar 12-well cell culture plate	Greiner bio-one	665180
Cellstar 24-well cell culture plate	Greiner bio-one	662160
Cellstar 96-well cell culture plate	Greiner bio-one	655180
Coverslips	Menzel GmbH & Co. KG	631-1580
10 µl pipette filter tips	Starlab	S1121-3810
200 µl pipette filter tips	Starlab	S1120-8810
1000 µl pipette filter tips	Starlab	S1126-7810
5 ml serological pipette	Greiner bio-one	606180
10 ml serological pipette	Greiner bio-one	607180
25 ml serological pipette	Greiner bio-one	760180
50 ml serological pipette	Greiner bio-one	768160
Kimwipes-Science	Roth	AA63.1
1.5 ml microcentrifuge tubes	Eppendorf AG	0030120086
2.0 ml microcentrifuge tubes	Eppendorf AG	0030120094
200 µl PCR tubes	Eppendorf AG	72.737.002
Petri dish	BD Biosciences	351058
Superfrost® plus microscope Slides	Menzel GmbH & Co. KG	6310108

Equipment

Machine Name	Company
Axio Observer. Z1(invers)	Carl Zeiss
Centrifuge 3K12	Sigma
Centrifuge 5804R	Eppendorf AG
Centrifuge 5415D	Eppendorf AG
Disperser T10 basic Package	IKA®-Werke GmbH & Co. KG
Fusion Solo	PeqLab (VWR)
GelIX Imager	INTAS
GeneAmp® PCR System 9700	Thermo Fisher Scientific
HERAcell® 240 Incubator	Heraeus
Hera safe	Heraeus
Mastercycler personal	Eppendorf AG
Mini-PROTEAN® 3 Cell	Bio-Rad Laboratories GmbH
Mini-Sub® Cell GT	Bio-Rad Laboratories GmbH

Mini Trans-Blot® Electrophoretic Transfer Cell	Bio-Rad Laboratories GmbH
Trans-Blot® Turbo™ Transfer System	Bio-Rad Laboratories GmbH
NanoDrop® Spectrophotometer ND-1000	PEQLAB Biotechnology GmbH
Peqstar Light cycler	Peqlab
pH-Meter 766 calimatic	Knick
Pipettes	Eppendorf AG
Power Supply EV245	Consort
PowerPac Basic	Bio-Rad
Real Time machine 7900HT Sequence Detection System	Applied Biosystems
Shaker Certomat HK	B. Braun Biotech international
Table-cool centrifuge	Eppendorf AG
Tecan Infinite M200 microplate reader	TECAN Group Ltd.
Vortexer Reax 2000	Heidolph
Water bath Certomat WR	B. Braun
Water system ELGA	Millipore
StainTray 10 Place	newscomersupply
StainTray 20 Place	newscomersupply
Microtome	Leica

2.2 Methods

2.2.1 Cell culture

All cell lines used (HEK293T, SW480 and HCT116) sourced from American Type Culture Collection (ATCC, Manassas, VA) were subjected to culture in DMEM (Gibco, US) blended with 10% FBS (Gibco) and 1% Penicillin-Streptomycin (PS) (Gibco, US) in an incubator device with controlled humidity containing with 5% CO₂ at 37°C (all from Thermo Fisher Scientific, Waltham, MA).

2.2.2 Immunocytochemistry (IHC)

Prior to use, all samples were fixed in 4% paraformaldehyde (PFA) (w/v) overnight, were then embedded in paraffin and dried on Superfrost slides (Menzel GmbH & Co. KG, Bielefeld, DE). Before starting the IHC procedure, the slides underwent a one-hour incubation at 37°C for drying. For antigen retrieval, a citrate solution (1:100 in dH₂O, pH 9) was heated in a steamer for 40 minutes, followed by a 20-minute cooling, subsequent to dewaxing and rehydration. Subsequently, the slides were blocked with

goat serum (Ab7481, Abcam, Cambridge, UK) and subjected to 3% H₂O₂ treatment to suppress peroxidase activity. Slides were subjected to overnight incubation with non-phosphorylated β -catenin (19807S, CST, Danvers, USA) at a dilution of 1:200. Following PBS washes, the slides were treated with a biotinylated goat anti-rabbit Ab (1:500) for 30 minutes. Subsequent steps involved a 30-min incubation with the ABC solution at room temperature (RT), followed by exposure to the DAB solution. The reaction was halted with dH₂O and slides underwent counterstaining with hematoxylin and were then covered with a mounting medium and sealed with a cover slip. The information on the use of antibodies is listed in Table 7.

Table 7: Antibodies dilution

Antibody	Order Number	Dilution ratio	Company
phosphorylated β -catenin	19807S	1:200	CST
biotinylated goat anti-rabbit antibody	BA-5000-1.5	1:500	Vector Laboratories

2.2.3 Plasmid DNA purification

Plasmid DNA purification methods were implemented following the guidelines provided by the Qiagen midi prep kit (12143, Qiagen, Hilden, DE).

2.2.4 Co-immunoprecipitation (Co-IP)

Confluent monolayers of three distinct cell lines (HEK293T, SW480 and HCT116) were disrupted through treatment with a hypotonic lysis buffer devoid of detergents. This hypotonic lysis buffer comprised 20 mM Tris-HCl (pH 7.4), 2 mM EDTA, 2 mM MgCl₂, 1 mM Na₃VO₄, and 1x protease inhibitor cocktail (4693124001, Roche, Basel, Switzerland). Co-IP was conducted using Protein G Plus/Protein A Agarose Suspension (IP05, Merk Millipore, Darmstadt, DE). Antibodies utilized in the process included Pan RAS (Sc-166691, Santa Cruz, Texas, USA), β -catenin (8480S, CST, Danvers, USA), and MTMR7 (MBS9406043, MybioSource, Eching, DE). Following an overnight Ab incubation at 4 °C, two rounds of soft bead washing (with the hypotonic lysis buffer) were performed before preparation of the SDS-PAGE. Protein expression was detected by Western blotting, and the chemiluminescence signals were visualized using ECL (A38554, Thermo Fisher Scientific, Karlsruhe, DE). The information on the use of antibodies is listed in Table 8 and Table 9.

Table 8: Antibodies for Co-IP

Antibody	Order Number	Total antibodies level per well	Company
Pan RAS	Sc-166691	10 μ g	CST
β -catenin	8480S	10 μ g	CST
MTMR7	MBS9406043	10 μ g	MybioSource

Table 9: Antibodies dilution

Antibody	Dilution ratio
1 st antibody	1:1000
2 nd antibody	1:2000

2.2.5 Immunoprecipitation (IP)

To detect Ubiquitin by Immunoblotting, HEK293T cells were seeded in 10 cm dishes and transfected with empty vector (EV)+ubiquitin-HA or MTMR7-FL+ubiquitin-HA plasmids overnight. After 72 hours, cell disruption was carried out using a hypotonic lysis buffer comprising 20 mM Tris-HCl (pH 7.4), 2 mM EDTA, 2 mM MgCl₂, 1 mM Na₃VO₄, and 1x protease inhibitor cocktail (4693124001, Roche, Basel, Switzerland). IP was executed using Protein G Plus/Protein A Agarose Suspension (IP05, Merk Millipore, Darmstadt, DE). The antibodies employed encompassed Pan RAS (Sc-166691, Santa Cruz, Texas, USA), β -catenin (8480S, CST, Danvers, USA), and HA-tag (3724S, CST, Danvers, USA). Following an overnight Ab incubation at 4 °C, two rounds of bead washing (using hypotonic lysis buffer + 150 mM NaCl + 0.1% Triton X-100) and two cycles of bead washing (using 500 mM LiCl) were performed before preparation of the SDS-PAGE. Protein expression was detected by Western blotting, and the chemiluminescence signals were visualized using ECL (A38554, Thermo Fisher Scientific, Karlsruhe, DE). The information on the use of antibodies is listed in Table 10 and Table 11.

Table 10: Antibodies for IP

Antibody	Order Number	Total antibodies level per well	Company
Pan RAS	Sc-166691	10 μ g	CST
β -catenin	8480S	10 μ g	CST
HA-tag	3724S	10 μ g	CST

Table 11: Antibodies dilution

Antibody	Dilution ratio
1 st antibody	1:1000
2 nd antibody	1:2000

2.2.6 Cell transfection and drug treatments

For transient transfection of adherent cells, HEK293T, SW480, and HCT116 cells were seeded at 5×10^5 cells/ well in 6-well plates or 4×10^6 cells/ dish in 10 cm culture dishes with complete DMEM medium and were grown overnight. For the ubiquitination experiment, the cells were co-transfected with MTMR7 or EV and pRK5-HA-Ubiquitin-WT using Turbofect® transfection reagent (R0532, Thermo Fisher Scientific, Karlsruhe, DE) overnight in serum-free DMEM. For drug treatment, the drugs were diluted in complete DMEM and added to the plates 48 hours after transfection. Following a 24-hour incubation with the drugs, cells were harvested, and the transfection efficiency along with protein expressions were analyzed by Western blotting.

2.2.7 Luciferase Reporter gene assay

The dual luciferase reporter gene detection system was employed to measure the direct effect of MTMR7 on the β -catenin reporter gene plasmid.

In summary, HEK293T, SW480, and HCT116 cells were co-transfected with MTMR7 or EV and the β -catenin reporter gene plasmid. After an overnight transfection, the medium was substituted with complete DMEM, and cells were left to recover for 24 hours. For drug treatment, a panel of pharmacological agents were diluted in complete DMEM and plated on the cells 48 hours after they were transfected. After a 24-hour incubation with the drugs, luciferase activity was quantified utilizing the dual-luciferase reporter assay (Promega, USA). TCF activity was assessed employing a multi-mode microplate reader (Tecan, Switzerland).

2.2.8 Reverse transcription (RT) PCR and real-time quantitative PCR (qPCR)

Total RNA was isolated with the RNeasy Mini kit (Qiagen, Hilden, DE), and reverse transcription was carried out employing the Verso cDNA Synthesis Kit (AB1453B, Thermo Fisher Scientific). Subsequently, real-time quantitative PCR (RT-qPCR) was executed employing SYBR™ Green PCR Master Mix (4385610, Thermo Fisher Scientific). Table 7 lists the reagents that comprised the reaction mix for one single sample. The PCR reaction program started with an initial denaturation at 95 °C for 5 min, followed by 45 cycles of 95 °C for 5 s, 60 °C for 30 s, and 72 °C for 10 s. A negative control reaction lacking cDNA template was incorporated. Relative quantification of the reference genes *β 2-microglobulin (B2m)*, *Axin2*, *Ephb*, *Lgr5*, and *Asclc* [78], and the $2^{-\Delta\Delta CT}$ method was utilized for data analysis [79].

Table 12: RT-qPCR

Reagent (per well)	Volume (per well, μ L)
SYBR™ Green PCR Master Mix	10
Primer (Forward) 10 μ M	1
Primer (Reverse) 10 μ M	1
cDNA	2
dH ₂ O	6

2.2.9 Immunofluorescence (IF)

The standard IF protocol involved the following steps. First, cells on coverslips underwent a PBS wash, followed by fixation with 4% PFA (w/v) at RT for 20 minutes, and subsequent permeabilization with 0.1% Triton X-100 in PBS for 10 minutes. To prevent nonspecific binding, a 20-minute incubation with 100% FBS at RT was carried out. Overnight incubation at 4°C followed, utilizing antibodies which were listed in below. After three PBS washes, coverslips were exposed to Alexa Fluor 594-conjugated donkey anti-goat IgG (1:200, Invitrogen; RRID: AB_141359) and Alexa Fluor 488-conjugated goat antirabbit IgG (1:200, Invitrogen; RRID: AB_141607). DAPI (Sigma-Aldrich) was used for nuclei staining. Image capture was performed using a

Zeiss Microscope (Axio Observer.Z1/Apotome, inverted). The information on the use of antibodies is listed in Table 13 and Table 14.

Table 13: Antibodies for IF

Immunofluorescence (IF)			
Application	Clone (Add-Ons)	Cat. No.	Company
Pan-RAS	Mouse IgG	Sc-166691	Santa Cruz
β -catenin	Rabbit IgG	8480S	CST
Non-phosphorylated β -catenin	Rabbit IgG	19807S	CST
Phalloidin	Alexa Fluor 488	A12381	Invitrogen
Streptavidin	Alexa Fluor 594	S11227	Invitrogen
DAPI		D1306	Invitrogen
Alexa Fluor 594	Donkey anti-rabbit	A21207	CST
Alexa Fluor 488	Donkey anti-mouse	A21206	CST
Mounting buffer		GM304	DAKO

Table 14: Antibodies dilution

Antibodies	Dilution ratio
Pan-RAS	1:250
β -catenin	1:250
Non-phosphorylated β -catenin	1:250
Phalloidin	1:1000
Streptavidin	1:1000
DAPI	1:20000
Alexa Fluor 594	1:1000
Alexa Fluor 488	1:1000

2.2.10 Proximity Ligation Assays (PLA)

In situ Proximity Ligation Assay (PLA) was conducted with a Duolink II In Situ Red Starter Kit Mouse/Rabbit (Sigma-Aldrich) following instructions provided by the manufacturer. HEK293T/SW480 cells were cultured on collagen-coated coverslips in Chamber Slides, followed by fixation, permeabilization, blocking, and overnight incubation with anti-Pan-RAS monoclonal and anti-MTMR7 antibodies. The information on the use of antibodies is listed in Table 15 and Table 16.

Table 15: Antibodies for PLA

Proximity Ligation Assay (PLA)			
Application	Clone (Add-Ons)	Cat. No.	Company
Pan-RAS	Mouse IgG	Sc-166691	Santa Cruz
β -catenin	Rabbit IgG	8480S	CST
Non-phospho β -catenin	Rabbit IgG	19807S	CST
Phalloidin	Alexa 488	A12381	Invitrogen
DAPI		D1306	Invitrogen
Duolink® in Situ PLA		DUO92101	Olink Bioscience
Alexa Fluor 594	Donkey anti-rabbit	A21207	CST
Alexa Fluor 488	Donkey anti-mouse	A21206	CST
Mounting buffer		GM304	DAKO

Table 16: Antibodies dilution

Antibody	Dilution ratio
Pan-RAS	1:250
β -catenin	1:250
Non-phosphorylated β -catenin	1:250
Phalloidin	1:1000
Streptavidin	1:1000
DAPI	1:20000
Alexa Fluor 594	1:1000
Alexa Fluor 488	1:1000

Duolink anti-rabbit PLUS and anti-mouse MINUS secondary antibodies, along with red detection reagents, were subsequently employed. The antibodies incubation, ligation, amplification, and washing were executed as given by the instruction manual. Finally, coverslips were mounted using Duolink Mounting Media with DAPI for visualization of the nuclei. Images were captured by microscopy (Zeiss Microscope Light, Axio Observer.Z1/Apotome, inverted).

2.2.11 Cellular peptide uptake

To investigate cellular uptake, we utilized the MTMR7 peptide which had been biotinylated and myristoylated at the N-terminus. The peptide was dissolved in DMSO, aliquoted, and stored at -20°C. The SW480/HT29 cells were seeded (5×10^4 cells/mL) in μ -Slide 8 Well chambers (ibidi GmbH, DE) and grown to subconfluency for 1 day. Following fixation with 4% PFA for 20 min, cells were subjected to thrice mild PBS washings, 10-min permeabilization using 0.1% Triton X-100, and another thrice washings with mild PBS. To block non-specific binding, FBS was utilized for a 20-min incubation at RT, followed by sequential staining with fluorescent streptavidin conjugates, phalloidin, and DAPI. Finally, image capture was conducted by microscopy (Zeiss Microscope Light, Axio Observer.Z1/Apotome, inverted). The information on the use of antibodies information is listed in Table 17.

Table 17: Antibodies dilution

Antibody	Dilution ratio
Streptavidin	1:1000
Phalloidin	1:1000
DAPI	1:20000

2.2.12 Western blotting

Cells underwent washing with ice-cold PBS before being lysed in SDS lysis buffer comprising 2% SDS, 10 mM Tris (pH 7.4), 150 mM NaCl, 10 mM EDTA, 10% Glycerol, protease inhibitor cocktail (Sigma-Aldrich). Then, 25-50 μ g cell lysates of protein sample were loaded into a 10% SDS-PAGE gel (Table 10) and subsequently transferred onto a nitrocellulose membrane (Whatman). After a 1-hour block with 5% skim milk in PBST at RT, the membranes underwent incubation overnight with the specified first Ab, followed by a 1-hour incubation with the secondary Ab at RT. Protein expression was then for detection of chemiluminescence visualized using ECL (A38554, Thermo Fisher Scientific, Karlsruhe, DE). The information on the use of antibodies is listed in Table 18-20.

Table 18: SDS-PAGE

Components	Separating gels (10%)	Stacking gels (4%)
H ₂ O	32.9 ml	14.4 ml
Acrylamide 30 (29:1)	28 ml	3.33 ml
Tris-HCl 1.5M, pH 8.8	21 ml	-
Tris-HCl 0.5M, pH 6.8	-	6.25 μ l
SDS 10%	830 μ l	250 μ l
APS 10%	840 μ l	250 μ l
TEMED	46 μ l	50 μ l

Table 19: Antibodies for Western blotting

Application	Clone (Add-Ons)	Cat. No.	Company
Western blotting (WB)			
Axin1	Rabbit IgG	2087S	CST
Axin2	Rabbit IgG	2151S	CST
MTMR7	Rabbit IgG	MBS9406043	Mybiosource
MTMR7	Rabbit IgG	PA5-113535	Invitrogen
MTMR7	Rabbit IgG	25990-1-AP	Proteintech
ERK1/2	Rabbit IgG	9102S	CST
β -catenin	Rabbit IgG	8480S	CST
Phospho β -catenin	Rabbit IgG	9565S	CST
Non- phosphorylated β -catenin	Rabbit IgG	19807S	CST
GSK3b	Rabbit IgG	12456S	CST
Phospho GSK3b	Rabbit IgG	9332S	CST
Pan-RAS	Mouse IgG	Sc-166691	Santa Cruz
K-RAS	Rabbit IgG	415700	CST
HSP90	Mouse IgG	sc-13119	Santa Cruz
β actin	Mouse IgG	sc-47778	Santa Cruz
Anti-HA	Rabbit IgG	3724S	CST
Cortactin	Rabbit IgG	3503S	CST
GAPDH	Mouse IgG	sc-47724	Santa Cruz
Lamin A/C	Rabbit IgG	sc-7292	Santa Cruz
Anti-rabbit IgG	Goat IgG	7074	CST
Anti-mouse IgG	Horse IgG	7076	CST

Table 20: Antibodies dilution

Antibody	Dilution ratio
1 st antibody	1:1000
2 nd antibody	1:2000

2.3 Ethics statement

Animal studies adhered to the ethical guidelines of the University of Heidelberg and obtained approval from the government of Baden-Württemberg, Karlsruhe (G-188/18)[69].

2.4 Statistics and software

Statistical analyses utilized Prism version 10 (GraphPad, LA Jolla, CA). Continuous variables were presented as means \pm S.E. Protein expression levels were quantitatively assessed through densitometric analysis of Western blot bands, captured using an imaging device (Fusion solo, VWR). For quantification, the optical density (OD) values of the protein bands were measured employing ImageJ software (<https://imagej.net/ij/>). Normalization was performed against the housekeeping protein HSP90, serving as an internal control. This approach corrected for potential variations in sample loading and transfer efficiency. Comparative analysis was conducted between the experimental groups and the control group, e.g. the EV+DMSO group, to quantify relative protein expression levels. Statistical significance was determined based on data aggregated from a minimum of three independent experiments. Initially, data were tested for Gauss normal distribution. Those conforming to a parametric (Gauss normal) distribution were analyzed by Student's t-test or one-way ANOVA. Non-parametric data were analyzed using the Mann-Whitney test, Wilcoxon signed-rank test and Kruskal-Wallis test. Two-way ANOVA was applied for multivariate data. All p-values < 0.05 were considered significant.

3 Results

3.1 Overexpression of MTMR7 in HEK293T cells.

HEK293T cells, characterized by their low endogenous MTMR7 expression, were chosen as a non-cancerous model to evaluate the efficacy of MTMR7 overexpression. The determination of this efficacy facilitated a precise delineation of the effects attributable to the overexpression of exogenous MTMR7.

Five distinct transfection groups were established in HEK293T cells: empty vector (EV), MTMR7-GFP, MTMR7, EV-GFP, and a group utilizing mouse brain tissue, serving as a positive control to validate the overexpression of MTMR7.

At 72 hours post-transfection, cellular proteins were harvested employing SDS lysis buffer and subjected to analysis via Western blotting (Figure 11). In the EV group transfected with PUC19 as EV control, no MTMR7 expression was discernible. Transfection with EV-GFP and MTMR7-GFP was implemented as a positive control to assess transfection efficacy and non-specific binding on the Western blot membranes.

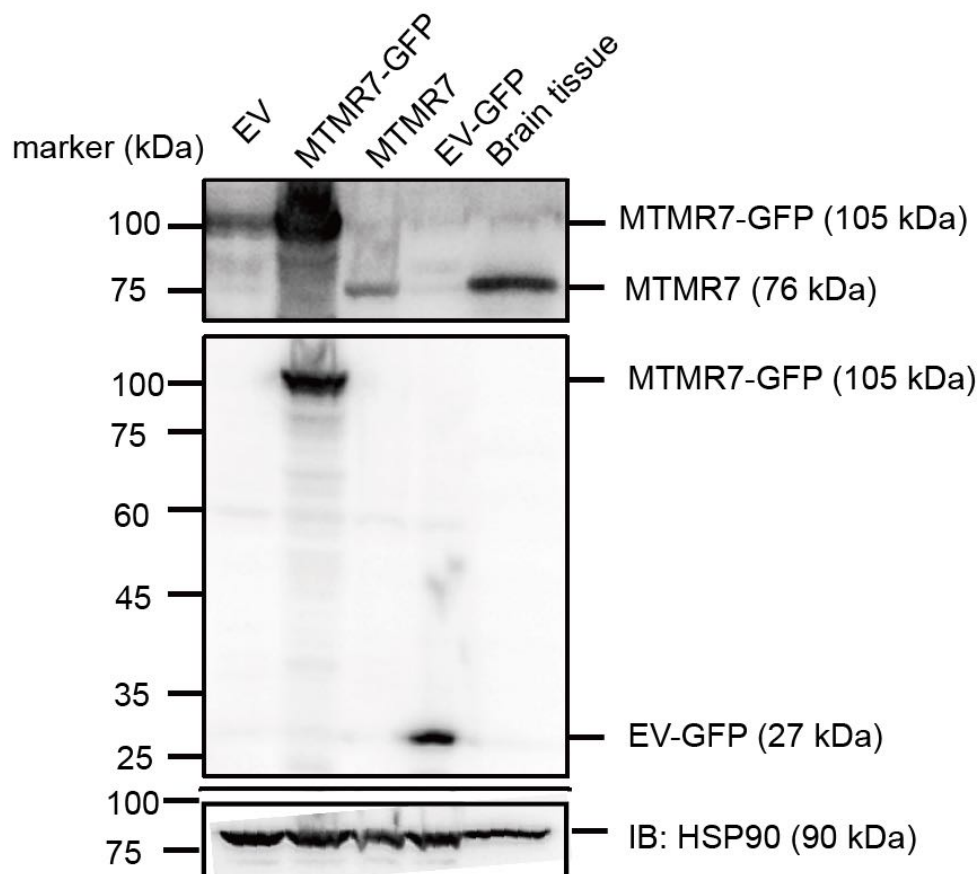


Figure 11. Overexpression of MTMR7 in HEK293T cells.

HEK293T cells were seeded at 4×10^6 cells per/dish (10 cm) in complete DMEM medium for overnight. Subsequently, the adherent cells underwent transient transfection with either EV, MTMR7, MTMR7-GFP or EV-GFP plasmid, respectively. Turbofect transfection reagent was used in a serum-free DMEM. At 72 hours post-transfection, the cells were harvested, followed by protein lysate extraction and SDS-PAGE analysis. Western blot was conducted to examine the protein expression. Presented here are representative Western blot images derived from three independent experiments ($n=3$).

3.2 *In vitro* analysis of WNT signaling after MTMR7 overexpression.

3.2.1 MTMR7 reduces TCF/LEF-dependent transcription.

To elucidate the effect of MTMR7 on TCF/LEF-mediated transcription, a luciferase reporter assay utilizing three distinct cell lines was conducted: HEK293T, SW480, and HCT116. These cells were co-transfected with a TCF/LEF driven reporter plasmid (TOP-FLASH) and with either EV or MTMR7 expression plasmid for a 24-hour period under serum-free conditions. Additionally, to further dissect the pathway, cells were treated with a panel of pharmacological agents (Table 21): DMSO served as a vehicle control, XAV939 (10 μ M), SAR405 (1 μ M), MG132 (3 μ M), and Chir99021 (Chir, 10 μ M) were utilized (Figure 12).

Table 21. Pharmacological agents

Pharmacological agents	Concentration	Therapeutic target
XAV939	10 μ M	Tankyrase inhibitor (inhibits WNT signaling)
SAR405	10 μ M	PIK3C/Vps inhibitor (potentially inhibits WNT signaling)
MG132	3 μ M	Proteasome inhibitor (potentially activates WNT signaling)
Chir99021	10 μ M	GSK3 α/β inhibitor (activates WNT signaling)

Transfection with MTMR7 led to suppression of TCF/LEF-driven transcription across all cell models, highlighting the potent inhibitory role of MTMR7 in this context. The use of DMSO as a vehicle control for the pharmacological inhibitors further validated the specific downregulation of TCF/LEF activity following MTMR7 overexpression [80].

The analysis was extended to evaluate the impact of XAV939, a tankyrase inhibitor known to impede the WNT signaling pathway [80], and SAR405, a PIK3C/Vps inhibitor with potential effects on WNT signaling [81]. Additionally, the proteasome inhibitor MG132 was considered to enhance WNT signaling by stabilization of β -catenin [82,83]. Conversely, Chir was employed as a benchmark activator of WNT signaling due to its specificity regarding inhibition of GSK3 [84,85].

Treatment with SAR405 resulted in inhibition of TCF/LEF-mediated transcription in HEK293T, SW480, and HCT116 cell lines, underscoring the efficacy of this compound in suppressing TCF/LEF-dependent transcription. Particularly noteworthy, SAR405 treatment in HCT116 cells elicited a significant decrease in luciferase activity, with an observed reduction of approximately 85% (EV + DMSO vs. EV + SAR405). However, XAV939 and MG132 did not reach statistical significance.

Chir significantly enhanced TCF-LEF transcriptional activity by inhibiting GSK3, thereby activating the WNT signaling pathway. We observed a marked increase (approx. 100-fold) in expression when comparing HCT116+EV+DMSO vs. HCT116+EV+Chir. Remarkably, even in the presence of WNT pathway activation induced by Chir, MTMR7 consistently exhibited an inhibitory effect on the pathway across all tested cell lines. Specifically, we observed a reduction of approximately 85% in HCT116 cell line (EV + Chir vs. MTMR7 + Chir), demonstrating a statistically significant difference. Collectively, our findings affirm the inhibitory influence of MTMR7 on TCF/LEF transcriptional activity, extending across APC-mutant cell lines (SW480

and HCT116) and the non-malignant cell line (HEK293T). This underscores the broad regulatory role of MTMR7 in modulating WNT/ β -catenin signaling.

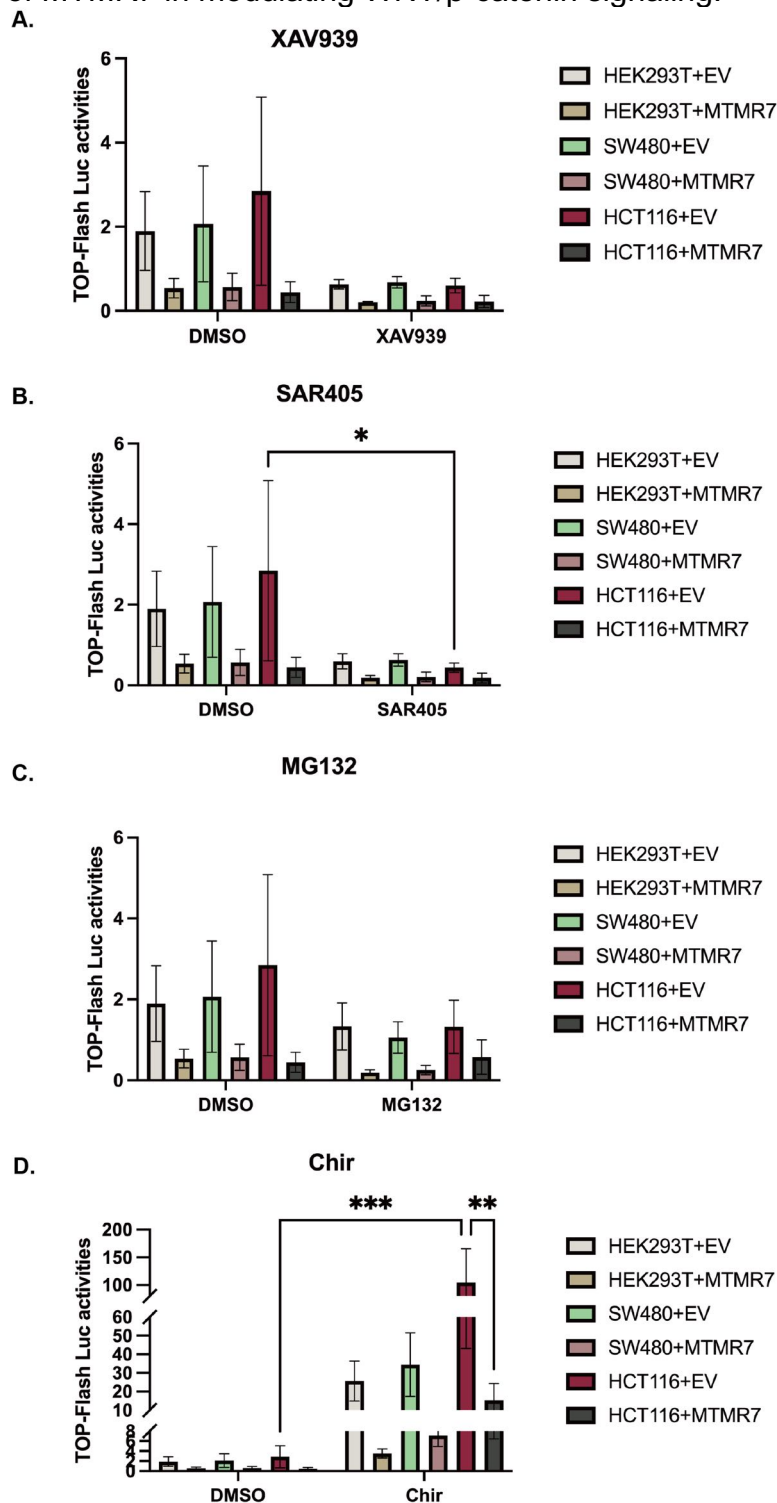


Figure 12. MTMR7 reduces the transcriptional response of TCF/LEF.

Three different cell lines were co-transfected with a TCF/LEF reporter plasmid and either MTMR7 or an EV control for 24 hours. Subsequently, the cells were exposed to pharmacological agents for an additional 24-hour period: **A.** XAV939 (10 μ M), **B.** SAR405 (1 μ M), **C.** MG132 (3 μ M), **D.** Chir (10 μ M), with equal volumes of DMSO serving as the vehicle control. The luciferase activity, assessed in total cell lysates, was normalized to protein content, and presented as -fold \pm S.E. based on three independent experiments. (n=3; * p <0.05 HCT116 + EV + DMSO vs. HCT116 + EV + SAR405; ** P <0.01 HCT116 + EV + Chir vs. HCT116 + MTMR7 + Chir; *** P <0.005 HCT116 + EV + DMSO vs. HCT116 + EV + Chir; Two-way ANOVA followed by Bonferroni's multiple comparisons).

3.2.2 MTMR7 and KYA1797K inhibit the transcriptional response of TCF/LEF.

Previous investigations have demonstrated that KY1220 effectively inhibits the WNT pathway through the destabilization of β -catenin and RAS. Moreover, KYA1797K, a derivative of KY1220, activates the β -catenin destruction complex and facilitates RAS degradation. Hence, KYA1797K serves as a potent and selective antagonist of the WNT signaling cascade with significant therapeutic potential in CRC [74,86,87].

To assess and compare the inhibitory effects of KYA1797K and MTMR7 on TCF/LEF transcriptional activity *in vitro*, luciferase assays were implemented for the assessment of concentration-dependent effects. In Figure 13, MTMR7 exhibits a stronger inhibitory effect on the WNT pathway compared to KYA1797K. KYA1797K demonstrated inhibitory effects on TCF/LEF activity at concentrations exceeding 60 μ M to 100 μ M. Meanwhile, MTMR7 independently suppressed TCF/LEF activity in both control conditions using medium alone or DMSO as vehicle. Under DMSO conditions, transfection with MTMR7 resulted in an 86% decrease in luciferase activities relative to the EV control, strongly indicating that MTMR7 significantly downregulated the transcription levels of TCF/LEF without the involvement of KYA1797K.

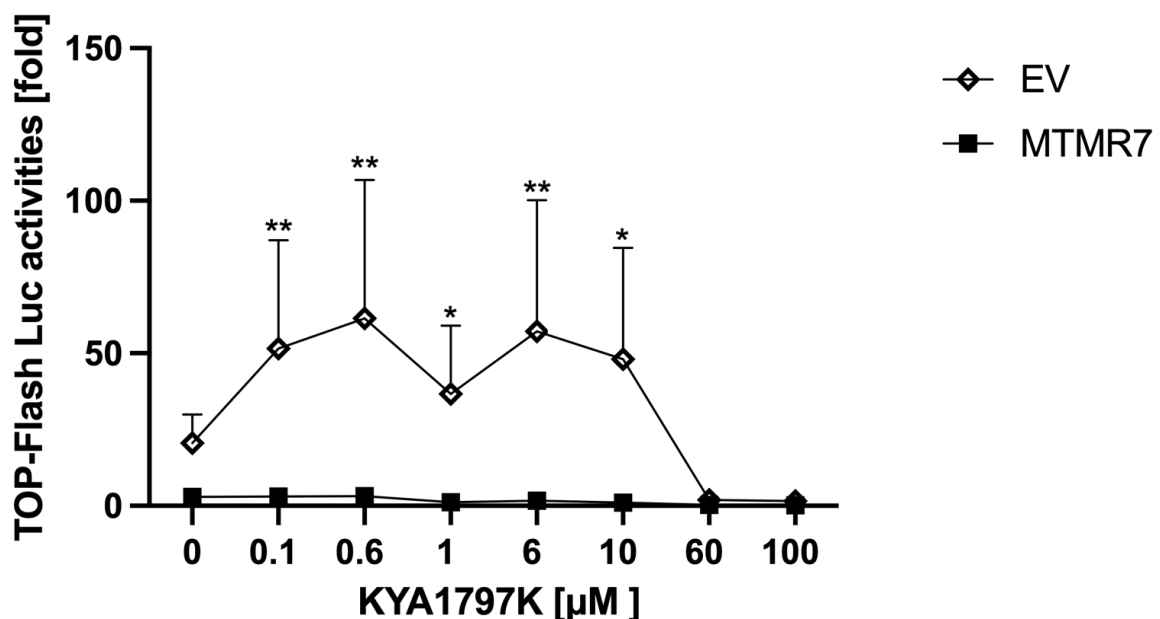


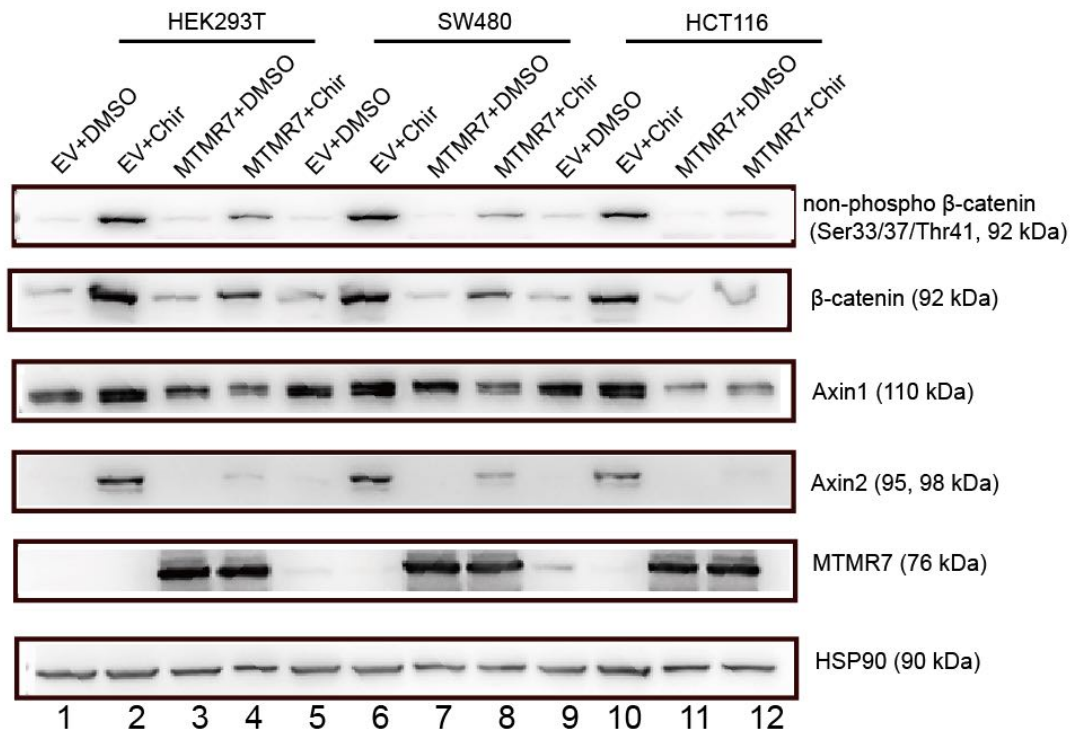
Figure 13. MTMR7 overexpression abrogates TCF/LEF transcription similar to high concentrations of KYA1797K.

SW480 cells were co-transfected with TCF/LEF reporter plasmid and either MTMR7 or an EV control for 24 hours. Following transfection, cells were treated with different concentrations of KYA1797K, ranging from 0.1 μ M to 100 μ M, as well as DMSO (KYA1797K = 0 μ M). Luciferase activity in total cell lysates was normalized to protein content and presented as -fold \pm S.E. (n=3; * P <0.05; ** P <0.01; Two-way ANOVA followed by Bonferroni's multiple comparisons).

3.2.3 MTMR7 inhibits WNT signaling in presence of GSK3i.

To further elucidate the effect of MTMR7 on the WNT signaling on the protein level, Western blotting was performed on protein lysate extracted from three distinct cell lines: HEK293T, SW480, and HCT116. Our findings from Figure 14A demonstrate that MTMR7 transfection combined with GSK3i treatment (MTMR7+Chir) decreased the levels of non-phosphorylated β -catenin level compared to the EV + Chir group. Conversely, in the absence of GSK3i treatment, MTMR7 overexpression (MTMR7 + DMSO) did not exhibit a considerable difference from the EV controls (EV + DMSO) due to overall low β -catenin expression.

A.



B.

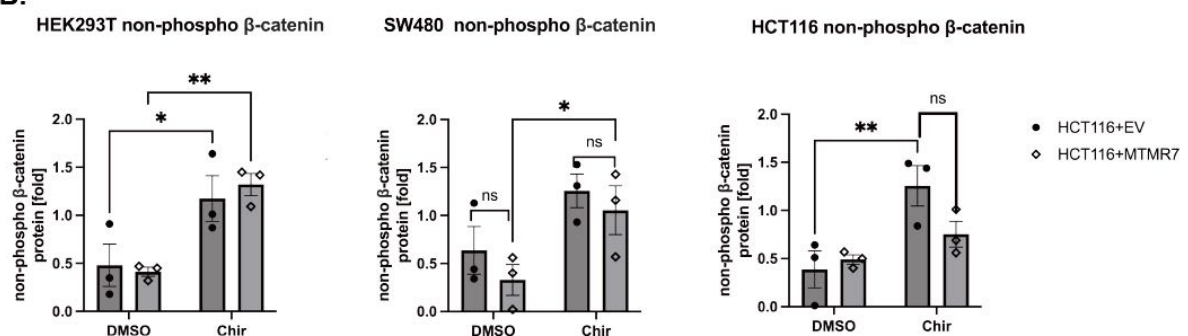


Figure 14. Changes of β -catenin protein upon MTMR7 overexpression in the presence of GSK3i.

A. HEK293T, SW480, and HCT116 were transiently transfected with either MTMR7 or EV control and incubated overnight in serum-free medium, followed by the treatment with Chir (10 μ M) or an equivalent volume of DMSO for 24 hours. Subsequently, the cells were harvested, and protein lysates were extracted for SDS-PAGE analysis. Western blot analysis was performed to evaluate the expression levels of the respective proteins. Presented here are representative Western blot images derived from three independent experiments (n=3). **B.** Quantitative analyses of Western blots from total lysates are depicted. O.D. values of bands were normalized to HSP90 and presented as -fold \pm S.E. (n=3 independent cell passages, * P <0.05; ** P <0.01; Two-way ANOVA followed by Bonferroni's multiple comparisons)

3.3 *In vivo* analysis of WNT signaling after MTMR7 peptide treatment.

3.3.1 Therapy of *APC*^{min/+} and SV40-Tag mice.

For previous experiments, we developed and characterized a peptide mimicking the effect of MTMR7 with regard to the activation of PPAR γ *in vitro* and *in vivo* [69]. The same peptide (MT) alongside with a scrambled control peptide (SC) and a vehicle control (VC) were used in these experiments. The characteristics and efficacy of these peptides are comprehensively outlined in Figure 7E and have been documented in our previously published work [69].

For the *in vivo* studies, two genetically modified murine cancer models were employed: C57BL6/J mice harboring the pCEA-SV40-Tag transgene and *APC*^{min/+} mice, both approximately 2 months of age [88,89]. Two peptides, MT and SC, were solubilized in a sterile solution of DMSO and PBS. This solution was administered intraperitoneally at a consistent dosage of 30 mg/kg, four times per week for a total of 2 weeks. The vehicle control (VC) received only DMSO and PBS. The experimental design, including the VC (4 mice), MT (8 mice), and SC (8 mice) groups, is depicted in Figure 15, which illustrates the specific treatments administered to each group.

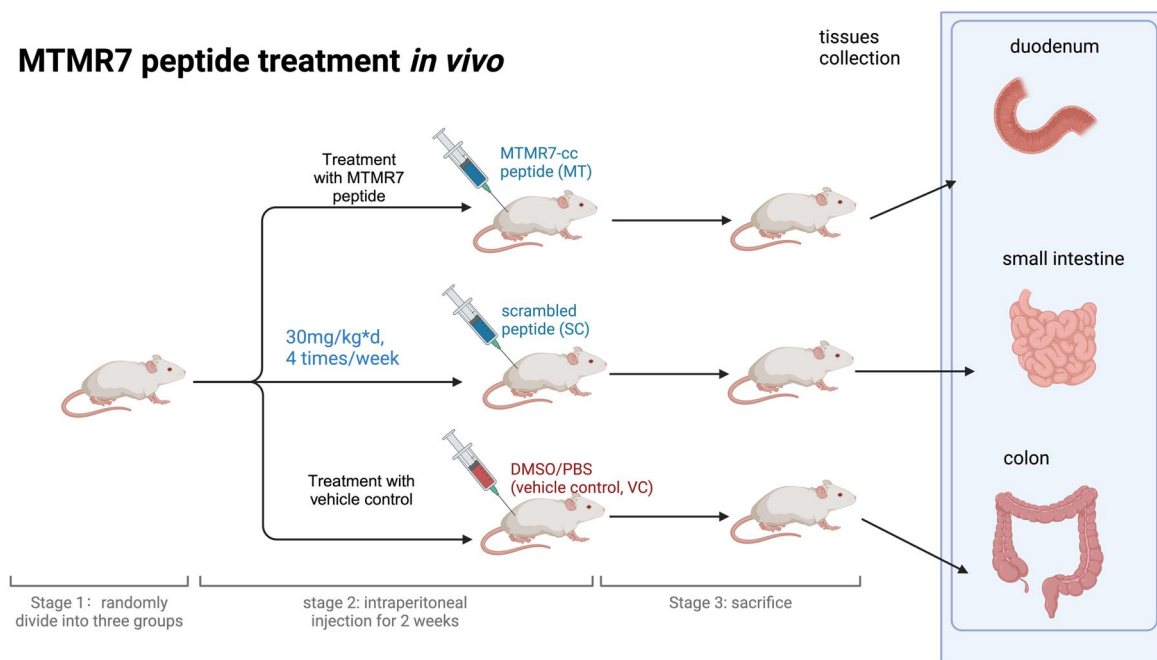


Figure 15. Schematic diagram of MTMR7 peptide treatment *in vivo*.

Therapeutic interventions were administered to *APC*^{min/+} and SV40-Tag transgenic mice, which had been previously randomized across three distinct treatment cohorts. The schematic representation of the treatment allocation and experimental design was crafted using the BioRender application (<https://www.biorender.com/>).

3.3.2 MTMR7 peptide inhibits WNT signaling *in vivo*.

The canonical WNT signaling pathway promotes CRC progression. β -catenin, a central effector molecule within this pathway, activates the downstream transcriptional response of WNT-signaling. Dysregulation of its intracytoplasmic degradation results in its accumulation in the nucleus, enabling target gene transcription, thereby facilitating tumorigenesis [78,90]. This mechanism entails the relocation of β -catenin from the cytoplasm to the nucleus, where it engages with transcription factors such as TCF/LEF, leading to the upregulation of WNT target genes. Therefore, the subcellular distribution of β -catenin serves as a surrogate marker for active WNT signaling [91,92].

To assess the impact of MT peptide treatment on WNT signaling, immunohistochemical staining (IHC) of gastric tumor and duodenal tissues obtained from SV40-Tag mice was conducted. This enabled us to monitor alterations in the expression and localization of non-phosphorylated (active) β -catenin. Following treatment, a marked decrease in the nuclear fraction of non-phosphorylated β -catenin expression was identified within the tumor tissues, with a similar trend observed in the stained duodenal sections (Figure 16A). Subsequently, the nucleus-to-cytoplasm ratio in non-phosphorylated β -catenin-positive cells was quantified. Figure 16B and 16C depict stained sections of tumor tissues and duodenal tissues, respectively. Our analysis revealed a robust reduction in the fraction of nuclear non-phosphorylated β -catenin across all mice following MTMR7 peptide treatment.

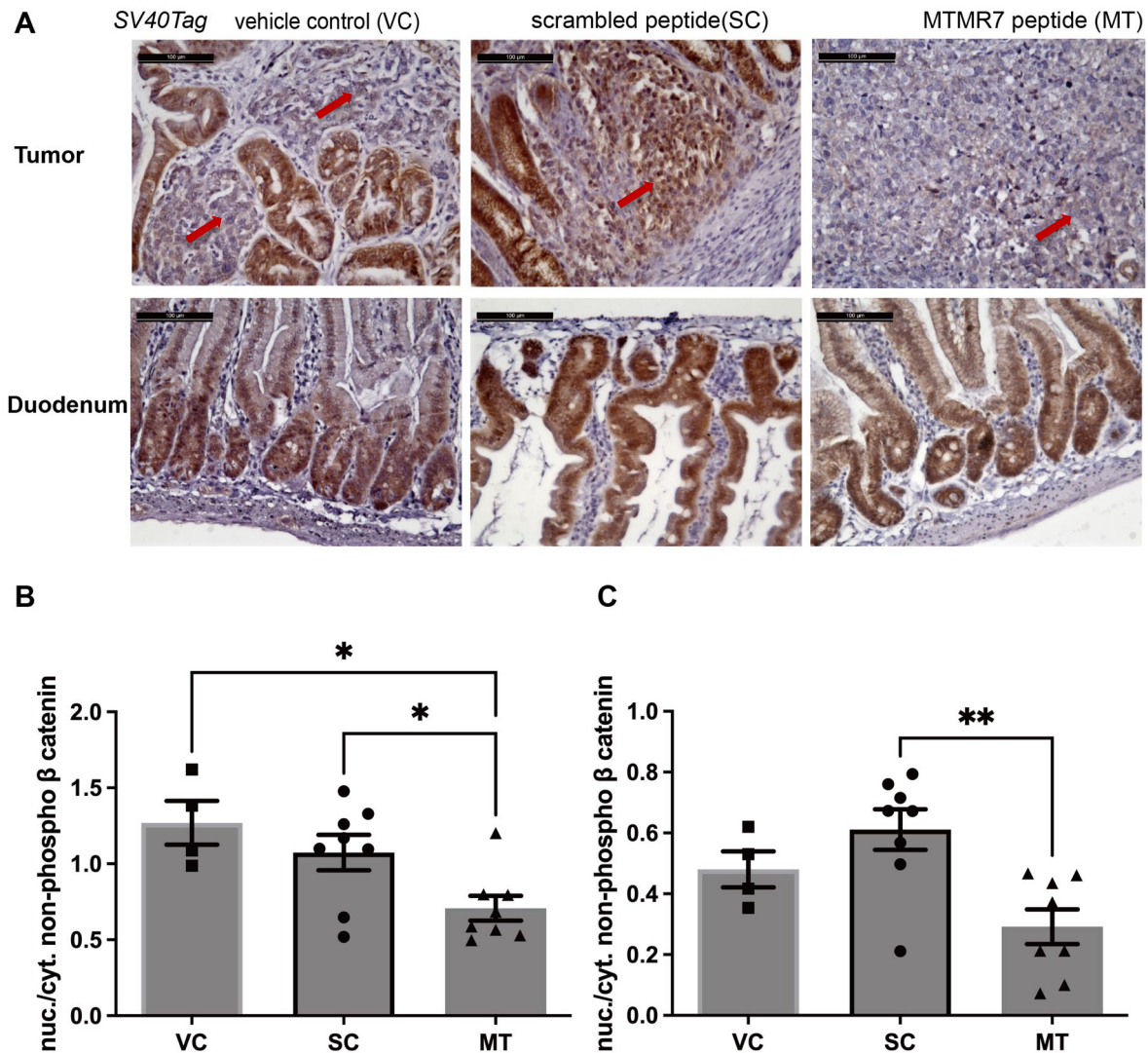


Figure 16. IHC analysis of non-phosphorylated β -catenin following MTMR7 peptide treatment.

A. IHC analysis of non-phosphorylated β catenin (cat:19807S) in gastric tumor and duodenal tissues derived from SV40-Tag transgenic mice subjected to interventions detailed in Figure 12, including vehicle control (VC), scramble peptide (SC) and MTMR7-CC peptide (MT). Regions displaying positive staining are highlighted by red arrows. **B.** Quantification of the nuclear-to-cytoplasmic ratio of non-phosphorylated β -catenin-positive cells in gastric tumor tissues. **C.** Assessment of the nuclear-to-cytoplasmic ratio in non-phosphorylated β -catenin-positive cells within duodenum tissues. Treatment groups are denoted as VC (vehicle control), SC (scramble peptide control), and MT (MTMR7 peptide treatment). Images of tumor or duodenal tissue were captured at a magnification of 200 \times . Nuclear staining positivity was manually counted in five fields of view per animal using *Image J* (imagej.nih.gov/ij) in tumor cells/ epithelial cells of the proliferative compartment of the duodenal crypts. Count of cells exhibiting positive results responding to nuclear staining was normalized to the total cell count in the tumor/proliferative compartment. Data were presented as means \pm S.E (Significance indicated by $*p < 0.05$, one-way ANOVA, $n = 4-8$ /group).

3.3.3 MTMR7 peptide reduces WNT-target gene expression.

Subsequent to IHC analysis aimed at determining the localization and expression of non-phosphorylated β -catenin, the transcriptional activity of key WNT pathway target genes were quantitatively assessed (*Axin2*, *Ephb*, *Lgr5*, and *Asclc*), in the small intestine of *APC^{min/+}* mice by RT-qPCR.

In *APC^{min/+}* mice subjected to MT peptide treatment, analysis of small intestine tissues unveiled a reduction in the expression of WNT target genes, as illustrated in Figure 17. However, this reduction, in comparison to the VC group, did not attain statistical significance. Nevertheless, the expression levels of *Ephb* and *Asclc* exhibited a discernible trend, suggesting a potential modulatory effect of MTMR7 peptide therapy on WNT signaling.

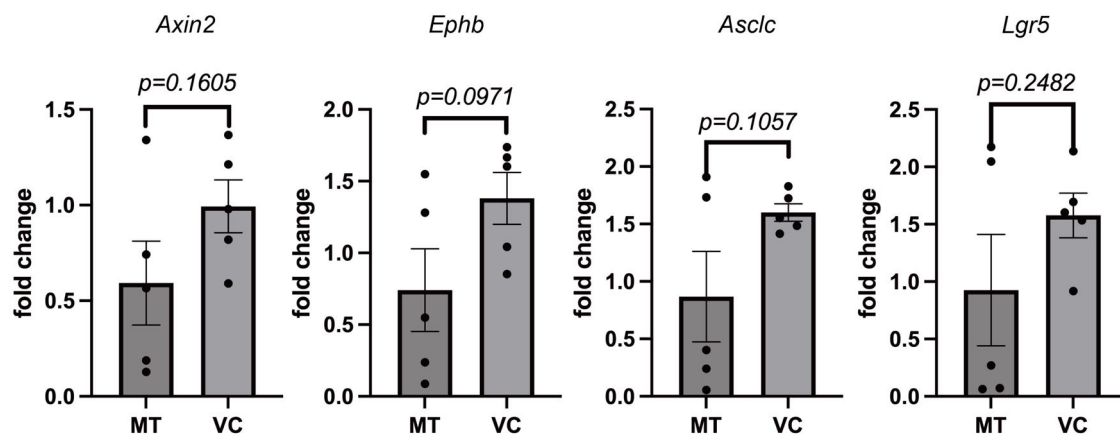


Figure 17. Expression of WNT target genes in the mouse small intestine.

Total RNA was isolated from frozen mouse tissues obtained from the small intestine. cDNA was assessed using RT-qPCR with 40 cycles to detect *Axin2*, *Ephb*, *Asclc* and *Lgr5*. The cycle threshold (CT) values of total RNA were normalized to β 2-microglobulin (*B2m*). The expression levels were calculated as -fold \pm S.E. compared to the vehicle control group (VC). (n=3 per organ; n.s vs. VC, unpaired t-student test).

3.4 MTMR7 regulates β -catenin translocation *in vitro*.

Next, the influence of MTMR7-FL enzyme on the subcellular localization of β -catenin in SW480 cells was assessed by immunofluorescence microscopy (IF). To explore β -catenin translocation dynamics, importazole (IPZ) and leptomycin B (LMB) were employed to modulate nuclear-cytoplasmic trafficking. IPZ inhibits the importin- β receptor, thereby suppressing the cytosol-to-nucleus import of proteins and downregulating nuclear protein accumulation [93]. Conversely, LMB impedes the CRM-1-dependent nuclear export pathway, resulting in reduced cytosolic protein export [94]. Additionally, GSK3i elevates the non-phosphorylated β -catenin level by inhibiting GSK3b [84], thereby enhancing WNT signaling in SW480 cells.

The IF staining (Figure 18) unveiled a down-regulation in non-phosphorylated β -catenin expression in SW480 cells after MTMR7 transfection in comparison to the EV group, accompanied by a noticeable shift in localization from the cytoplasm to the nucleus. In the EV + DMSO group, non-phosphorylated β -catenin in vehicle-treated cells predominantly localized in the cytoplasm. Conversely, the EV + LMB group exhibited a distinct translocation of non-phosphorylated β -catenin from the cytoplasm to the nucleus. Notably, overexpression of MTMR7 in SW480 led to nuclear accumulation of non-phosphorylated β -catenin, indicating that MTMR7 is crucial in mediating the translocation of β -catenin from the cytoplasm to the nucleus. Conversely, MTMR7 + IPZ led to the cytoplasmic aggregation of non-phosphorylated β -catenin, suggesting that IPZ inhibits the translocation from cytoplasm to nucleus by targeting the importin- β receptor, thereby modulating the MTMR7-mediated regulation of the distribution of non-phosphorylated β -catenin.

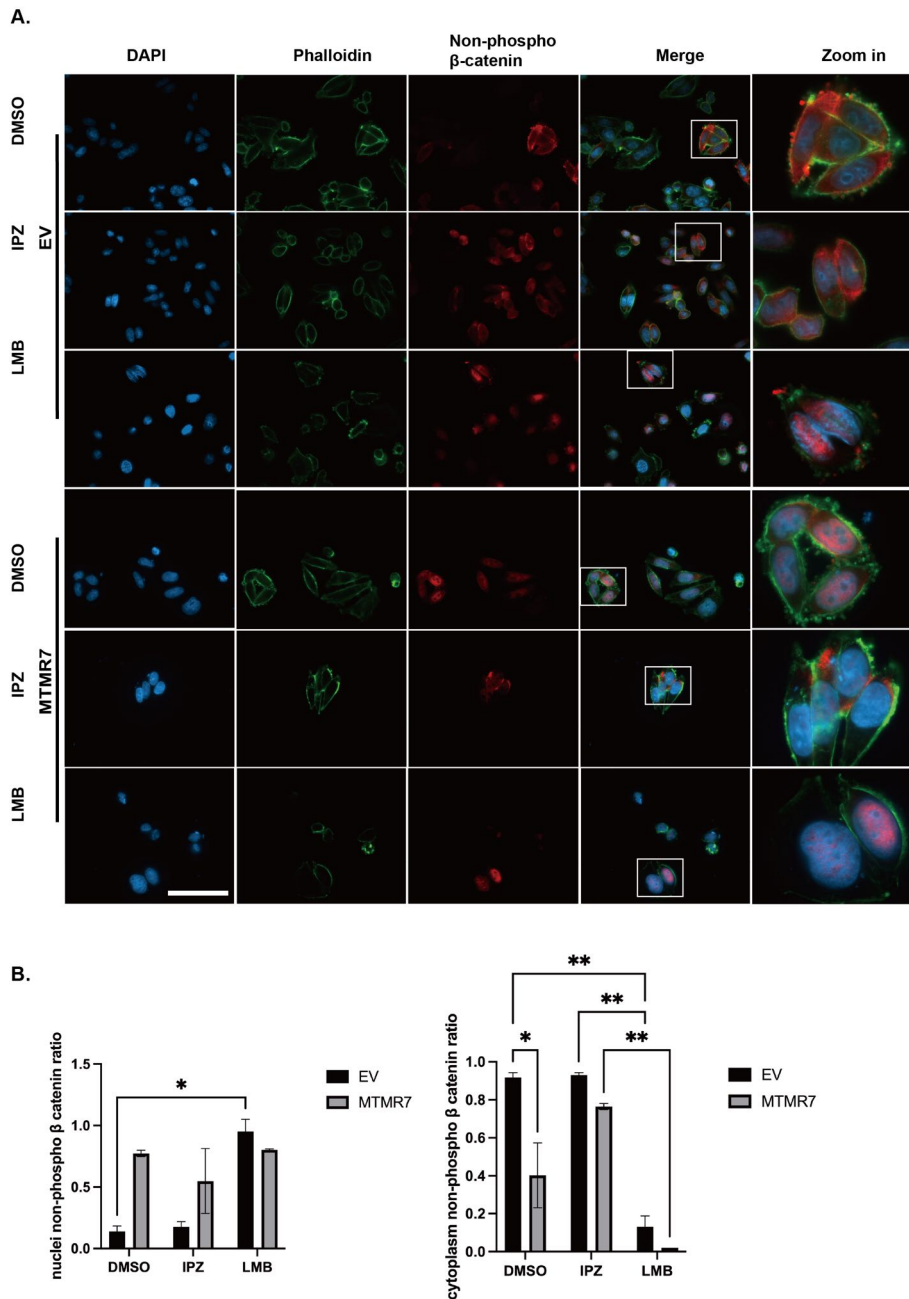


Figure 18. Subcellular localization of non-phosphorylated β -catenin in SW480 cells.

A. SW480 cells were cultured at a density of 5×10^4 cells/mL in μ -Slide 8 Well chambers and transfected with either an EV or MTMR7 plasmid for 24 hours in serum-free media. Following transfection, cells were treated with Chir (10 μ M) in combination with either LMB (0.1 μ M), IPZ (5 μ M), or DMSO as a control for an additional 24 hours. Cells were then fixed and stained for IF. Colors: green=phalloidin, red=non-phosphorylated β -catenin, blue=DAPI (nuclei). Magnification 630 \times . Representative images from $n=2$ independent experiments. **B.** Quantitative analysis of non-phosphorylated β -catenin localization in nuclei and cytoplasm across experimental groups. The prevalence of cells with nuclear positivity or cytoplasm positivity for non-phosphorylated β -catenin was expressed as a normalized ratio against the total cell count. Experimental groups were categorized based on transfection variables (EV vs. MTMR7) and treatment with pharmacological agents (DMSO, IPZ, and LMB). Positive staining for non-phosphorylated β -catenin in nuclei or cytoplasm was quantified in five randomly selected fields of view per well, employing *ImageJ* software (imagej.nih.gov/ij). Results are depicted as mean ratios \pm S.E (Significance indicated by $*p < 0.05$, $**p < 0.01$, two-way ANOVA followed by Bonferroni's multiple comparisons). IF images derived from two independent experiments ($n=2$).

3.5 MTMR7 inhibits WNT signaling by interfering with RAS- β -catenin interaction.

3.5.1 RAS and β -catenin form a protein interaction complex.

The precise mechanism underlying the inhibitory effect of MTMR7 on the WNT pathway remains to be fully elucidated. Given the established stability and degradation resistance of β -catenin and RAS due to their mutual interactions, as demonstrated in prior research [86,87], we hypothesized that MTMR7 may disrupt this interaction, consequently enhancing their degradation via phosphorylation and ubiquitination processes. To investigate this hypothesis, we transfected HEK293T, SW480, and HCT116 cell lines with the MTMR7 plasmid and conducted co-immunoprecipitation (Co-IP) to explore potential interactions between MTMR7 and the RAS- β -catenin complex. The assay involved the use of polyclonal antisera against RAS for pull-down, followed by immunoblotting (IB) to detect β -catenin.

Our results presented in Figure 19 confirm an interaction between RAS and β -catenin under both EV and MTMR7-transfected conditions. Notably, the presence of β -catenin in the immunoprecipitated (IP) sample from SW480 and HCT116 cells following pull-down with an Ab against RAS confirms the interplay between RAS and β -catenin. Importantly, overexpression of MTMR7 led to a prominent reduction in β -catenin levels in both the input and the IP from SW480 and HCT116 cells in comparison to the control groups. This decrease corroborates the hypothesis that MTMR7 interrupts the RAS- β -catenin interactions, thereby reducing the cellular levels of β -catenin.

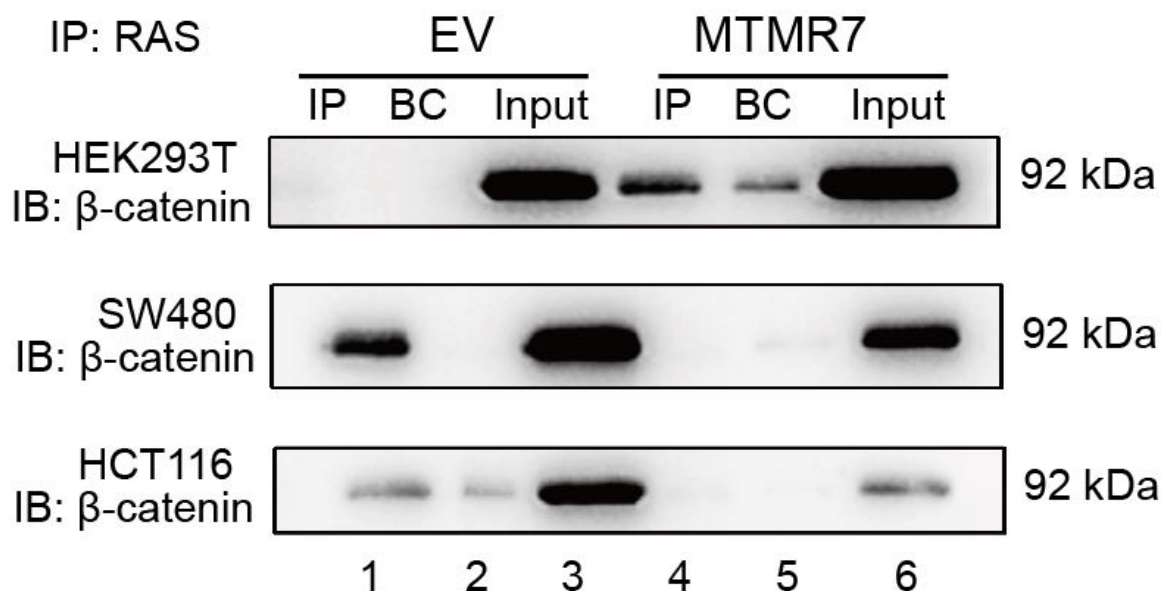


Figure 19. Co-IP detecting MTMR7 interference with the β -catenin-RAS interaction complex.

IP was performed using an Ab specific for RAS, with a no-Ab (beads control, BC) serving as the negative control. Coprecipitated proteins were identified by IB employing an Ab against β -catenin. "Input" represents the total protein from cell lysates. Presented here are representative Western blot images derived from three independent experiments (n=3).

3.5.2 MTMR7 does not directly interact with full-length (FL) RAS by Co-IP.

The previous data suggested that MTMR7 impedes the assembly of the RAS- β -catenin complex, resulting in the destabilization and subsequent degradation of RAS and β -catenin. Such phenomenon hints at a direct mechanistic intervention by MTMR7, yet the specifics of such interference remain elusive. To elucidate this, we proposed that MTMR7 might target RAS directly at its β -catenin interaction domains, effectively preventing the formation of the RAS- β -catenin complex [73,74,86]. To assess this hypothesis, Co-IP experiments were designed in HEK293T cells, utilizing a polyclonal antiserum against FL RAS for IP, followed by IB for both FL-RAS and MTMR7.

Figure 20A illustrates a discernible decrease in RAS protein levels in cells transfected with MTMR7 compared to the EV group, suggesting a role for MTMR7 in the targeted degradation of RAS. Contrary to our initial hypothesis, subsequent analyses demonstrated no direct interaction between MTMR7 and FL-RAS, as evidenced by the absence of IB of MTMR7 in IP of RAS in both EV and MTMR7 group.

To further investigate the potential interaction between MTMR7 and RAS, IF staining was conducted in HEK293T cells following transfection with MTMR7. The IF imaging (Figure 20B) unveiled distinct localization patterns of RAS (green) and MTMR7 (red). While both proteins exhibited positive expression and could co-localize within the same cellular regions, as indicated by the merged yellow fluorescence.

Expanding our inquiry, we employed Proximity Ligation Assay (PLA) in MTMR7-transfected SW480 cells to detect *in situ* interactions between MTMR7 and RAS. Despite the sensitivity of PLA in highlighting proximal interactions via a red fluorescent signal, Figure 20C revealed no observable interaction between MTMR7 and endogenous FL RAS in the transfected cells. These findings collectively suggest that while MTMR7 impacts RAS- β -catenin assembly, it likely does not directly bind to FL-RAS. In the meantime, Our cooperation partners demonstrated that the isolated globular domain of KRAS directly interacts with the CC domain of MTMR7 [95]. Therein, the hypervariable region (HVR) tail of KRAS hindered the interaction of FL MTMR7 with FL RAS, consistent with the IP results above.

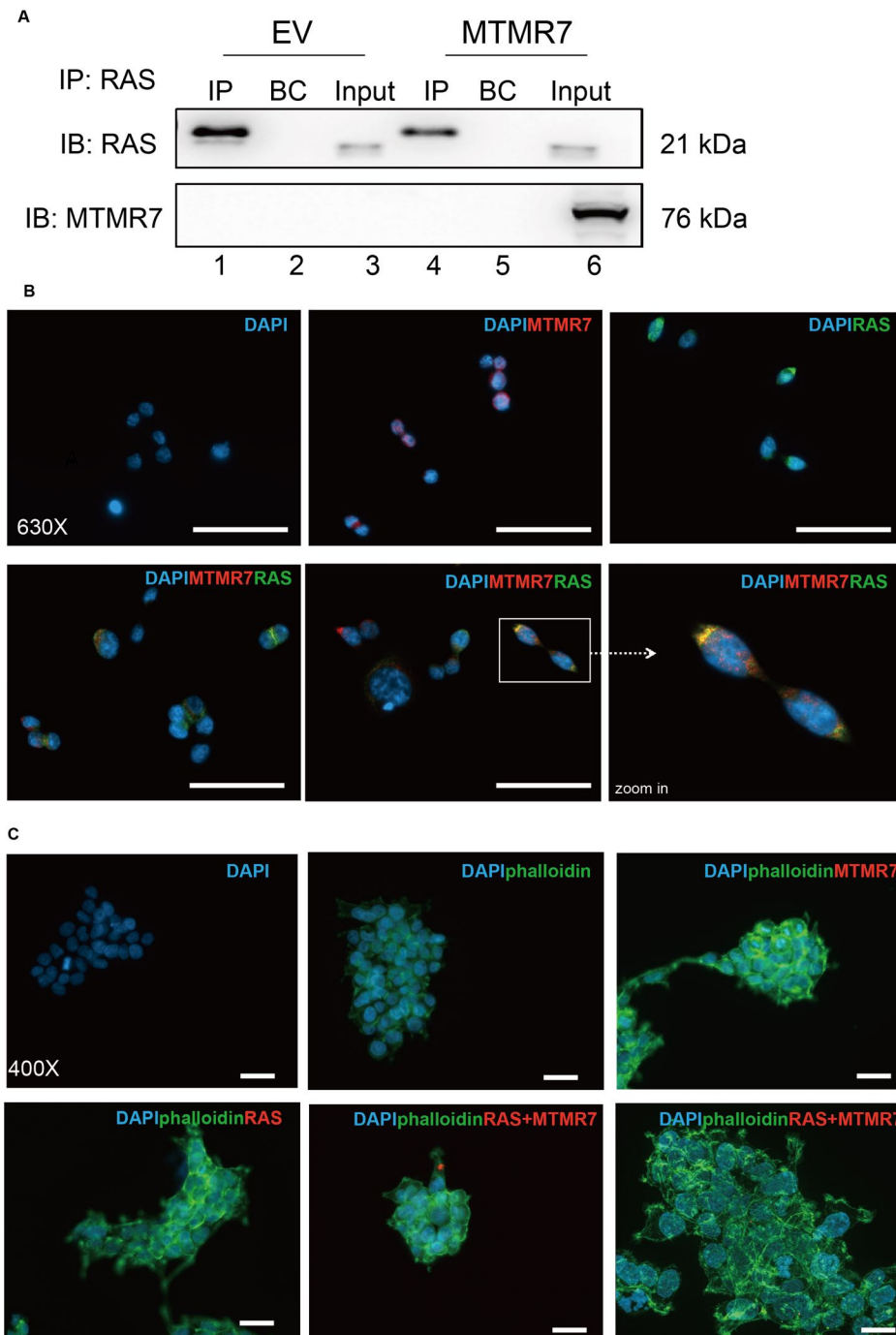


Figure 20. MTMR7-RAS interaction and localization.

A. IP assays were conducted using antibodies against FL RAS, with a no-Ab (beads control, BC) serving as the negative control. Western blot analysis detected both RAS and MTMR7. Presented here are representative Western blot images derived from three independent experiments (n=3).

B. Subcellular localization of MTMR7 and FL RAS in HEK293T cells. Following transfection with MTMR7 plasmid, cells underwent IF staining to elucidate the distribution of MTMR7 and RAS. Colors: green=RAS, red=MTMR7, blue=DAPI (nuclei). Magnification 630 \times . Representative images from n=3 independent experiments.

C. PLA in MTMR7-transfected SW480 cells to detect *in situ* interactions between MTMR7 and FL RAS. Following transient transfection with the MTMR7-FL plasmid, PLA was performed using specific antibodies against MTMR7 and RAS. The assay, designed to visualize protein-protein interactions through fluorescent signals (red dots for MTMR7-RAS proximity), along with phalloidin (green) and DAPI (blue) staining for cytoskeletal and nuclear visualization respectively, showed an absence of red fluorescence signals at 400 \times magnification. The utilization of a singular Ab served as negative control. Representative images from n=1 experiment.

3.5.3 Inhibition of WNT signaling by MTMR7 through destabilization of RAS and β -catenin.

To further elucidate the effect of MTMR7 expression on the WNT signaling pathway, specifically its impact on RAS and β -catenin stability, IP assays in HEK293T cells were employed in the presence of Chir and MG132. This investigative approach, involving the co-transfection with ubiquitin-HA and either an MTMR7 plasmid or an EV, followed by treatment with Chir and/or MG132, facilitated the assessment of β -catenin levels via Ab-specific pulldown assays.

The experimental outcomes demonstrated that MTMR7 expression fosters the degradation of β -catenin. By analyzing the normalized OD values of protein complexes precipitated by different antibodies post-MTMR7 overexpression, we bypassed the variability introduced by drug treatments. This strategy allowed for a direct comparison of β -catenin levels influenced by the presence or absence of MTMR7. Figures 21A-D display the original IB membranes, with subsequent image analysis revealing notable differences in β -catenin degradation between the MTMR7 and EV groups.

Comprehensive densitometric analyses, as shown in Figures 21E and 21F, illustrate the regulatory impact of MTMR7 on β -catenin levels within the WNT signaling pathway. Specifically, a marked reduction in β -catenin levels is observed with MTMR7 + aHA (anti-HA), MTMR7 + aRAS (anti-RAS), and MTMR7 + aBCAT (anti- β -catenin) compared to their EV counterparts. These findings confirm the role of MTMR7 as a negative regulator of the WNT/ β -catenin signaling. However, future repetitions of individual conditions of the experimental set-ups have to corroborate these findings and critically test for statistical significance.

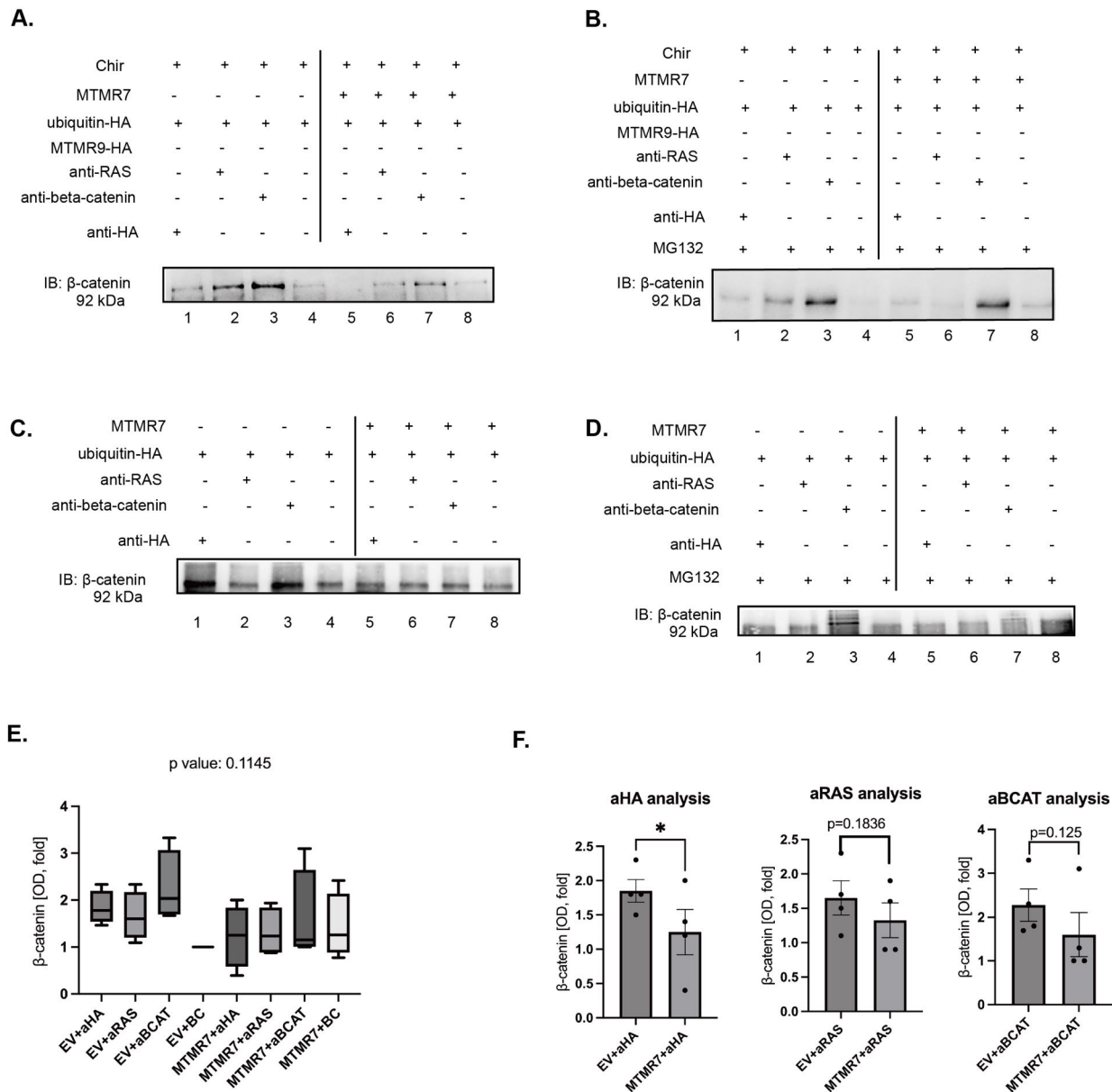


Figure 21. MTMR7 overexpression leads to destabilization of β -catenin and RAS.

Cells were co-transfected with ubiquitin-HA and either an EV or an MTMR7 plasmid, followed by treatment with **A.** Chir (10 μ M), **B.** Chir (10 μ M) and MG132 (3 μ M), **C.** no treatment (control), or **D.** MG132 (3 μ M) alone. IP was performed on cell lysates using anti-HA, pan-RAS, or anti- β -catenin antibodies, followed by IB to detect β -catenin. Densitometric analysis of immunoblots from treatments A-D, quantified using ImageJ software. Comparative analysis of β -catenin levels in cells overexpressing EV vs. MTMR7, independent of drug treatment, to inform future experimental directions. OD value of β -catenin levels was normalized to EV+BC group and calculated as -fold \pm S.E. **E.** OD values analyzed with one-way ANOVA and Kruskal-Wallis test and **F.** paired t-test for β -catenin levels, with Wilcoxon test applied for analysis of between-assay variance (aBAT). (n=1 per condition, total n=6 independent experiments.)

Abbreviations: aHA: anti-HA Ab, aBCAT: anti- β -catenin Ab, aRAS: anti-RAS Ab.

3.6 Cellular uptake of Biotin-MTMR7 peptide.

Our previous studies have demonstrated that MTMR7 inhibits WNT signaling both *in vivo* and *in vitro*, positioning it as a potential novel therapeutic agent for CRC [69,70]. Nevertheless, developing MTMR7 as a new peptide for synthesis and research purposes raises pivotal questions regarding its cellular uptake and retention time within the cells, which are crucial factors for its potential therapeutic efficacy. Consequently, experiments were designed to investigate the cellular uptake of the peptide.

To explore the cellular uptake dynamics, a myristoylated Biotin-MTMR7 peptide was employed, which features a myristoyl group at the N-terminus for membrane localization and a biotin moiety also at the N-terminus for detection purposes. As suggested by the literature, the retention of the myristoyl group may enhance the association of the peptide with cell membranes [96–99]. Moreover, the inherent non-fluorescent characteristics of biotin enable the introduction of fluorescently labeled streptavidin, thereby facilitating the visualization of the peptide through fluorescence microscopy.

Figure 22 presents the uptake and intracellular localization of the Biotin-MTMR7 peptide in SW480 and HT29 cells, as detected by IF microscopy. This series of images illustrates the peptide's uptake at specified time intervals—initially at administration, followed by various time points (0 min, 30 min, 1 hour, 2 hours, 4 hours, 6 hours, 16 hours, 48 hours) post-administration.

Peptide uptake was observed in both SW480 and HT29 cells. Nevertheless, HT29 cells exhibited a higher level of peptide absorption and retention. Specifically, the peptide levels could be detected after 30 minutes upon administration in SW480 cells. However, the peptide signal weakened from 1 to 6 hours post-injection compared to the signal at the 30-minute time point. In contrast, HT29 cells exhibited peptide accumulation within the cytoplasm at the 30-minute time point, a phenomenon that persisted consistently for up to 6 hours, with the peptide signal remaining observable even after 16 hours of injection. It is noteworthy that the signal diminished at the 48-hour time point.

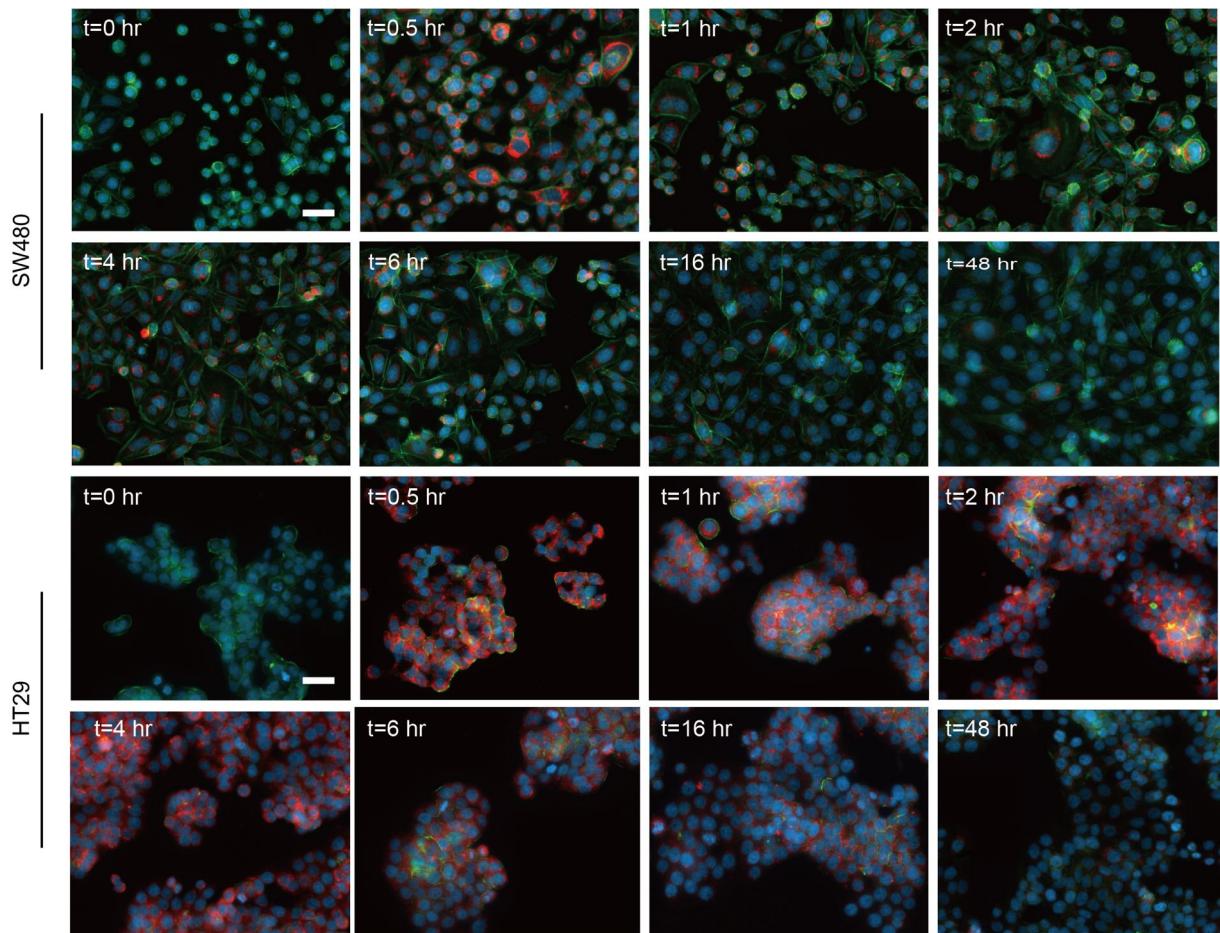


Figure 22. Time-courses of Biotin-MTMR7 peptide internalization in SW480 and HT29 cells.

Peptide uptake and localization were observed at various time points (0 min, 30 min, 1 hour, 2 hours, 4 hours, 6 hours, 16 hours, 48 hours) using a 1 μ M peptide concentration. Colors: red dots=Biotin-MTMR7 peptide, green=phalloidin, blue=DAPI (nuclei); magnification at 400 \times . Representative images from n=2 independent experiments.

4 Discussion

The findings in this study described the inhibitory effects of MTMR7, a myotubularin-related lipid phosphatase, on the WNT pathway in CRC. We evinced the potential of MTMR7 as a tentative therapeutic agent for the treatment of CRC.

The impact of MTMR7 on the transcriptional response of the TCF/LEF complex within the WNT pathway is complex and multifaceted. MTMR7 significantly diminished the transcriptional activity induced by TCF/LEF, thereby attenuating downstream expression of WNT target genes involved in cancer cell proliferation and tumor progression. Notably, MTMR7 inhibited the WNT pathway even in the presence of a GSK3 inhibitor, demonstrating its potent suppressive effect on this pathway. By interfering with the WNT pathway, MTMR7 also impeded the RAS- β -catenin interaction, crucially disrupting this pivotal linkage. Moreover, it promoted the destabilization of both RAS and β -catenin, leading to their enhanced degradation. Together, these findings demonstrate that MTMR7 exerts a comprehensive inhibitory effect on the WNT signaling cascade, underlining its potential as a regulatory target for modulating the WNT pathway.

4.1 Expression and function of MTMR7.

Despite extensive studies on the MTM family, research on its specific member MTMR7 remains limited. The MTM family, consisting of MTMs and related proteins, constitutes a growing group of enzymes crucial for regulating PtdIns(3)*P* levels. Specifically, MTMR7, a member of this family, exhibits targeted phosphatase activity on the phosphorylated forms of phosphatidylinositol [54,62,100].

MTMR7 primarily dephosphorylates PtdIns(3)*P* and PtdIns(3,5)*P*₂, as detailed in the Figure 23. This process is essential for the regulation of cell membrane dynamics. The subcellular localization of MTMR7 suggests its involvement in membrane trafficking. The localization of the MTMR7 varies with cellular state, possibly reflecting its regulatory role in intracellular membrane processes. For instance, MTMR7 is mainly identified in the nucleus in unicellular states and in the cytoplasm in confluent cells. This shift in localization might be related to its role in regulating membrane transport across various cell states [68].

Additionally, in 2003, Yasuhiro Mochizuki and Philip W. Majerus shed light on the molecular and biological characteristics of MTMR7, such as its coding sequence in mice and tissue-specific expression patterns [68]. They identified the CC domain of MTMR7 as its primary protein-binding region, a crucial factor for comprehending its function and action mechanism. Furthermore, their IF results revealed the primary localization of MTMR7 in Golgi-like granules and endosomes, and subcellular grading confirmed its presence in the cytoplasm and membranes of mouse neuronal cells [68].

In summary, while this study offers initial insights into the roles of MTMR7 in membrane trafficking, further experiments are imperative to elucidate its detailed molecular mechanisms and biological functions. Subsequent research endeavors should aim to delineate the specific pathways through which MTMR7 influences membrane vesicle dynamics and discern their impact on cell physiology and pathology.

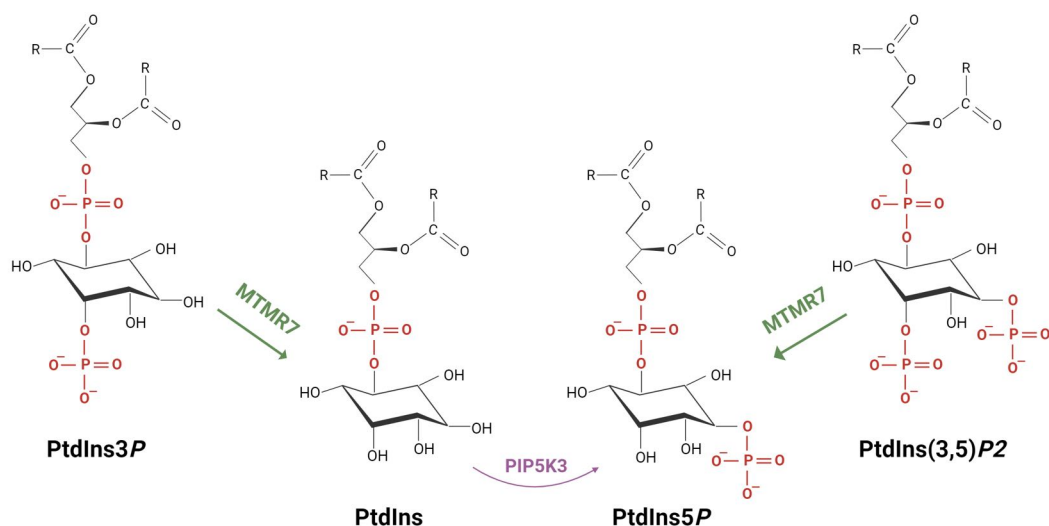


Figure 23. MTMR7 in phosphoinositide metabolism. The schematic representation of MTMR7 in phosphoinositide metabolism, was crafted using the ChemDraw application.

4.2 MTMR7 and the WNT pathway in colorectal cancer cells.

The aberrant regulation of the WNT/ β -catenin pathway is currently acknowledged as the central mechanism driving the carcinogenesis of both hereditary and sporadic CRC [90]. Traditionally, *APC* gene mutations were considered as a switch that activates this pathway [91,101]. Exploring the mechanisms through which regulators silence the WNT/ β -catenin pathway contributes to identifying innovative targeted therapeutic approaches for CRC. Our team has previously validated that an MTM phosphatase (i.e., MTMR7) inhibits the proliferation of CRC cells by involving the insulin pathway and reducing non-phosphorylated β -catenin through inhibition of TCF/LEF-driven promoter activity. These cumulative observations illuminate the role of MTMR7 in suppressing initiation and/or progression of CRC, a function associated with β -catenin degradation and the subsequent attenuation of WNT/ β -catenin pathway.

This study demonstrated that applying a MTMR7 CC domain-derived peptide in a murine cancer model with *APC* mutation can significantly decrease β -catenin levels within tumor tissues. Notably, only changes in mRNA levels of WNT target genes were observed in the intestinal tissues of *APC*^{min/+} mice. However, the *APC*^{min/+} mice are a genetically engineered model characterized by defective *APC* synthesis. This observation is noteworthy because although peptide treatment appears to exert a minimal impact on mRNA levels, IHC revealed significant effects (Figure 16). These findings confirm that changes at the protein level are more substantial and informative. Additionally, to assess the therapeutic efficacy of MTMR7 peptide on CRC, 11-week-old mice were treated with the peptide for two weeks. However, this treatment duration may only reflect the short-term therapeutic efficacy. To observe the mid- and long-term effectiveness of MTMR7 treatment, extended time points should be included in the future studies. Moreover, the alterations of mRNA and protein levels related to WNT signaling pathway as well as the survival rates after the treatment could provide a more comprehensive view of the *in vivo* function of MTMR7 [77,102].

Notably, diversifying experimental models to include 3D organoids, such as normal tissue, *APC*^{min/+}, and patient-derived organoids, will be beneficial in future research endeavors. Unlike 2D cultures such as cell lines, organoids better simulate the tumor microenvironment, which are essential for understanding tumor immunology and drug responses of CRC. In addition, tumor organoids could reduce the use of animal experiments by closely mimicking the pathophysiological conditions of cancer. Specifically, when used in conjunction with CRISPR-based gene editing, organoids enable a more effective and in-depth exploration of the molecular mechanisms underlying CRC development and metastasis [103].

Furthermore, our in vitro observations by demonstrating a notable reduction in the quantity of β -catenin protein in CRC cells. Collectively, our findings indicate that MTMR7 down-regulates β -catenin. Notably, this study identified that the exogenous transfection and ectopic overexpression of MTMR7 correlates with diminished transcriptional activity of TCF/LEF, which is activated by the binding of intranuclear β -catenin. All observations of TCF/LEF transcriptional activity were assessed using the luciferase reporter gene assay, a widely adopted method for studying the WNT pathway. In this assay, the TCF/LEF promoter regulates the expression of the luciferase reporter gene. Activation of the WNT signaling participates in the increase in luciferase activity, facilitating the quantification of WNT signaling intensity. In the meanwhile, we have observed a notable phenomenon: treatment with SAR405, a PIK3C/Vps inhibitor, consistently suppressed TCF/LEF transcriptional activity in three distinct cell lines. SAR405 not only inhibits autophagy but also synergizes with the inhibition of mechanistic target of rapamycin (mTOR) in tumor cells [81]. This suggests a multifaceted role of SAR405 in cellular signaling networks [104]. The inhibitory effects of SAR405 on TCF/LEF activity potentially mediated through mechanisms involving the stabilization and degradation processes of β -catenin. Additionally, the role of class III PI3K in the endocytosis of proteins and receptors may further influence WNT pathway modulation [81,104,105]. The intriguing findings from our luciferase reporter gene assay prompt further investigation into its underlying mechanisms within the WNT pathway.

Before exploring the mechanistic impact of MTMR7 on nuclear transcription factors, the inhibitory effects elicited by MTMR7 and KAY1797K (a small molecule known for destabilizing β -catenin) were comparatively analyzed. Notably, MTMR7 demonstrated a more pronounced inhibitory effect on the WNT signaling compared to KYA1797K, significantly reducing the transcription levels of TCF/LEF independently of KYA1797K. The mechanisms by which MTMR7 and KYA1797K inhibit the WNT signaling pathway differ substantially. Previous research by Choi et al. identified the RGS (Regulator of G protein Signaling) domain of Axin, a key component of destruction complex on WNT pathway, as a direct interaction site for KYA1797K [73,86,87]. This interaction is mediated through a direct binding to the Axin-domain, which results in inhibition of WNT pathway activity. In contrast, overexpression of MTMR7 in three distinct cell lines in this dissertation led to a downregulation of key WNT pathway proteins such as Axin and β -catenin (Figure 17), not by direct interaction with Axin, but rather through destabilizing the RAS- β -catenin complex, thereby promoting the degradation of both components. Furthermore, our previously published work demonstrated that the isolated globular domain of KRAS directly interacts with the CC domain of MTMR7, as observed by NMR spectroscopy [95]. Interestingly, the HVR tail of KRAS obstructs the interaction between full-length MTMR7 and full-length RAS. This observation

elucidates why MTMR7 downregulated the transcription levels of TCF/LEF without the involvement of KYA1797K.

MTMR7 suppressed the activity of effector proteins in the WNT pathway, leading to a marked inhibition of the TCF/LEF transcriptional activity. This inhibition directly constrained downstream mRNA synthesis. Notably, reductions were observed in the levels of *Axin2*, *Ephb*, *Lgr5*, and *Ascl2*—key target genes associated with the WNT pathway. These findings suggested that MTMR7 may inhibit the accumulation of β -catenin within the nucleus or interfere with its trafficking from the cytoplasm to the nucleus.

In our study, we hypothesized that MTMR7 disrupts the WNT pathway by interfering with the RAS- β -catenin complex formation in the cytoplasm, and the hypothesis was supported by our Co-IP and IP experiments. However, the inhibition by MTMR7 likely does not occur through a direct interaction with RAS, possibly due to incompatible structural features that prevent stable binding, as evidenced by our Co-IP and PLA experiments. This conclusion was supported by our Collaborators findings using NMR on the direct interaction of MTMR7 CC domain with the globular domain of KRAS lacking the HVR [95]. Instead, MTMR7 might interact with β -catenin directly, disrupting its interaction with RAS. This possibility is bolstered by Sang-Kyu Lee's findings, which highlighted the stability of the RAS- β -catenin complex in the cytoplasm and the disruptive effect of KYA1797K on this complex [74,86]. Consequently, further studies are imperative to elucidate the exact mechanism through which MTMR7 inhibits the WNT pathway, along with an exploration of its binding site on β -catenin. We will plan to further explore this mechanism in future studies.

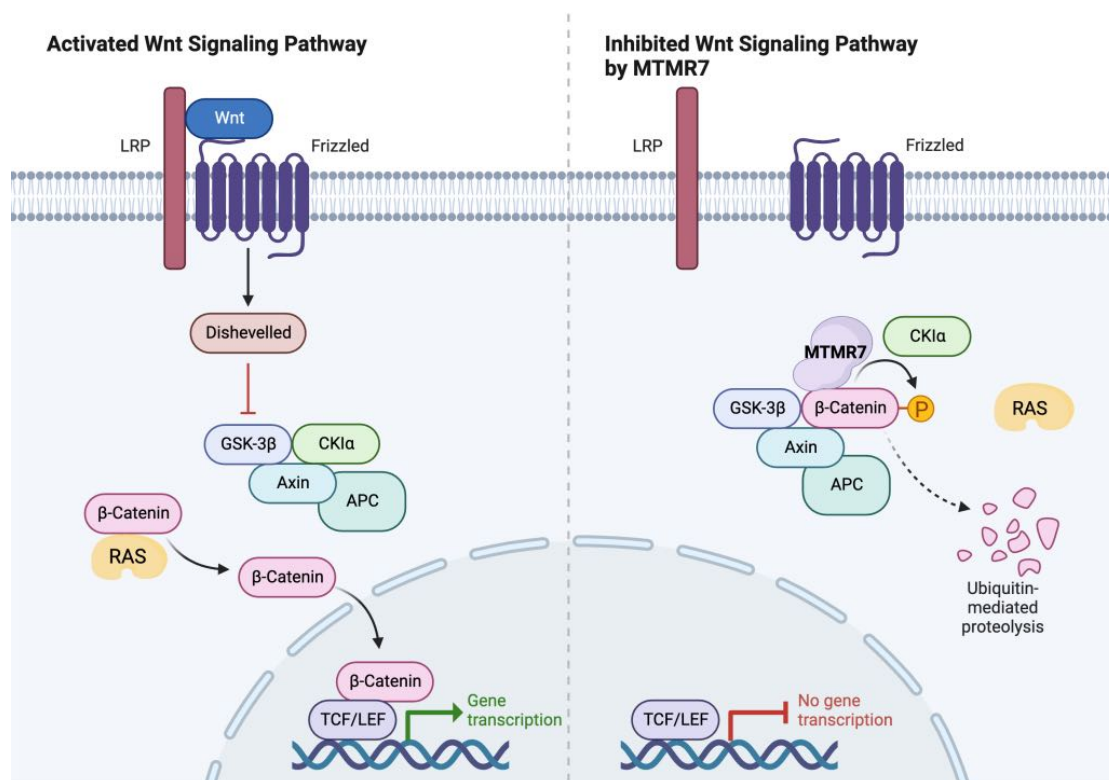


Figure 24. Schematic diagram for involvement of MTMR7 in the WNT pathway. (Left: activated state of WNT signaling. Right: inhibited state of WNT signaling by MTMR7). The diagram was generated by using the BioRender application (<https://www.biorender.com/>).

Our study primarily focused on inhibiting and downregulating the WNT pathway, with special emphasis on the distribution patterns of β -catenin. Upon activation of the WNT pathway, β -catenin avoids degradation by dissociation from the destruction complex, leading to its accumulation within the cytoplasm [91]. Subsequently, it undergoes translocation into the nucleus, where it binds to TCF/LEF, thus enhancing the transcriptional activity of WNT target genes [101]. Consequently, the expression of WNT target genes is predominantly associated with the translocation of β -catenin [92]. Nevertheless, the precise mechanism governing the nuclear entry of β -catenin remains to be fully elucidated [106].

Previous investigations into WNT signaling have predominantly focused on the processes behind the degradation of β -catenin, potentially overlooking the mechanisms associated with its nuclear translocation. In general, most nuclear proteins possess a nuclear localization sequence (NLS) that facilitates their transport from the cytoplasm into the nucleus [107]. This process involves the interaction with nuclear pore proteins (such as importin β), facilitated by RAN GTPase [108,109]. In contrast, β -catenin lacks a conventional NLS, which is typically essential for the recognition and transportation of proteins by importins/karyopherins into the nucleus [110]. However, despite this absence, β -catenin (arm repeats) exhibits a structural resemblance to importin β (HEAT repeats), signifying the presence of overlapping regions. These regions could potentially assume a pivotal role in the translocation process through the nuclear pore complexes (NPC) [111]. This structural similarity enables β -catenin to traverse the NPC without binding to importin β .

Therefore, our data underscored the potential role of MTMR7 in preventing β -catenin from translocating into the nucleus. Unexpectedly, overexpression of MTMR7 induced a relocation of β -catenin from the cytoplasm to the nucleus, escalating the nuclear accumulation of β -catenin in comparison to the condition in the control group transfected with EV. This observation stands surprisingly in contrast to the findings in established literatures where nuclear translocation of β -catenin typically correlates with the activation of numerous WNT target genes, often indicative of tumorigenesis. However, this finding differs from several previous studies. For instance, the pituitary tumor-transforming gene 1 stabilizes β -catenin and promotes its nuclear translocation, hence fostering hepatic tumor development. Therefore, the exact mechanism by which MTMR7 facilitates the nuclear translocation of β -catenin while concurrently reducing the transcriptional activity of TCF/LEF should be further investigated [112].

4.3 Pathways involved in MTMR7 regulation.

This study proposed novel therapeutic strategies for CRC by harnessing MTMR7. Specifically, it highlights the crucial roles of MTMR7 in inhibiting the WNT pathway and disrupting the RAS- β -catenin complex. This action facilitates the degradation of RAS and β -catenin, offering promising avenues for both diagnosis and treatment, especially in patients exhibiting treatment resistance due to *CTNBB1*, *APC*, or *KRAS* mutations. Moreover, this study suggests that mutations in the WNT and RAS pathways create a synergistic interplay, fostering crosstalk between these pathways. This interaction may result in tumor progression, posing a significant challenge to the efficacy of treatment strategies for patients.

Our previous investigation revealed that MTMR7 plays a multifaceted role by not only inhibiting ERK1/2 and AKT/mTOR pathways but also establishing a complex association with PPAR γ , enhancing the transcriptional activity of PPAR γ -responsive enhancer element (PPRE) in the nucleus [69,70]. While our findings shed light on these aspects, the specific mechanism by which MTMR7 inhibits the WNT signaling pathway remains less elucidated. In this study, we proposed several potential mechanisms through which MTMR7 may exert influence on the WNT signaling pathway, in addition to its direct effect on the RAS- β -catenin complex.

(1) PPAR γ

PPAR γ acts as a negative regulator in various tumorigenic processes and developmental pathways [113]. Our prior research has demonstrated a collaborative role between PPAR γ and MTMR7, functioning as chaperones and synergistically enhancing PPRE-driven promoters and transcripts levels. Additionally, a substantial crosstalk exists between the PPAR γ and WNT signaling pathways.

A study by Farshbaf et al. illustrated that PPAR γ agonists contribute to enhanced synaptic plasticity through interactions with the WNT/PI3K/AKT pathway [114]. Moreover, Gregorio et al. revealed that in instances where intestinal fibrosis correlates with robust WNT signaling activation, the use of PPAR γ agonists can mitigate fibrosis by deactivating WNT signaling [115]. Furthermore, Gustafson et al. employed thiazolidinediones (TZDs) to decrease β -catenin levels and increase DKK1 (an inhibitor of the WNT pathway) expression [116]. Therefore, PPAR γ activates GSK3b, fostering a stable destruction complex that contributes to diminishing β -catenin levels.

In normal cellular conditions, PPAR γ inhibits tumorigenesis and WNT signaling by directing phosphorylated β -catenin to proteasomes, which is a process involving the connexin-binding domain of PPAR γ [117,118]. Conversely, there exists a bidirectional regulation between PPAR γ and β -catenin. Studies have demonstrated that β -catenin signaling activates the AKT pathway, resulting in downregulated PPAR γ expression in adipocytes and 2T2-L1 preadipocytes [114,119]. Moreover, the activation of β -catenin has been observed to reduce PPAR γ expression, with numerous studies identifying PPAR γ as a negative target gene of β -catenin [117].

Conclusively, existing literatures suggest that the inhibitory effect of MTMR7 on the WNT pathway may stem from the activation of PPAR γ , which in turn can further suppress WNT signaling.

(2) AKT

The AKT and the WNT pathways intersect at the level of GSK3b regulation [120]. AKT, positioned downstream of PI3K, phosphorylates GSK3b. However, this phosphorylation disrupts the formation of the destruction complex, comprising GSK3b, APC, CK1, and Axin. Consequently, the disruption allows the β -catenin to accumulate and translocate, thereby activating and sustaining the WNT pathway [121–123]. Additionally, our previous study demonstrated that MTMR7 inhibits two downstream pathways of receptor tyrosine kinase (RTK), including the AKT signaling. This inhibitory impact by MTMR7 weakens the activity of AKT, allowing GSK3b to activate and degrade β -catenin through phosphorylation and ubiquitination.

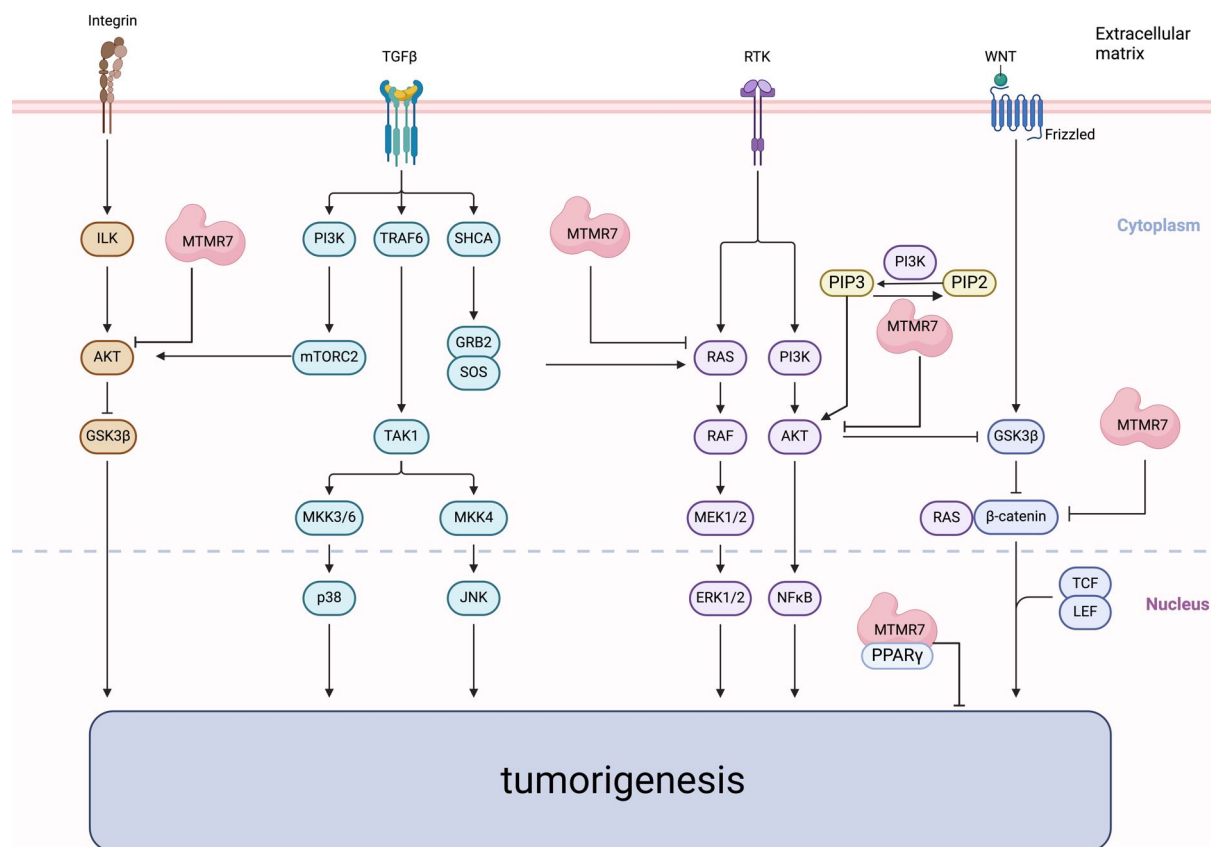


Figure 25. Schematic diagram of pathways involved in MTMR7 regulation. The diagram was generated by using the BioRender application (<https://www.biorender.com/>).

4.4 MTMR7 as novel therapeutic target for colorectal cancer.

The dysregulation of the WNT/ β -catenin pathway has been established as a critical factor in the tumorigenesis and progression of CRC [90–92]. Consequently, it represents a potentially promising therapeutic target for impeding cancer proliferation. Various small-molecule inhibitors targeting WNT/ β -catenin signaling have been identified so far. However, none of them have been approved for clinical use. Given that β -catenin functions as the central player in canonical WNT signaling and is continuously synthesized and accumulated in APC-mutated CRC, it stands out as an attractive target for cancer therapy. There has been exploration into disrupting the interaction between β -catenin and CREB binding protein (CBP), a co-activator crucial for β -catenin-dependent transcription. For instance, PRI-724, a pioneering small molecule that hinders the interaction between β -catenin and CBP, has undergone evaluation in clinical trials [124,125]. However, the outcomes of the combinatorial therapy involving PRI-724 and bevacizumab for treating newly diagnosed mCRC have not been published yet (NCT02413853). Moreover, MSAB is a small-molecule capable of inducing β -catenin degradation in WNT-dependent cancer cells and in mouse cancer models [126].

Peptides demonstrate greater therapeutic efficacy in their interaction with β -catenin when compared to small molecules. However, they encounter persistent challenges associated with limited membrane permeability and susceptibility to protease

degradation. Our study revealed a substantial inhibition of the WNT signaling pathway in CRC following treatment with an MTMR7-derived peptide. Although this initial experiment focused on assessing the short-term efficacy, we strongly advocate for future studies to delve into the long-term durable efficacy of this therapeutic approach.

In addition, Hongwei et al. have reported that xStAx-VHLL, a peptide synthesized by proteolysis targeting chimeras (PROTAC) technique, can directly bind to β -catenin, strongly inhibiting WNT signaling in cancer cells and impacting the survival of CRC patient-derived organoids [127]. In forthcoming investigations, the potential modification of MTMR7 using the PROTAC technique, in collaboration with experts in pharmacology, will hold promise for enhancing its anti-tumor properties and strengthening its resilience against protease activity. The exploration of this approach stands to significantly augment the therapeutic efficacy of MTMR7 in combating tumors while concurrently bolstering its resilience against proteolytic degradation.

In conclusion, our research presented a pioneering approach to CRC treatment, particularly for patients carrying *APC*, *CTNNB1* and *KRAS* mutations. The mechanism through which MTMR7 inhibits CRC offers a potential novel therapeutic strategy against drug-resistant forms of the disease, holding potential to shape future clinical practices. In addition, our findings lay the groundwork for the development of MTMR7-based therapies, which are expected to enhance the treatment outcomes for CRC patients.

5 CONCLUSION

This study delineated the inhibitory impact of MTMR7 on the WNT pathway in CRC and underscored its therapeutic potential for CRC treatment. MTMR7 exhibited the capability to modulate various oncogenic signaling pathways, particularly through inhibition of RAS/WNT signaling interactions. Moreover, we validated that MTMR7 effectively disrupts the WNT pathway, specifically by inhibiting RAS- β -catenin interactions, thus impeding this vital association. While the specific binding site and degradation mechanism of MTMR7 in this complex remain unclear, these aspects will be subjects of investigation in future research. In summary, our findings emphasize the complex mechanism of MTMR7 inhibition of the WNT signaling cascade, highlighting its potential as a regulatory target.

6 REFERENCES

- [1] Brenner H, Kloor M, Pox CP. Colorectal cancer. *The Lancet* 2014;383:1490–502. [https://doi.org/10.1016/S0140-6736\(13\)61649-9](https://doi.org/10.1016/S0140-6736(13)61649-9).
- [2] Stewart BW, Wild CP, editors. *World cancer report 2014*. Lyon, France: International Agency for Research on Cancer; 2014.
- [3] Global cancer observatory. <https://gco.iarc.fr/> n.d.
- [4] Rawla P, Sunkara T, Barsouk A. Epidemiology of colorectal cancer: incidence, mortality, survival, and risk factors. *Pg* 2019;14:89–103. <https://doi.org/10.5114/pg.2018.81072>.
- [5] Patel SG, Karlitz JJ, Yen T, Lieu CH, Boland CR. The rising tide of early-onset colorectal cancer: a comprehensive review of epidemiology, clinical features, biology, risk factors, prevention, and early detection. *The Lancet Gastroenterology & Hepatology* 2022;7:262–74. [https://doi.org/10.1016/S2468-1253\(21\)00426-X](https://doi.org/10.1016/S2468-1253(21)00426-X).
- [6] Lang D, Ciombor KK. Diagnosis and Management of Rectal Cancer in Patients Younger Than 50 Years: Rising Global Incidence and Unique Challenges. *Journal of the National Comprehensive Cancer Network* 2022;20:1169–75. <https://doi.org/10.6004/jnccn.2022.7056>.
- [7] Dekker E, Tanis PJ, Vleugels JLA, Kasi PM, Wallace MB. Colorectal cancer. *The Lancet* 2019;394:1467–80. [https://doi.org/10.1016/S0140-6736\(19\)32319-0](https://doi.org/10.1016/S0140-6736(19)32319-0).
- [8] Kanth P, Grimmett J, Champine M, Burt R, Samadder JN. Hereditary Colorectal Polyposis and Cancer Syndromes: A Primer on Diagnosis and Management. *American Journal of Gastroenterology* 2017;112:1509–25. <https://doi.org/10.1038/ajg.2017.212>.
- [9] Ma H, Brosens LAA, Offerhaus GJA, Giardiello FM, De Leng WWJ, Montgomery EA. Pathology and genetics of hereditary colorectal cancer. *Pathology* 2018;50:49–59. <https://doi.org/10.1016/j.pathol.2017.09.004>.
- [10] Guh DP, Zhang W, Bansback N, Amarsi Z, Birmingham CL, Anis AH. The incidence of co-morbidities related to obesity and overweight: A systematic review and meta-analysis. *BMC Public Health* 2009;9:88. <https://doi.org/10.1186/1471-2458-9-88>.
- [11] Dai Z. Obesity and colorectal cancer risk: A meta-analysis of cohort studies. *WJG* 2007;13:4199. <https://doi.org/10.3748/wjg.v13.i31.4199>.
- [12] Moghaddam AA, Woodward M, Huxley R. Obesity and Risk of Colorectal Cancer: A Meta-analysis of 31 Studies with 70,000 Events. *Cancer Epidemiology, Biomarkers & Prevention* 2007;16:2533–47. <https://doi.org/10.1158/1055-9965.EPI-07-0708>.
- [13] Reaven GM. Role of Insulin Resistance in Human. *INSULIN RESISTANCE* 1988;37.
- [14] Schoen RE, Tangen CM, Kuller LH, Burke GL, Cushman M, Tracy RP, et al. Increased Blood Glucose and Insulin, Body Size, and Incident Colorectal Cancer. *JNCI Journal of the National Cancer Institute* 1999;91:1147–54. <https://doi.org/10.1093/jnci/91.13.1147>.
- [15] Barb D, Williams CJ, Neuwirth AK, Mantzoros CS. Adiponectin in relation to malignancies: a review of existing basic research and clinical evidence. *The American Journal of Clinical Nutrition* 2007;86:858S-866S. <https://doi.org/10.1093/ajcn/86.3.858S>.

-
- [16] Kim Y-I. Diet, Lifestyle, and Colorectal Cancer: Is Hyperinsulinemia the Missing Link? *Nutrition Reviews* 2009;56:275–9. <https://doi.org/10.1111/j.1753-4887.1998.tb01765.x>.
- [17] Hanahan D, Weinberg RA. Hallmarks of Cancer: The Next Generation. *Cell* 2011;144:646–74. <https://doi.org/10.1016/j.cell.2011.02.013>.
- [18] Botteri E, Iodice S, Raimondi S, Maisonneuve P, Lowenfels AB. Cigarette Smoking and Adenomatous Polyps: A Meta-analysis. *Gastroenterology* 2008;134:388-395.e3. <https://doi.org/10.1053/j.gastro.2007.11.007>.
- [19] Fedirko V, Tramacere I, Bagnardi V, Rota M, Scotti L, Islami F, et al. Alcohol drinking and colorectal cancer risk: an overall and dose–response meta-analysis of published studies. *Annals of Oncology* 2011;22:1958–72. <https://doi.org/10.1093/annonc/mdq653>.
- [20] Grady WM, Carethers JM. Genomic and Epigenetic Instability in Colorectal Cancer Pathogenesis. *Gastroenterology* 2008;135:1079–99. <https://doi.org/10.1053/j.gastro.2008.07.076>.
- [21] Guinney J, Dienstmann R, Wang X, de Reyniès A, Schlicker A, Soneson C, et al. The consensus molecular subtypes of colorectal cancer. *Nat Med* 2015;21:1350–6. <https://doi.org/10.1038/nm.3967>.
- [22] Mármol I, Sánchez-de-Diego C, Pradilla Dieste A, Cerrada E, Rodriguez Yoldi M. Colorectal Carcinoma: A General Overview and Future Perspectives in Colorectal Cancer. *IJMS* 2017;18:197. <https://doi.org/10.3390/ijms18010197>.
- [23] Boland CR, Goel A. Microsatellite Instability in Colorectal Cancer. *Gastroenterology* 2010;138:2073-2087.e3. <https://doi.org/10.1053/j.gastro.2009.12.064>.
- [24] Inamura K. Colorectal Cancers: An Update on Their Molecular Pathology. *Cancers* 2018;10:26. <https://doi.org/10.3390/cancers10010026>.
- [25] Nguyen LH, Goel A, Chung DC. Pathways of Colorectal Carcinogenesis. *Gastroenterology* 2020;158:291–302. <https://doi.org/10.1053/j.gastro.2019.08.059>.
- [26] Huang Z, Yang M. Molecular Network of Colorectal Cancer and Current Therapeutic Options. *Front Oncol* 2022;12:852927. <https://doi.org/10.3389/fonc.2022.852927>.
- [27] Koveitypour Z, Panahi F, Vakilian M, Peymani M, Seyed Forootan F, Nasr Esfahani MH, et al. Signaling pathways involved in colorectal cancer progression. *Cell Biosci* 2019;9:97. <https://doi.org/10.1186/s13578-019-0361-4>.
- [28] Luo X-J, Zhao Q, Liu J, Zheng J-B, Qiu M-Z, Ju H-Q, et al. Novel Genetic and Epigenetic Biomarkers of Prognostic and Predictive Significance in Stage II/III Colorectal Cancer. *Molecular Therapy* 2021;29:587–96. <https://doi.org/10.1016/j.ymthe.2020.12.017>.
- [29] Pagès F, Mlecnik B, Marliot F, Bindea G, Ou F-S, Bifulco C, et al. International validation of the consensus Immunoscore for the classification of colon cancer: a prognostic and accuracy study. *The Lancet* 2018;391:2128–39. [https://doi.org/10.1016/S0140-6736\(18\)30789-X](https://doi.org/10.1016/S0140-6736(18)30789-X).
- [30] Müller MF, Ibrahim AEK, Arends MJ. Molecular pathological classification of colorectal cancer. *Virchows Arch* 2016;469:125–34. <https://doi.org/10.1007/s00428-016-1956-3>.
- [31] Lenz H-J, Ou F-S, Venook AP, Hochster HS, Niedzwiecki D, Goldberg RM, et al. Impact of Consensus Molecular Subtype on Survival in Patients With Metastatic Colorectal Cancer: Results From CALGB/SWOG 80405 (Alliance). *JCO* 2019;37:1876–85. <https://doi.org/10.1200/JCO.18.02258>.

-
- [32] Akiyoshi T, Wang Z, Kaneyasu T, Gotoh O, Tanaka N, Amino S, et al. Transcriptomic Analyses of Pretreatment Tumor Biopsy Samples, Response to Neoadjuvant Chemoradiotherapy, and Survival in Patients With Advanced Rectal Cancer. *JAMA Netw Open* 2023;6:e2252140. <https://doi.org/10.1001/jamanetworkopen.2022.52140>.
- [33] Deng J, Tian A-L, Pan H, Sauvat A, Leduc M, Liu P, et al. Everolimus and plicamycin specifically target chemoresistant colorectal cancer cells of the CMS4 subtype. *Cell Death Dis* 2021;12:978. <https://doi.org/10.1038/s41419-021-04270-x>.
- [34] Peters NA, Constantinides A, Ubink I, Van Kuik J, Bloemendal HJ, Van Dodewaard JM, et al. Consensus molecular subtype 4 (CMS4)-targeted therapy in primary colon cancer: A proof-of-concept study. *Front Oncol* 2022;12:969855. <https://doi.org/10.3389/fonc.2022.969855>.
- [35] Ubink I, Van Eden WJ, Snaebjornsson P, Kok NFM, Van Kuik J, Van Grevenstein WMU, et al. Histopathological and molecular classification of colorectal cancer and corresponding peritoneal metastases. *British Journal of Surgery* 2018;105:e204–11. <https://doi.org/10.1002/bjs.10788>.
- [36] Shaukat A, Kaltenbach T, Dominitz JA, Robertson DJ, Anderson JC, Cruise M, et al. Endoscopic Recognition and Management Strategies for Malignant Colorectal Polyps: Recommendations of the US Multi-Society Task Force on Colorectal Cancer. *Gastroenterology* 2020;159:1916-1934.e2. <https://doi.org/10.1053/j.gastro.2020.08.050>.
- [37] Kuipers EJ, Grady WM, Lieberman D, Seufferlein T, Sung JJ, Boelens PG, et al. Colorectal cancer. *Nat Rev Dis Primers* 2015;1:15065. <https://doi.org/10.1038/nrdp.2015.65>.
- [38] Taylor FGM, Quirke P, Heald RJ, Moran B, Blomqvist L, Swift I, et al. Preoperative High-resolution Magnetic Resonance Imaging Can Identify Good Prognosis Stage I, II, and III Rectal Cancer Best Managed by Surgery Alone: A Prospective, Multicenter, European Study. *Annals of Surgery* 2011;253:711–9. <https://doi.org/10.1097/SLA.0b013e31820b8d52>.
- [39] Hurwitz H, Fehrenbacher L, Novotny W, Cartwright T, Hainsworth J, Heim W, et al. Bevacizumab plus Irinotecan, Fluorouracil, and Leucovorin for Metastatic Colorectal Cancer. *N Engl J Med* 2004;350:2335–42. <https://doi.org/10.1056/NEJMoa032691>.
- [40] Grothey A, Cutsem EV, Sobrero A, Siena S, Falcone A, Ychou M, et al. Regorafenib monotherapy for previously treated metastatic colorectal cancer (CORRECT): an international, multicentre, randomised, placebo-controlled, phase 3 trial. *The Lancet* 2013;381:303–12. [https://doi.org/10.1016/S0140-6736\(12\)61900-X](https://doi.org/10.1016/S0140-6736(12)61900-X).
- [41] Adenis A, De La Fouchardiere C, Paule B, Burtin P, Tougeron D, Wallet J, et al. Survival, safety, and prognostic factors for outcome with Regorafenib in patients with metastatic colorectal cancer refractory to standard therapies: results from a multicenter study (REBECCA) nested within a compassionate use program. *BMC Cancer* 2016;16:412. <https://doi.org/10.1186/s12885-016-2440-9>.
- [42] Kasi PM, Kotani D, Cecchini M, Shitara K, Ohtsu A, Ramanathan RK, et al. Chemotherapy induced neutropenia at 1-month mark is a predictor of overall survival in patients receiving TAS-102 for refractory metastatic colorectal cancer: a cohort study. *BMC Cancer* 2016;16:467. <https://doi.org/10.1186/s12885-016-2491-y>.

-
- [43] Le DT, Uram JN, Wang H, Bartlett BR, Kemberling H, Eyring AD, et al. PD-1 Blockade in Tumors with Mismatch-Repair Deficiency. *N Engl J Med* 2015;372:2509–20. <https://doi.org/10.1056/NEJMoa1500596>.
- [44] Qin S, Xu L, Yi M, Yu S, Wu K, Luo S. Novel immune checkpoint targets: moving beyond PD-1 and CTLA-4. *Mol Cancer* 2019;18:155. <https://doi.org/10.1186/s12943-019-1091-2>.
- [45] Wang X. The biomarkers of hyperprogressive disease in PD-1/PD-L1 blockage therapy 2020:15.
- [46] Kopetz S, Guthrie KA, Morris VK, Lenz H-J, Magliocco AM, Maru D, et al. Randomized Trial of Irinotecan and Cetuximab With or Without Vemurafenib in BRAF-Mutant Metastatic Colorectal Cancer (SWOG S1406). *Journal of Clinical Oncology* n.d.;39.
- [47] Van Cutsem E, Huijberts S, Grothey A, Yaeger R, Cuyle P-J, Elez E, et al. Binimetinib, Encorafenib, and Cetuximab Triplet Therapy for Patients With *BRAF* V600E-Mutant Metastatic Colorectal Cancer: Safety Lead-In Results From the Phase III BEACON Colorectal Cancer Study. *JCO* 2019;37:1460–9. <https://doi.org/10.1200/JCO.18.02459>.
- [48] Knudsen AB, Zauber AG, Rutter CM, Naber SK, Doria-Rose VP, Pabiniak C, et al. Estimation of Benefits, Burden, and Harms of Colorectal Cancer Screening Strategies: Modeling Study for the US Preventive Services Task Force. *JAMA* 2016;315:2595. <https://doi.org/10.1001/jama.2016.6828>.
- [49] Baron JA, Beach M, Mandel JS, Stolk RU, Haile RW, Sandler RS, et al. Calcium Supplements and Colorectal Adenomas. *Annals NY Acad Sci* 1999;889:138–45. <https://doi.org/10.1111/j.1749-6632.1999.tb08731.x>.
- [50] Keum N, Aune D, Greenwood DC, Ju W, Giovannucci EL. Calcium intake and colorectal cancer risk: Dose-response meta-analysis of prospective observational studies: Calcium intake and colorectal cancer. *Int J Cancer* 2014;135:1940–8. <https://doi.org/10.1002/ijc.28840>.
- [51] Gorham ED, Garland CF, Garland FC, Grant WB, Mohr SB, Lipkin M, et al. Vitamin D and prevention of colorectal cancer. *The Journal of Steroid Biochemistry and Molecular Biology* 2005;97:179–94. <https://doi.org/10.1016/j.jsbmb.2005.06.018>.
- [52] Rothwell PM, Wilson M, Elwin C-E, Norrving B, Algra A, Warlow CP, et al. Long-term effect of aspirin on colorectal cancer incidence and mortality: 20-year follow-up of five randomised trials. *The Lancet* 2010;376:1741–50. [https://doi.org/10.1016/S0140-6736\(10\)61543-7](https://doi.org/10.1016/S0140-6736(10)61543-7).
- [53] Nishihara R, Lochhead P, Kuchiba A, Jung S, Yamauchi M, Liao X, et al. Aspirin Use and Risk of Colorectal Cancer According to BRAF Mutation Status. *JAMA* 2013;309:2563. <https://doi.org/10.1001/jama.2013.6599>.
- [54] Taylor GS, Maehama T, Dixon JE. Myotubularin, a protein tyrosine phosphatase mutated in myotubular myopathy, dephosphorylates the lipid second messenger, phosphatidylinositol 3-phosphate. *Proc Natl Acad Sci USA* 2000;97:8910–5. <https://doi.org/10.1073/pnas.160255697>.
- [55] Majerus PW, York JD. Phosphoinositide phosphatases and disease. *Journal of Lipid Research* 2009;50:S249–54. <https://doi.org/10.1194/jlr.R800072-JLR200>.
- [56] Phan TK, Williams SA, Bindra GK, Lay FT, Poon IKH, Hulett MD. Phosphoinositides: multipurpose cellular lipids with emerging roles in cell death. *Cell Death Differ* 2019;26:781–93. <https://doi.org/10.1038/s41418-018-0269-2>.
- [57] Hnia K, Vaccari I, Bolino A, Laporte J. Myotubularin phosphoinositide phosphatases: cellular functions and disease pathophysiology. *Trends in*

-
- Molecular Medicine 2012;18:317–27.
<https://doi.org/10.1016/j.molmed.2012.04.004>.
- [58] Begley MJ, Taylor GS, Kim S-A, Veine DM, Dixon JE, Stuckey JA. Crystal Structure of a Phosphoinositide Phosphatase, MTMR2: Insights into Myotubular Myopathy and Charcot-Marie-Tooth Syndrome. *Molecular Cell* n.d.
- [59] Doerks T, Strauss M, Brendel M, Bork P. GRAM, a novel domain in glucosyltransferases, myotubularins and other putative membrane-associated proteins. *Trends in Biochemical Sciences* 2000;25:483–5.
[https://doi.org/10.1016/S0968-0004\(00\)01664-9](https://doi.org/10.1016/S0968-0004(00)01664-9).
- [60] Choudhury P, Srivastava S, Li Z, Ko K, Albaqumi M, Narayan K, et al. Specificity of the Myotubularin Family of Phosphatidylinositol-3-phosphatase Is Determined by the PH/GRAM Domain. *J Biol Chem* 2006;281:31762–9.
<https://doi.org/10.1074/jbc.M606344200>.
- [61] Tsujita K, Itoh T, Ijuin T, Yamamoto A, Shisheva A, Laporte J, et al. Myotubularin Regulates the Function of the Late Endosome through the GRAM Domain-Phosphatidylinositol 3,5-Bisphosphate Interaction. *Journal of Biological Chemistry* 2004;279:13817–24. <https://doi.org/10.1074/jbc.M312294200>.
- [62] Laporte J, Bedez F, Bolino A, Mandel J-L. Myotubularins, a large disease-associated family of cooperating catalytically active and inactive phosphoinositides phosphatases. *Human Molecular Genetics* 2003;12:R285–92.
<https://doi.org/10.1093/hmg/ddg273>.
- [63] George K, van Wijngaarden, Paul Fleury, Jaap Bethlem, A. E. F. Hugo Meijer. Familial “myotubular” myopathy. *Neurology* 1969;19:901.
<https://doi.org/10.1212/WNL.19.9.901>.
- [64] Laporte J, Biancalana V, Tanner SM, Kress W, Schneider V, Wallgren-Pettersson C, et al. MTM1 mutations in X-linked myotubular myopathy. *Hum Mutat* 2000;15:393–409. [https://doi.org/10.1002/\(SICI\)1098-1004\(200005\)15:5<393::AID-HUMU1>3.0.CO;2-R](https://doi.org/10.1002/(SICI)1098-1004(200005)15:5<393::AID-HUMU1>3.0.CO;2-R).
- [65] Buj-Bello A, Laugel V, Messaddeq N, Zahreddine H, Laporte J, Pellissier J-F, et al. The lipid phosphatase myotubularin is essential for skeletal muscle maintenance but not for myogenesis in mice. *Proc Natl Acad Sci USA* 2002;99:15060–5. <https://doi.org/10.1073/pnas.212498399>.
- [66] Firestein R, Nagy PL, Daly M, Huie P, Conti M, Cleary ML. Male infertility, impaired spermatogenesis, and azoospermia in mice deficient for the pseudophosphatase Sbf1. *J Clin Invest* 2002;109:1165–72.
<https://doi.org/10.1172/JCI0212589>.
- [67] Zheng B, Yu X, Chai R. Myotubularin-Related Phosphatase 3 Promotes Growth of Colorectal Cancer Cells. *The Scientific World Journal* 2014;2014:1–8.
<https://doi.org/10.1155/2014/703804>.
- [68] Mochizuki Y, Majerus PW. Characterization of myotubularin-related protein 7 and its binding partner, myotubularin-related protein 9. *Proceedings of the National Academy of Sciences* 2003;100:9768–73.
<https://doi.org/10.1073/pnas.1333958100>.
- [69] Weidner P, Söhn M, Schroeder T, Helm L, Hauber V, Gutting T, et al. Myotubularin-related protein 7 activates peroxisome proliferator-activated receptor-gamma. *Oncogenesis* 2020;9:59. <https://doi.org/10.1038/s41389-020-0238-8>.
- [70] Weidner P, Söhn M, Gutting T, Friedrich T, Gaiser T, Magdeburg J, et al. Myotubularin-related protein 7 inhibits insulin signaling in colorectal cancer. *Oncotarget* 2016;7:50490–506. <https://doi.org/10.18632/oncotarget.10466>.

-
- [71] Ogino S, Shima K, Baba Y, Nosho K, Irahara N, Kure S, et al. Colorectal Cancer Expression of Peroxisome Proliferator-Activated Receptor γ (PPARG, PPARGgamma) Is Associated With Good Prognosis. *Gastroenterology* 2009;136:1242–50. <https://doi.org/10.1053/j.gastro.2008.12.048>.
- [72] Burgermeister E, Chuderland D, Hanoch T, Meyer M, Liscovitch M, Seger R. Interaction with MEK Causes Nuclear Export and Downregulation of Peroxisome Proliferator-Activated Receptor γ . *Molecular and Cellular Biology* 2007;27:803–17. <https://doi.org/10.1128/MCB.00601-06>.
- [73] Choi JK, Kwak I-S, Yoon S-B, Cho H, Moon B-S. A Small Molecule Promoting Neural Differentiation Suppresses Cancer Stem Cells in Colorectal Cancer. *Biomedicines* 2022;10:859. <https://doi.org/10.3390/biomedicines10040859>.
- [74] Lee S, Jeong W, Cho Y, Cha P, Yoon J, Ro EJ, et al. β -Catenin- RAS interaction serves as a molecular switch for RAS degradation via GSK 3 β . *EMBO Rep* 2018;19. <https://doi.org/10.15252/embr.201846060>.
- [75] Ahmed D, Eide PW, Eilertsen IA, Danielsen SA, Eknæs M, Hektoen M, et al. Epigenetic and genetic features of 24 colon cancer cell lines. *Oncogenesis* 2013;2:e71–e71. <https://doi.org/10.1038/oncsis.2013.35>.
- [76] Friedrich T, Richter B, Gaiser T, Weiss C, Janssen K-P, Einwächter H, et al. Deficiency of caveolin-1 in Apcmin/+ mice promotes colorectal tumorigenesis. *Carcinogenesis* 2013;34:2109–18. <https://doi.org/10.1093/carcin/bgt142>.
- [77] Ren J, Sui H, Fang F, Li Q, Li B. The application of ApcMin/+ mouse model in colorectal tumor researches. *J Cancer Res Clin Oncol* 2019;145:1111–22. <https://doi.org/10.1007/s00432-019-02883-6>.
- [78] Wallmen B, Schrempp M, Hecht A. Intrinsic properties of Tcf1 and Tcf4 splice variants determine cell-type-specific Wnt/ β -catenin target gene expression. *Nucleic Acids Research* 2012;40:9455–69. <https://doi.org/10.1093/nar/gks690>.
- [79] Livak KJ, Schmittgen TD. Analysis of Relative Gene Expression Data Using Real-Time Quantitative PCR and the 2- $\Delta\Delta$ CT Method. *Methods* 2001;25:402–8. <https://doi.org/10.1006/meth.2001.1262>.
- [80] Huang S-MA, Mishina YM, Liu S, Cheung A, Stegmeier F, Michaud GA, et al. Tankyrase inhibition stabilizes axin and antagonizes Wnt signalling. *Nature* 2009;461:614–20. <https://doi.org/10.1038/nature08356>.
- [81] Pasquier B. SAR405, a PIK3C3/Vps34 inhibitor that prevents autophagy and synergizes with MTOR inhibition in tumor cells. *Autophagy* 2015;11:725–6. <https://doi.org/10.1080/15548627.2015.1033601>.
- [82] Ji L, Lu B, Zamponi R, Charlat O, Aversa R, Yang Z, et al. USP7 inhibits Wnt/ β -catenin signaling through promoting stabilization of Axin. *Nat Commun* 2019;10:4184. <https://doi.org/10.1038/s41467-019-12143-3>.
- [83] Wu C, Luo K, Zhao F, Yin P, Song Y, Deng M, et al. USP20 positively regulates tumorigenesis and chemoresistance through β -catenin stabilization. *Cell Death Differ* 2018;25:1855–69. <https://doi.org/10.1038/s41418-018-0138-z>.
- [84] Yoshida Y, Soma T, Matsuzaki T, Kishimoto J. Wnt activator CHIR99021-stimulated human dermal papilla spheroids contribute to hair follicle formation and production of reconstituted follicle-enriched human skin. *Biochemical and Biophysical Research Communications* 2019;516:599–605. <https://doi.org/10.1016/j.bbrc.2019.06.038>.
- [85] Li Y, Gong H, Ding J, Zhao F, Du J, Wan J, et al. Inhibition of GSK3 Represses the Expression of Retinoic Acid Synthetic Enzyme ALDH1A2 via Wnt/ β -Catenin Signaling in WiT49 Cells. *Front Cell Dev Biol* 2020;8:94. <https://doi.org/10.3389/fcell.2020.00094>.

-
- [86] Cha P-H, Cho Y-H, Lee S-K, Lee J, Jeong W-J, Moon B-S, et al. Small-molecule binding of the axin RGS domain promotes β -catenin and Ras degradation. *Nat Chem Biol* 2016;12:593–600. <https://doi.org/10.1038/nchembio.2103>.
- [87] Jeong W-J, Ro EJ, Choi K-Y. Interaction between Wnt/ β -catenin and RAS-ERK pathways and an anti-cancer strategy via degradations of β -catenin and RAS by targeting the Wnt/ β -catenin pathway. *Npj Precision Onc* 2018;2:5. <https://doi.org/10.1038/s41698-018-0049-y>.
- [88] Thompson JA, Eades-Perner A-M, Ditter M, Muller WJ, Zimmermann W. Expression of transgenic carcinoembryonic antigen (CEA) in tumor-prone mice: An animal model for CEA-directed tumor immunotherapy. *Int J Cancer* 1997;72:197–202. [https://doi.org/10.1002/\(SICI\)1097-0215\(19970703\)72:1<197::AID-IJC28>3.0.CO;2-F](https://doi.org/10.1002/(SICI)1097-0215(19970703)72:1<197::AID-IJC28>3.0.CO;2-F).
- [89] Kim SH, Roth KA, Moser AR, Gordon JI. Transgenic mouse models that explore the multistep hypothesis of intestinal neoplasia. *The Journal of Cell Biology* 1993;123:877–93. <https://doi.org/10.1083/jcb.123.4.877>.
- [90] Li Y-R. Wnt/ β -catenin signaling pathway and colorectal cancer. *WCJD* 2015;23:1930. <https://doi.org/10.11569/wcjd.v23.i12.1930>.
- [91] Clevers H, Nusse R. Wnt/ β -Catenin Signaling and Disease. *Cell* 2012;149:1192–205. <https://doi.org/10.1016/j.cell.2012.05.012>.
- [92] MacDonald BT, Tamai K, He X. Wnt/ β -Catenin Signaling: Components, Mechanisms, and Diseases. *Developmental Cell* 2009;17:9–26. <https://doi.org/10.1016/j.devcel.2009.06.016>.
- [93] Soderholm JF, Bird SL, Kalab P, Sampathkumar Y, Hasegawa K, Uehara-Bingen M, et al. Importazole, a Small Molecule Inhibitor of the Transport Receptor Importin- β . *ACS Chem Biol* 2011;6:700–8. <https://doi.org/10.1021/cb2000296>.
- [94] Jans DA, Martin AJ, Wagstaff KM. Inhibitors of nuclear transport. *Current Opinion in Cell Biology* 2019;58:50–60. <https://doi.org/10.1016/j.ceb.2019.01.001>.
- [95] Weidner P, Saar D, Söhn M, Schroeder T, Yu Y, Zöllner FG, et al. Myotubularin-related-protein-7 inhibits mutant (G12V) K-RAS by direct interaction. *Cancer Letters* 2024;588:216783. <https://doi.org/10.1016/j.canlet.2024.216783>.
- [96] Nelson AR, Borland L, Allbritton NL, Sims CE. Myristoyl-Based Transport of Peptides into Living Cells. *Biochemistry* 2007;46:14771–81. <https://doi.org/10.1021/bi701295k>.
- [97] Wang B, Dai T, Sun W, Wei Y, Ren J, Zhang L, et al. Protein N-myristoylation: functions and mechanisms in control of innate immunity. *Cell Mol Immunol* 2021;18:878–88. <https://doi.org/10.1038/s41423-021-00663-2>.
- [98] Youn P, Chen Y, Furgeson DY. A Myristoylated Cell-Penetrating Peptide Bearing a Transferrin Receptor-Targeting Sequence for Neuro-Targeted siRNA Delivery. *Mol Pharmaceutics* 2014;11:486–95. <https://doi.org/10.1021/mp400446v>.
- [99] Yuan M, Song Z, Ying M, Zhu H, He Q, Yang B, et al. N-myristoylation: from cell biology to translational medicine. *Acta Pharmacol Sin* 2020;41:1005–15. <https://doi.org/10.1038/s41401-020-0388-4>.
- [100] Posor Y, Jang W, Haucke V. Phosphoinositides as membrane organizers. *Nat Rev Mol Cell Biol* 2022;23:797–816. <https://doi.org/10.1038/s41580-022-00490-x>.
- [101] Clevers H. Wnt/ β -Catenin Signaling in Development and Disease. *Cell* 2006;127:469–80. <https://doi.org/10.1016/j.cell.2006.10.018>.

-
- [102] Moser AR, Luongo C, Gould KA, McNeley MK, Shoemaker AR, Dove WF. ApcMin: A mouse model for intestinal and mammary tumorigenesis. *European Journal of Cancer* 1995;31:1061–4. [https://doi.org/10.1016/0959-8049\(95\)00181-H](https://doi.org/10.1016/0959-8049(95)00181-H).
- [103] Tuveson D, Clevers H. Cancer modeling meets human organoid technology. *Science* 2019;364:952–5. <https://doi.org/10.1126/science.aaw6985>.
- [104] Ronan B, Flamand O, Vescovi L, Dureuil C, Durand L, Fassy F, et al. A highly potent and selective Vps34 inhibitor alters vesicle trafficking and autophagy. *Nat Chem Biol* 2014;10:1013–9. <https://doi.org/10.1038/nchembio.1681>.
- [105] Wu H, Lu X-X, Wang J-R, Yang T-Y, Li X-M, He X-S, et al. TRAF6 inhibits colorectal cancer metastasis through regulating selective autophagic CTNNB1/ β -catenin degradation and is targeted for GSK3B/GSK3 β -mediated phosphorylation and degradation. *Autophagy* 2019;15:1506–22. <https://doi.org/10.1080/15548627.2019.1586250>.
- [106] Griffin JN, Del Viso F, Duncan AR, Robson A, Hwang W, Kulkarni S, et al. RAPGEF5 Regulates Nuclear Translocation of β -Catenin. *Developmental Cell* 2018;44:248-260.e4. <https://doi.org/10.1016/j.devcel.2017.12.001>.
- [107] Fahrenkrog B, Aebi U. The nuclear pore complex: nucleocytoplasmic transport and beyond. *Nat Rev Mol Cell Biol* 2003;4:757–66. <https://doi.org/10.1038/nrm1230>.
- [108] Quimby BB, Corbett AH. Nuclear transport mechanisms: CMLS, *Cell Mol Life Sci* 2001;58:1766–73. <https://doi.org/10.1007/PL00000816>.
- [109] Komeili A, O’Shea EK. New Perspectives on Nuclear Transport. *Annu Rev Genet* 2001;35:341–64. <https://doi.org/10.1146/annurev.genet.35.102401.090720>.
- [110] Hwang WY, Kostiuik V, González DP, Lusk CP, Khokha MK. Kap- β 2/Transportin mediates β -catenin nuclear transport in Wnt signaling. *eLife* 2022;11:e70495. <https://doi.org/10.7554/eLife.70495>.
- [111] Jamieson C, Sharma M, Henderson BR. Targeting the β -catenin nuclear transport pathway in cancer. *Seminars in Cancer Biology* 2014;27:20–9. <https://doi.org/10.1016/j.semcancer.2014.04.012>.
- [112] Zhang X, Wu N, Huang H, Li S, Liu S, Zhang R, et al. Phosphorylated PTTG1 switches its subcellular distribution and promotes β -catenin stabilization and subsequent transcription activity. *Oncogene* 2023;42:2439–55. <https://doi.org/10.1038/s41388-023-02767-7>.
- [113] Vallée A, Lecarpentier Y, Guillevin R, Vallée J-N. Thermodynamics in Gliomas: Interactions between the Canonical WNT/Beta-Catenin Pathway and PPAR Gamma. *Front Physiol* 2017;8:352. <https://doi.org/10.3389/fphys.2017.00352>.
- [114] Farshbaf MJ, Ghaedi K, Shirani M, Nasr-Esfahani MH. Peroxisome proliferator activated receptor gamma (PPAR γ) as a therapeutic target for improvement of cognitive performance in Fragile-X. *Medical Hypotheses* 2014;82:291–4. <https://doi.org/10.1016/j.mehy.2013.12.012>.
- [115] Di Gregorio J, Sferra R, Specca S, Vetuschi A, Dubuquoy C, Desreumaux P, et al. Role of glycogen synthase kinase-3 β and PPAR- γ on epithelial-to-mesenchymal transition in DSS-induced colorectal fibrosis. *PLoS ONE* 2017;12:e0171093. <https://doi.org/10.1371/journal.pone.0171093>.
- [116] Gustafson B, Eliasson B, Smith U. Thiazolidinediones increase the wingless-type MMTV integration site family (WNT) inhibitor Dickkopf-1 in adipocytes: a link with osteogenesis. *Diabetologia* 2010;53:536–40. <https://doi.org/10.1007/s00125-009-1615-1>.

-
- [117] Jansson EÅ, Are A, Greicius G, Kuo I-C, Kelly D, Arulampalam V, et al. The Wnt/ β -catenin signaling pathway targets PPAR γ activity in colon cancer cells. *Proc Natl Acad Sci USA* 2005;102:1460–5. <https://doi.org/10.1073/pnas.0405928102>.
- [118] Lecarpentier Y, Claes V, Vallée A, Hébert J-L. Interactions between PPAR Gamma and the Canonical Wnt/Beta-Catenin Pathway in Type 2 Diabetes and Colon Cancer. *PPAR Research* 2017;2017:1–9. <https://doi.org/10.1155/2017/5879090>.
- [119] Huelsken J, Behrens J. The Wnt signalling pathway. *Journal of Cell Science* 2002;115:3977–8. <https://doi.org/10.1242/jcs.00089>.
- [120] Hermida MA, Dinesh Kumar J, Leslie NR. GSK3 and its interactions with the PI3K/AKT/mTOR signalling network. *Advances in Biological Regulation* 2017;65:5–15. <https://doi.org/10.1016/j.jbior.2017.06.003>.
- [121] Fleming-de-Moraes CD, Rocha MR, Tessmann JW, De Araujo WM, Morgado-Diaz JA. Crosstalk between PI3K/Akt and Wnt/ β -catenin pathways promote colorectal cancer progression regardless of mutational status. *Cancer Biology & Therapy* 2022;23:1–13. <https://doi.org/10.1080/15384047.2022.2108690>.
- [122] Freyberg Z, Ferrando SJ, Javitch JA. Roles of the Akt/GSK-3 and Wnt Signaling Pathways in Schizophrenia and Antipsychotic Drug Action. *AJP* 2010;167:388–96. <https://doi.org/10.1176/appi.ajp.2009.08121873>.
- [123] Prossomariti A, Piazzini G, Alquati C, Ricciardiello L. Are Wnt/ β -Catenin and PI3K/AKT/mTORC1 Distinct Pathways in Colorectal Cancer? *Cellular and Molecular Gastroenterology and Hepatology* 2020;10:491–506. <https://doi.org/10.1016/j.jcmgh.2020.04.007>.
- [124] Moroney MR, Woodruff E, Qamar L, Bradford AP, Wolsky R, Bitler BG, et al. Inhibiting Wnt/beta-catenin in *CTNNB1* -mutated endometrial cancer. *Molecular Carcinogenesis* 2021;60:511–23. <https://doi.org/10.1002/mc.23308>.
- [125] Katoh M. Multi-layered prevention and treatment of chronic inflammation, organ fibrosis and cancer associated with canonical WNT/ β -catenin signaling activation (Review). *Int J Mol Med* 2018. <https://doi.org/10.3892/ijmm.2018.3689>.
- [126] Hwang S-Y, Deng X, Byun S, Lee C, Lee S-J, Suh H, et al. Direct Targeting of β -Catenin by a Small Molecule Stimulates Proteasomal Degradation and Suppresses Oncogenic Wnt/ β -Catenin Signaling. *Cell Reports* 2016;16:28–36. <https://doi.org/10.1016/j.celrep.2016.05.071>.
- [127] Liao H, Li X, Zhao L, Wang Y, Wang X, Wu Y, et al. A PROTAC peptide induces durable β -catenin degradation and suppresses Wnt-dependent intestinal cancer. *Cell Discov* 2020;6:35. <https://doi.org/10.1038/s41421-020-0171-1>.

7 CURRICULUM VITAE

PERSONAL INFORMATION

First and Last Name: Yanxiong Yu

Date of Birth: 30.07.1994

Place of Birth: China

EDUCATION

- | | |
|--------------------|--|
| 02.2021- | Heidelberg University (Medical Faculty Mannheim)
Mannheim, Germany
Doctor, Internal Medicine |
| 09.2017 – 06.2020 | Nanjing Medical University (NMU), China
Master, Pathogenic Biology |
| 09. 2012 – 06.2017 | Guangdong pharmaceutical university (GDPU), China
Bachelor, Clinical Medicine |

PUBLICATION:

1. Gutting T., Merkel A., Fink DJ., Hetjens S., Weidner P., **Yu Y.**, Burgermeister E., Belle S. et al. Expression of the EGFR-RAS Inhibitory Proteins DOK1 and MTMR7 and its Significance in Colorectal Adenoma and Adenoma Recurrence. *Journal of Gastrointestinal Liver Diseases*. 2021 Dec 21;30(4):446-455.
2. **Yu, Y.***, Farooq, M. S. *, Eberhart Meessen, S., Jiang, Y., Kato, D., Zhan, T., Ebert, M. P. A., & Burgermeister, E. et al. Nuclear pore protein POM121 regulates subcellular localization and transcriptional activity of PPAR γ . *Cell Death & Disease*, 15(1), 7. (**Co-first author**)
3. Weidner, P., Saar, D., Söhn, M., Schroeder, T., **Yu, Y.**, Burgermeister, E. et al. Myotubularin-related-protein-7 inhibits mutant (G12V) K-RAS by direct interaction. *Cancer Letters*, 588, 216783.

8 ACKNOWLEDGEMENTS

First and foremost, I extend my sincerest gratitude to Prof. Matthias Ebert, the Director of II. Med. Klinik. His provision of research opportunities and unwavering support facilitated the completion of my MD project in the research laboratory of the II. Med. Klinik (UMM), University of Heidelberg.

I owe a profound debt of gratitude to my supervisor, PD Elke Burgermeister. Her professional and meticulous guidance, both in my scientific endeavors and personal life, have rendered my three-year MD journey both smooth and fulfilling.

I appreciate the guidance provided by Dr. Sabine Eberhart, Dr. Philip Weidner and Frank Herweck. Their expertise relating to my project and in experimental techniques has been very helpful.

I am deeply thankful to Nachi, both a friend and lab colleague, for his experimental and reagent support over the past three years. His contributions fostered a friendly working environment and sparked insightful discussions.

I wish to express my gratitude to Gabriela, our technician, for her indispensable support in my day-to-day tasks. Further, my heartfelt thanks go out to all members of the lab and clinic for their constant support.

I would also like to acknowledge the China Scholarship Council (CSC) for their generous financial support and recognition throughout this period.

Lastly, I must thank my parents for their support throughout my three-year MD journey, my friends Xuanxuan and Luna for their unwavering encouragement and comfort amid experimental setbacks, which greatly contributed to the successful completion of my thesis.